Title:

Microglia signals to fibroblasts and neural progenitor cells to control regenerative neurogenesis after spinal cord injury in zebrafish

Authors:

Alberto Docampo-Seara[1], M. Ilyas Cosacak[1§], Kim Heilemann[1§], Friederike Kessel[1], Ana-Maria Oprişoreanu[1], Markus Westphal[1], Özge Çark[1], Daniela Zöller[1], Josi Arnold[1], Anja Bretschneider[1], Alisa Hnatiuk[1], Nikolay Ninov[1], Catherina G. Becker[1,2,3]*, Thomas Becker[1,2]*

Addresses:

1 Center for Regenerative Therapies Dresden at the TU Dresden, Fetscherstraße 105, 01307 Dresden, Germany

2 Centre for Discovery Brain Sciences, University of Edinburgh Medical School: Biomedical Sciences, Edinburgh EH16 4SB, UK

3 Cluster of Excellence Physics of Life, TU Dresden, 01062 Dresden, Germany

§ equal contribution

*Senior author

Key words:

spinal cord regeneration; cell-cell interactions; scRNAseq; neurogenesis; blood-derived macrophages; fibroblasts; *sema4ab*; *tgfb3*

HIGHLIGHTS

- Microglia control signalling from fibroblasts in a spinal injury site
- Fibroblasts promote regenerative neurogenesis via Tgfb3 signalling
- scRNAseq reveals full complement of *sema4ab*-dependent cell type interactions in a spinal injury site
- *sema4ab* stabilises activation state of microglia after injury

ABSTRACT

Zebrafish, in contrast to mammals, regenerate neurons after spinal cord injury, but little is known about the control mechanisms of this process. Here we show that microglia are the main cell type to express the evolutionarily conserved signalling molecule *sema4ab* in the injury site. Deletion of *sema4ab* doubles the number of newly generated progenitor cells and neurons after spinal injury. Using scRNAseq of all lesion site cell types after gene disruption, we find that *sema4ab* supports the microglial activation state and promotes interactions with fibroblasts and neural progenitor cells. Mechanistically, *sema4ab* signals through *plxn1a/b* receptors on spinal progenitors and attenuates expression of the neurogenesis-promoting cytokine *tgfb3* in fibroblasts. Hence, microglia regulate neurogenesis via *sema4ab* in successful spinal cord regeneration in zebrafish, which may be one of the mechanisms preventing regenerative neurogenesis in the mammalian spinal cord.

INTRODUCTION

Mammals, including humans, fail to regenerate neurons lost to protracted secondary cell death around a spinal injury site (Dusart & Schwab, 1994; Liu *et al*, 1997). Spinal progenitor cells can generate new neurons in a conducive environment and can even be re-programmed *in vivo* to produce oligodendrocytes, but not neurons (Llorens-Bobadilla *et al*, 2020; Shihabuddin *et al*, 2000; Stenudd *et al*, 2022). The environment in a spinal injury site consists of immune cells, such as invading blood-derived macrophages (BDMs) and tissue-resident microglia, astrocytes, oligodendrocytes, and fibroblasts. Interactions of these cell types result in an inhibitory environment for regenerative neurogenesis in which prolonged inflammation, as well as fibrotic and astrocytic scarring predominates (Anderson *et al*, 2016; Dias *et al*, 2018; Francos-Quijorna *et al*, 2022; Griffin & Bradke, 2020; Tran *et al*, 2018).

In contrast to mammals, zebrafish functionally regenerate their spinal cord at the adult and larval stage (Becker *et al*, 2004; Chang *et al*, 2021; Mokalled *et al*, 2016; Ohnmacht *et al*, 2016; Vandestadt *et al*, 2021). This includes regeneration of new neurons from resident progenitors (Briona & Dorsky, 2014; Briona *et al*, 2015; Huang *et al*, 2021; Ohnmacht *et al.*, 2016; Reimer *et al*, 2008). In zebrafish, these progenitor cells are termed ependymo-radial glial cells (ERGs), by virtue of their combination of ependymal and astroglial features (Becker & Becker, 2015).

A large number of signalling molecules from various cellular sources have been discovered that promote regenerative neurogenesis and axon growth in the zebrafish model (Becker & Becker, 2022). Importantly, regenerative neurogenesis avoids over-proliferation, which may be encountered when transplanting neural

progenitor cells to a spinal lesion (Sharp *et al*, 2014), or exhaustion of the progenitor pool, for example observed in a stroke model in mice (Carlen *et al*, 2009). Hence production of new neurons must be precisely regulated in zebrafish.

Microglia signal in the lesion via cytokines and are therefore in a key position to provide such regulation. In the injured telencephalon, microglia have been found to promote regenerative neurogenesis (Kyritsis *et al*, 2012). However, after a spinal cord injury, microglial cells proliferate (Becker & Becker, 2001), but lack expression of the neurogenesis-promoting cytokine *tnfa*, found in BDMs (Cavone *et al*, 2021; Tsarouchas *et al*, 2018).

Microglia likely interact with a number of other regeneration-relevant cell types that also influence regenerative neurogenesis. For example, ERGs and astrocyte-like cells produce a range of regeneration-promoting growth factors in central nervous system (CNS) injuries in zebrafish (Cigliola *et al*, 2023; Goldshmit *et al*, 2012; Mokalled *et al.*, 2016) and fibroblasts that invade a spinal lesion site promote regeneration by producing favourable extracellular matrix components for axonal regeneration (Kolb *et al*, 2023; Tsata *et al*, 2021; Wehner *et al*, 2017).

To understand how microglia influence the signalling landscape in the injury site and regenerative neurogenesis, we analysed the role of the conserved signalling molecule Semaphorin 4A (Sema4A). *Sema4a* that is mainly expressed by microglia and BDMs and can change their activation state (Leitner *et al*, 2015; Meda *et al*, 2012). Sema4a has been shown to promote a pro-fibrotic phenotype in fibroblasts *in vitro*, suggesting possible interactions with fibroblasts (Carvalheiro *et al*, 2019). Knock out of the principal Sema4A receptors Plexin B1 and B2 impairs neurogenesis

in the developing mouse brain (Daviaud *et al*, 2016), suggesting microglia to progenitor cell communication.

Here, we find that a zebrafish orthologue of *Sema4A*, *semaphorin4ab (sema4ab)*, in microglia maintains their activation state and attenuates neural progenitor proliferation. *Sema4ab* likely acts directly on ERGs via *plxnb1a/b* and indirectly, by reducing the production of the pro-neurogenic factor *tgfb3* in fibroblasts. Hence, *sema4ab*+ microglia regulate regenerative neurogenesis in the regeneration-permissive cellular environment of the zebrafish spinal cord.

RESULTS

scRNAseq indicates changes in microglia signalling interactions in the absence of *sema4ab* that increase neurogenesis

To better understand possible microglia/ERG communication in the complex lesion site environment, we decided to mutagenize the potential microglia activation factor *sema4ab* and analyse the consequences simultaneously for all relevant cell types by using scRNAseq. After a complete spinal lesion at 3 days post-fertilization (dpf), lesion-induced neurogenesis peaks at 24 hours post-lesion (hpl) in larval zebrafish; axons have regrown over the lesion site and swimming function is largely recovered by 48 hpl (Ohnmacht *et al.*, 2016; Wehner *et al.*, 2017). Thus, major regenerative processes occur within 48 hpl.

We injected larvae with highly-active CrRNAs (haCRs) that lead to mutagenesis of the targeted site in nearly all somatic cells, allowing phenotype analysis already in haCR-injected somatic mutants for *sema4ab* (Keatinge *et al*, 2021). We generated scRNAseq profiles of lesion site tissue from 50 control gRNA-injected and 50 *sema4ab* haCR-injected larvae at 24 hpl, the peak of regenerative neurogenesis (Ohnmacht *et al.*, 2016) (Fig. 1A).

Our scRNAseq experiments yielded 11788 cells for the control gRNA-injected sample (gControl), 11621 cells for sample 1 (gSema4abR1), and 11330 cells for sample 2 (gSema4abR2) of two technical repeats of *sema4ab* haCR-injected larvae after quality control. (Suppl. Tables 1, 2). The haCR manipulation of *sema4ab* was highly penetrant, as no intact reads of the targeted site could be retrieved, contrary to controls (151 correct reads in controls; 4 reads, none of which were correct, in *sema4ab* haCR-injected larvae; Suppl. Table 3, see Suppl. Table 4 for example

reads). Moreover, principal component analysis indicated that the two technical repeats of the *sema4ab* haCR treated condition were very closely related and more distant from the control sample (Suppl. Fig. 1A).

Unsupervised clustering and annotation revealed 44 distinct cell clusters that fell into 15 major cell categories (Fig. 1B,C). Fibroblast-like cells constituted the majority of all cells (21.13 %), consisting of 7 clusters, followed by neural cells (14.86 %), consisting of ERGs, oligodendrocytes and 4 neuronal clusters, red blood cells (13.54 %), consisting of three clusters, muscle cells (13.54 %), consisting of 5 clusters, and immune cells (11.63 %), consisting of 4 BDM/microglia and 2 neutrophil clusters. Hence, all major cell types expected from histology were represented in the samples, allowing for comprehensive analyses of cell interactions in the lesioned larval zebrafish spinal cord.

High and selective expression of *sema4ab* was found in a cluster of BDM/microglia (Fig. 1D), cluster MM #1. Using microglia marker *apoeb (Peri & Nusslein-Volhard, 2008)* and a marker set from adult zebrafish brain (Zambusi *et al*, 2022) we found that MM#1 and MM#2 expressed higher levels of microglial marker genes, compared to MM#3 and MM#4, which expressed more BDM-related genes. Population MM#2, in contrast to population MM#1, expressed proliferation markers, but otherwise marker expression was very similar between the two populations (Fig. 1E). Therefore, MM#2 likely is a proliferative sub-group of microglia and together with population MM#1 represent microglia. Hence, microglia is the main cell type expressing *sema4ab* in the injury site.

To determine gene expression changes in microglia in the absence of *sema4ab* function, we used GOstats for KEGG analysis (Falcon & Gentleman, 2007)

on microglia cluster MM#1. This indicated changes in activation pathways, namely RIG-I-like receptor signalling (Yoneyama *et al*, 2024), Toll-like receptor signalling pathways (Alhamdan *et al*, 2024) and NOD-like receptor signalling (Almeida-da-Silva *et al*, 2023) (Fig. 1F). Most of the indicator genes were under-represented in the sample in which *sema4ab* was disrupted compared to the control sample (20 of 21 genes for RIG-I-pathway, 29 of 32 for Toll-like receptor pathway; 16 of 17 genes for NOD-like receptor signalling; Suppl. Data file 1), suggesting reduced activation of microglia in the absence of *sema4ab*.

Analysis of the top down-regulated genes in MM#1 confirms this result (Table 1). For example, one of the most underrepresented genes, *lyz* (5.91-fold down), is related to a pro-inflammatory state (Barros et al., 2015; MacParland et al., 2018). Similarly, *grn1* (6.87-fold down), is linked to a pro-inflammatory state and cytokine production (Horinokita et al., 2019).

Reduced activation of microglia likely influences a number of cell types in the injury site. Comparing cell numbers between samples indicated no major changes in cell type representation resulting from *sema4ab* disruption (Suppl. Fig. 1B), with the possible exception of peridermis cluster 2 (PD#2), which showed a ~50 % reduction in cell number (Suppl. Fig. 1C). However, we observed alterations in gene expression. The highest changes in gene expression (> 300 differentially expressed genes) were present in microglia (MM#1, MM#2), neutrophils (NP#1), neurons (NN#2), fibroblasts (FB#1, FB#2, FB#3, FB#5), muscle (MC#1), peridermal cells (PD#1, PD#2), as well as in keratinocytes (KC#1, KC#2) and red blood cells (RB#1) (Suppl. Fig. 1D). Interestingly, most clusters showed reduced gene expression, with the exception of one neuronal cluster NN#2, which showed increased gene

expression. This indicates changes in gene expression across many cell types when *sema4ab* is disrupted in microglia.

To get a comprehensive view of how cell types could be affected by changes in microglia, we used CellChat, which evaluates cell interactions based on known ligand-receptor interactions in scRNAseq data (Jin *et al*, 2021). An analysis of the outgoing interactions of microglia indicated potentially altered signal/receptor interactions with all identified cell cluster, including ERGs (black circle) and fibroblasts (red line), but also with themselves and their proliferative version MM#2 (square) (Fig. 1G). Most of these signal/ligand interactions were diminished when *sema4ab* was disrupted. To determine potential direct signalling from microglia to ERGs, we analysed potentially altered signal/receptor interactions between microglia and ERGs. That indicated reduced interactions of *sema4ab* with *plxnb1a, plxnb1b* and *plxn2a* (Fig. 1H). Hence, scRNAseq predicts microglia to directly signal to ERGs using Sema4ab to Plexin receptors.

Of note, fibroblasts have pivotal functions in successful spinal cord regeneration in zebrafish (Tsata & Wehner, 2021), and all 7 clusters of fibroblasts show reduced incoming signals from microglia, when *sema4ab* is disrupted. Affected signal/receptor interactions included cytokine signalling (*e.g. tnfb, tgfb1b)*, among other pathways (Suppl. Fig. 1E). In addition, KEGG analysis for the three fibroblast populations that showed highest levels of differentially expressed genes after *sema4ab* disruption (FB#1, FB#2, FB#3) indicated ECM-receptor interactions, TGF-beta signalling, and adherens junction pathways as changed (Fig. 1I). This data suggests that signalling and ECM-related functions were changed in fibroblasts when *sema4ab* was disrupted. Hence, scRNA-seq indicates multiple simultaneous

signalling events of *sema4ab*+ microglia with other non-neural lesion cells, such as fibroblasts, that likely condition the lesion environment.

To determine whether such changed interactions influence regenerative neurogenesis, we analysed changes in proliferation and in gene expression related to neuronal differentiation in ERGs. Using the “Cell-Cycling Scoring and Regression” analysis code in Seurat (Satija *et al*, 2015) we calculated the proportion of cells in different cells cycle phases. We found a substantial increase in cells in G2/M phase in sema4ab-injected larvae (gControl: 16%, gSema4ab: 28%) (Fig. 1J). Additionally, a comparison of neuronal differentiation markers (*neurog1*, *neurod1*, *ascl1a*) and motor neuron cell fate marker *mnx1*, showed increased expression in ERGs in the absence of *sema4ab* function (Fig. 1K). This is consistent with enhanced progenitor proliferation and neurogenesis. Overall, scRNA-seq suggests a scenario, in which direct signalling via *sema4a* from microglial cells to spinal progenitors, as well as via other cell types, attenuates neurogenesis.

Sema4ab **is expressed mainly in microglia during regeneration**

To verify observations from scRNA-seq in vivo, we first analysed *sema4ab* expression during regeneration in whole-mounted larvae by multiplexed hybridization chain reaction fluorescence *in situ* hybridization (HCR-FISH) in combination with immune cell type-specific transgenic and HCR-FISH markers. Microglia were identified in *mpeg:mCherry* transgenic fish, in which mCherry is expressed under the *mpeg1.1* promoter (Ellett *et al*, 2011), and by additional expression of *apoeb* (*mpeg:mCherry*+/*apoeb*+). Putative BDMs were *mpeg:mCherry*+/*apoeb*-. Neutrophils

were detected in *mpx:GFP* transgenic fish, in which GFP is expressed under the *mpx* promoter (Renshaw *et al*, 2006) .

In uninjured three-day-old larvae, hardly any *sema4ab*+ cells were detectable, consistent with expression in injury-reactive immune cells. In contrast, at 6 hpl, numbers of *sema4ab*+ cells were strongly increased in the lesion site and remained high to at least 48 hpl (Fig. 2A-C; see Suppl. Fig. 2A for method control).

Co-labelling experiments at 24 hpl indicated that the majority of *sema4ab*+ cells were microglia (60.6 %, *sema4ab+; mpeg1:GFP+, apoeb*+). 17.7 % were putative BDMs (*sema4ab*+, *mpeg1:GFP*+, *apoeb*-), and 12.7% were unidentified (*sema4ab*+ only; Fig. 2D-G). Co-labelling of *sema4ab* with *mpx:GFP* expressing neutrophils indicated that 16 % of *sema4ab*+ cells were neutrophils at 6 hpl and at 24 hpl (Suppl. Fig. 2B-D), indicating that the few *sema4ab*+ cells not labelled by *mpeg:mCherry* were likely mostly neutrophils. In summary, a spinal lesion induced the presence of *sema4ab*+ immune cells, with few if any non-immune cells expressing the gene in the lesion site. The vast majority of *sema4ab*+ immune cells were microglial cells, confirming scRNAseq results.

***Sema4ab* disruption increases regenerative neurogenesis.**

For a loss-of-function analysis of *sema4ab* in regenerative neurogenesis, we targeted *sema4ab* in somatic mutants and generated a stable germline mutant from haCR-injected fish. The germline mutant introduced a 14 bp insertion in exon 6, leading to a premature stop codon, which is predicted to lead to a truncated protein lacking functionally important domains, such as sema superfamily domains, plexin repeat domains and the intracellular part, containing a sema4F domain (Suppl. Fig.

3A). Somatic mutants (Suppl. Fig. 3B-C) showed no differences in growth compared to control gRNA injected larvae, as measured by body length (Suppl. Fig. 3D), notochord thickness (Suppl. Fig. 3E), or spinal cord thickness (Suppl. Fig. 3F). However, a small decrease in eye size was observed (8 % reduction, Suppl. Fig. 3G) that may be related to compromised photoreceptor maintenance in the absence of Sema4a function (Toyofuku *et al*, 2012). Similarly, germline mutants (Suppl. Fig. 3H,I) showed an unchanged body length compared to wild type fish (Suppl. Fig. 3J) and also a small reduction in eye diameter (9 % reduction; Suppl. Fig. 3K). Adults were viable and fertile. Hence, gross development of larvae was largely unimpaired in the absence of *sema4ab*.

To analyse regenerative neurogenesis, we used 5-Ethynyl-2'-deoxyuridine (EdU) labelling in the *mnx1:GFP* transgenic line that labels motor neurons. Motor neurons represent the main cell type that is newly generated during lesion-induced neurogenesis (Cavone et al., 2021). In unlesioned *sema4ab* haCR-injected larvae (EdU added at 72 hpf, analysis at 96 hpf) few newly generated motor neurons (EdU+/*mnx1*:*GFP*+) were present, similar to control gRNA-injected larvae (Suppl. Fig. 4A-C). This was expected, since *sema4ab* was not detectable in the spinal cord without lesion and shows that *sema4ab* does not have a detectable role in ongoing low-level developmental neurogenesis.

After a lesion at 3 dpf, we observed a ~4-fold lesion-induced increase in numbers of new motor neurons in control gRNA-injected larvae at 48 hpl, as previously reported (Ohnmacht et al., 2016). Remarkably, in *sema4ab* haCR injected larvae, this number was further increased by 85 % compared to lesioned wild type control gRNA-injected larvae (Fig. 3A-C). Similarly, in the lesioned *sema4ab*

germline mutant, the number of new motor neurons almost doubled (95 % increase) compared to lesioned wild type control larvae (Fig. 3D).

For a gain-of-function approach, we generated a construct that leads to overexpression of *sema4ab* and a fluorescent reporter under the control of a heat-shock promotor (*hsp70l:sema4ab-t2a-mCherry,* abbreviated as *hsp70:sema4ab*, Suppl. Fig. 5A). We observed reporter gene expression mainly in muscle cells in heat-shocked lesioned plasmid injected-fish but not in heat-shocked lesioned fish that did not receive plasmid injection (Suppl. Fig. 5B). qRT-PCR in heat-shocked plasmid-injected fish vs heat-shocked controls indicated up to 140 times increased mRNA levels of *sema4ab* that returned to baseline by 24 hours post-induction (Suppl. Fig. 5C-D).

We used multiple (4 hours before lesion, 20 hpl, 36 hpl) heat-shocks in lesioned animals to ensure sufficient levels of over-expressed *sema4ab* mRNA. However, we did not observe significant changes in regenerative neurogenesis as determined by the number of EdU+/*mnx1:GFP*+ cells at 48 hpl (Suppl. Fig. 5E,F). This suggested that the endogenous levels of *sema4ab* expression already had maximal effects on lesion-induced neurogenesis. In addition, this experiment shows that added Sema4ab protein is not toxic for neurogenesis.

Next, we used the same heat-shock regime on *sema4ab* germline mutants, in which functional endogenous *sema4ab* was not present (Fig. 3E). Over-expression completely abolished the increased lesion-induced neurogenesis seen in the mutant (Fig. 3F,G). Given that reporter expression for the overexpressed gene was only detectable in muscle cells, rescuing activity in the spinal cord may be through signalling of soluble Sema4ab from muscle cells. Moreover, this observation

confirms that our *sema4ab* mutant carries a *loss-of-function* mutation and that Sema4ab controls regenerative neurogenesis.

To determine whether the increased number of new motor neurons observed after *sema4ab* disruption was a consequence of enhanced progenitor proliferation or neuronal differentiation, we cumulatively labelled ERGs with EdU (Fig. 3H). This indicated a doubling (97% increase) in Edu-labelled ERGs (*her4.1:GFP*+/EdU+) in *sema4ab* haCR injected lesioned larvae, compared to control-gRNA injected lesioned larvae (Fig. 3I,J).

To directly show a potential increase in neurogenic differentiation of ERGs, we analysed the expression of the proneural transcription factor *neurod1* (Pataskar et al, 2016) by qRT-PCR and HCR-FISH. Lesioned somatic *sema4a* mutants showed a 60% increase in *neurod1* mRNA expression, compared to lesioned control-gRNA injected larvae at 24 hpl in qRT-PCR (Fig. 3K,L), as predicted by scRNAseq (see Fig. 1K). Similarly, the number of *neurod1*-expressing motor neuron progenitor cells (*olig2:EGFP+/neurod1*+) was also increased by 50% in lesioned somatic mutants for *sema4ab*, compared to lesioned control-gRNA injected larvae at 24 hpl (Fig. 3M,N). Hence, in the absence of sema4ab function, the number of EdU label-retaining progenitor cells, the number of neurogenic progenitors, and newly generated neurons were all increased, consistent with *sema4ab* restricting proliferation of neurogenic progenitors.

Disruption of *plxnb1a/b* augments regenerative neurogenesis.

scRNAseq predicted direct signalling of microglia to ERGs via Plexin receptors. To find *plexin* receptor expression in ERGs, we performed HCR-FISH for

two *plxnb1* (*plxnb1a*, *plxnb1b) and plxn2b* (*plxnb2a* and *plxnb2b)* paralogs that code for potential Sema4a receptors (Meda *et al.*, 2012; Rajabinejad *et al*, 2020) in combination with *her4.1:EGFP* transgenic reporter line, in which ERG progenitor cells are fluorescently labelled under the promoter for *her4.1*.

Multiplexed HCR-FISH for *plxnb1a* and *plxnb1b* in the same larvae showed that *plxnb1a* mRNA was detectable at low levels in ERGs in unlesioned animals at 3 dpf, with no detectable increase at 24 hpl. The signal for *plxnb1b* was generally stronger than that for *plxnb1a*, and also did not show detectable changes after lesion (Fig. 4A-C). High magnifications indicated co-expression of *plxnb1a and plxnb1b* in the same ERGs (Fig. 4D). Only very low (*plxnb1a*) or no signal (*plxnb1b*) was detectable outside ERGs in the spinal cord for both *plxnb1a* and *plxnb1b.*

Selective expression of *plxnb1a* and *plxnb1b* in ERGs made these good candidates for receiving a *sema4ab* signal. Therefore, we disrupted *plxnb1a* and *plxnb1b* by haCR injection. While single somatic mutations had no effect (Fig. 4E,F), simultaneous mutation of *plxnb1a* and *plxnb1b* by co-injecting the respective haCRs increased numbers of newly generated motor neurons (EdU+/*mnx1:GFP*+) by 55 % at 48 hpl (Fig. 4G).

plxnb2a was only detectable in cells that were located lateral to ERGs in unlesioned and lesioned animals, whereas *plxnb2b* was expressed in ERGs in unlesioned and lesioned larvae (Suppl. Fig. 6A-D). In the lesion site, signal could be detected that was likely related to non-neuronal cells for both *plxnb2a* and *plxnb2b.* However, disrupting *plxnb2a* and *plxnb2b* with haCRs had no detectable effect on regenerative neurogenesis (Suppl. Fig. 6E-G). Hence, disrupting *plxnb1a/b*, which code for Sema4ab receptors and are selectively expressed in ERGs, partially

replicated the effect of *sema4ab* mutation. This suggests direct microglia to ERG interaction via Sema4ab signalling to Plxnb1a/b.

Disruption of *sema4ab* does not induce major changes in numbers and behaviours of invading cell types

To characterize the influence of *sema4ab* on the lesion site environment *in situ*, we analysed the numbers of cells invading the lesion site with known roles in regeneration, namely neutrophils, BDMs/microglia, and fibroblast-like cells (de Sena-Tomas *et al*, 2024; Tsarouchas *et al.*, 2018; Tsata *et al.*, 2021; Wehner *et al.*, 2017) (Suppl. Fig. 7A). The number of neutrophils (*mpx:GFP*+) in the lesion site was unchanged between lesioned control gRNA-injected larvae and *sema4ab* haCR-injected larvae at 4 hpl (peak of neutrophil invasion) and 24 hpl (peak of regenerative neurogenesis; Suppl. Fig. 7B,C). BDMs/microglia (*mpeg*:*mCherry*+) were moderately reduced in number by 12 % in *sema4ab* haCR injected larvae (Suppl. Fig. 7D) at 24 hpl and the density of fibroblasts (*pdgfrb:GFP*+) remained unchanged in the absence of *sema4ab* function (Suppl. Fig. 7E). Hence, numbers of crucial cell types that are recruited to the lesion site remained largely unchanged, confirming data from scRNAseq.

To determine whether BDMs/microglia behaviour was altered in the absence of *sema4ab*, we analysed phagocytosis of cellular debris, which is one of the major functions of BDMs/microglia (Yu *et al*, 2022). We used acridine orange staining to detect levels of cellular debris as a proxy for efferocytosis. The average fluorescence intensity of acridine orange in the lesion site was comparable between control gRNA-injected larvae and *sema4ab* haCR-injected ones at 24 hpl (Suppl. Fig. 7F).

Similarly, the number of BDMs/microglia with acridine orange-positive inclusions, as indicators of phagocytosed debris, did not show differences in these experimental groups (Suppl. Fig. 7G). This suggests that efferocytosis of debris by BDMs/microglia was not grossly altered in *sema4ab*-deficient BDMs/microglia.

Cytokine signalling is altered in *sema4ab*-deficient animals

scRNAseq indicated a change in the activation state of *sema4ab* deficient microglia, which could lead to an altered cytokine milieu in the injury site. Therefore, we analysed expression levels of *serum amyloid A* (*saa*), an inflammation marker and regulator of cytokine release (Song *et al*, 2009), and major pro- (*il1b, tnfa, il6, il11b*) and anti- (*tgfb1a, tgfb3*) inflammatory cytokines (Woodcock & Morganti-Kossmann, 2013) in the lesion site environment in control gRNA- and *sema4ab* haCR-injected lesioned larvae by qRT-PCR at 4 and 24 hpl (Fig. 5A). *il1b*, *tnfa*, and *il6* did not show any changes at 4 hpl (Fig. 5B), when the immune response was dominated by neutrophils. However, reduced expression levels of *il1b* (by 50 %), *tnfa* (by 75 %), and *il6* (by 65 %), together with those of *il11b* (by 45 %) and *saa* (by 75 %), were detected at 24 hpl (Fig. 5C), when microglia dominated the injury site. At that time point, levels of *tgfb1a* expression were slightly reduced (by 20 %), whereas those of *tgfb3* were more than doubled (120 % increase; Fig. 5D). Overall, qRT-PCR results indicate a shift from a pro-inflammatory to an anti-inflammatory lesion environment in the absence of *sema4ab* function.

To identify possible receptors mediating the effect of Sema4ab on the cytokine environment, we functionally screened additional potential Sema4ab receptors (*havcr1, havcr2, nrp1b, plxnd1*) using haCR disruption and analysis by

qRT-PCR, but none of these replicated the pattern of *sema4ab* disruption in reducing expression *il1b*, *tnfa*, *il11b* and *saa,* or increasing expression *of tgfb3* (Suppl. Fig. 8A-C). This suggests more complex interactions of *sema4ab*+ microglia with cells in the lesion site environment.

To track the cellular sources of the changes in cytokine gene expression observed after *sema4ab* disruption in the lesion site environment, we used transgenic reporter lines and HCR-FISH in histological preparations at 24 hpl (Suppl. Fig. 9A). We found that the number of *il1b:GFP* double-positive BDMs/microglia (*mpeg:mCherry*) remained unchanged, but *il1b:GFP* fluorescence intensity was reduced in *sema4ab* haCR-injected larvae, compared to control gRNA-injected larvae (Suppl. Fig. 9B). The number of *tnfa:EGFP*+ BDMs/microglia, as well as fluorescence intensity for *tnfa:EGFP* was likewise reduced (Suppl. Fig. 9C). In HCR-FISH we found that *saa* labelling intensity was decreased (Suppl. Fig. 9D). This confirms results from qRT-PCR.

Fibroblasts increase *tgfb3* expression in the absence of *sema4ab* function in immune cells

In HCR-FISH, the labelling intensity of *tgfb3* mRNA was generally increased in *sema4ab haCR* injected animals compared to control gRNA injected controls, in agreement with qRT-PCR results (Suppl. Fig. 10A,B). Remarkably, expression of *tgfb3* in fibroblasts (*pdgfrb*+), but not in BDMs or microglia (*mfap4*+) was observed in scRNAseq (Fig. 6A). In agreement with scRNAseq, HCR-FISH co-localisation studies indicated that the *tgfb3* signal was not detectable in *mfap4*:*mCherry*+ cells. Instead, the signal was present mostly in fibroblasts (*pdgfrb:GFP*+; Fig. 6B-D and

Suppl. Fig. 10C). In contrast, *sema4ab* was almost exclusively expressed in immune cells (Suppl. Fig. 10D, cf. Fig. 2: Suppl. Fig. 2). Indeed, quantifying the HCR-FISH signal by masking the *tgfb3* signal with those for BDMs/microglia and fibroblasts in *mfap4:mCherry* and *pdgfrb:GFP* transgenic fish and applying background subtraction (see Material and Methods) indicated that the signal was located in fibroblasts with no detectable signal in BDMs/microglia in either control gRNA- or *sema4ab* haCR-injected lesioned larvae. Moreover, the HCR-FISH signal was increased by 20 % in the fibroblasts (Fig. 6E,F). This suggests a scenario in which microglia signal to fibroblasts in the lesion site during regeneration. Indeed, live observation of BDMs/microglia (*mfap4:mCherry*) and fibroblasts *(pdgfrb:GFP)* from 10 to 25 hpl indicated close physical interactions between these cell types in the injury site, where *mfap4:mCherry*+ cells move along elongated stationary fibroblasts (Fig. 6G,H and supplemental movies 1 and 2). No obvious differences in these cell behaviours were detectable between control gRNA- and *sema4ab* haCR-injected larvae. These data suggest that *mfap4:mCherry*+ cells are in close contact with fibroblasts and may attenuate *tgfb3* expression in fibroblasts in the presence of *sema4ab*.

Fibroblasts promote regenerative neurogenesis via Tgfb3

Tgfb3 signalling has been implicated in neuronal regeneration in the zebrafish retina before (Lee et al., 2020). To test its role in regenerative neurogenesis in the zebrafish spinal cord, we disrupted *tgfb3* genetically in somatic mutants and in a temporally conditional way by pharmacologically blocking Tgfb receptors with the small molecule inhibitor SB431542 (Sun *et al*, 2006). Animals injected with *tgfb3* haCRs showed a 45 % reduction in the number of newly generated motor neurons

(EdU+/*mnx1:GFP*+) after spinal lesion, compared to control gRNA-injected lesioned larvae at 48 hpl (Fig. 7A,B). Similarly, adding SB431542 to the larvae reduced the number of newly generated motor neurons by 45 %, compared to DMSO treated controls, at 48 hpl (Fig. 7C,D). These observations support a promoting role of *tgfb3* for regenerative neurogenesis.

Disruption of *tgfb3* abolishes the effect of *sema4ab* disruption on lesion-induced neurogenesis

To determine whether control of *tgfb3* expression by Sema4ab signalling could explain at least in part the role of *sema4ab* in attenuating regenerative neurogenesis, we disrupted both genes simultaneously by co-injecting *sema4ab* and *tgfb3* haCRs. Disruption of both genes was effective, as indicated by internal RFLP controls for both targets. In these larvae, lesion-induced generation of motor neurons (EdU+/*mnx1:GFP*+) was indistinguishable from that in lesioned control gRNA-injected larvae (Fig. 7E,F). Hence, disruption of *tgfb3* abolished the augmenting effect of *sema4ab* disruption on regenerative neurogenesis. This suggests that control of *tgfb3* expression in fibroblasts is a major mechanism by which *sema4ab*+ microglia control lesion-induced neurogenesis.

Potential *sema4ab* signalling in adult zebrafish and mouse spinal cord injury

To estimate whether the regulation patterns observed here could be conserved across species, we analysed expression of relevant genes in published scRNAseq profiles of the lesioned spinal cord of adult zebrafish (Cigliola *et al.*, 2023)

and adult mice (Xue *et al*, 2024). In adult zebrafish, we found expression of *plxnb1a* and *plxnb1b* in clusters of *her4.3*+ ERGs. We confirmed this by HCR-FISH in cross sections of adult spinal cord, where we found expression in the ventricular layer (Suppl. Fig. 11A-C). In scRNAseq data, *sema4ab* reads were present in microglia (*mfap4*+/*p2ry12*+)*. tgfb3* reads were present in fibroblasts (*pgrfrb*+), but not in immune cells (Suppl. Fig. 11A,B). Similarly, in the sample from the lesioned spinal cord of adult mice, we found selective expression of *Sema4a* in microglia (*P2ry12*+) and *Plxnb1* selectively in potential ventricular progenitors (*Foxj1*+). *Tgfb3* was expressed in fibroblasts (*Pdgfra*+), but not in microglia (Suppl. Fig. 12A,B). This indicated that in the injured adult zebrafish and mouse spinal cords, microglia, fibroblasts and progenitor cells show comparable selective gene expression to what we observe in larval zebrafish. This is consistent with a potentially conserved role of *sema4ab* in spinal cord injury across vertebrates.

***sema4ab* disruption enhances axon regrowth and impairs recovery of swimming function**

We also tested a possible role of *sema4ab* in other modalities of lesion-induced repair, axon regrowth across a spinal lesion site, and recovery of swimming function. To analyse axon regrowth, we assessed the thickness (cross-sectional area) of the neuronal tissue bridge *(tubb5:dsred* line) re-connecting the spinal cord stumps (Wehner *et al.*, 2017) (Suppl. Fig. 13A,B). We observed a 59 % increase in bridge thickness at 48 hpl in lesioned *sema4ab* haCR injected animals, compared to lesioned control gRNA injected animals. This may reflect an inhibitory role of *sema4ab* on axon growth (Yoneyama *et al.*, 2024)*.*

Functional recovery was assessed by measuring the distance swum after a vibration stimulus. This indicated a 40 % reduction in swim distance in lesioned *sema4ab* germline mutants, compared to lesioned wild type animals (Suppl. Fig. 13C,D). Uninjured *sema4ab* germline mutants swam distances that were not different from those of uninjured wild type larvae (Suppl. Fig. 13E,F). These results demonstrate that *sema4ab* is necessary for recovery of swimming function after injury, but not for development of the locomotor system. This phenotype may be related to the role of Sema4A in synapse formation (McDermott *et al*, 2018) (see discussion).

In summary, we propose a model by which Sema4ab from microglia controls neurogenesis directly through Plxnb1a/b on ERGs and indirectly via control of fibroblast-derived Tgfb3 in successful spinal cord regeneration in zebrafish (Fig. 7G). Sema4ab has additional functions in axon regeneration and behavioural recovery.

DISCUSSION

Here we elucidate one of the mechanisms by which regenerative neurogenesis is controlled in a regenerative vertebrate. We show that *sema4ab*, mainly expressed by microglia, influences several cell types. We provide evidence for major functions of *sema4ab* in preventing ERG progenitor over-proliferation directly via Plxn1a/b receptors on ERGs and indirectly, by inhibiting Tgfb3 secretion from fibroblasts.

Even though mostly regeneration-promoting signals are reported for regenerating systems, regulation of growth is indispensable for appropriate repair. Here we show that Sema4ab attenuates regenerative neurogenesis. Some other attenuating signals have also been reported. For example, notch signalling is re-activated after spinal injury in adult zebrafish and attenuates neurogenesis there (Dias *et al*, 2012). In a recent functional screen in the regenerating retina of adult zebrafish, 11 out of 100 regeneration-associated genes have been found to promote and 7 genes to attenuate neuronal regeneration (Emmerich *et al*, 2024). Interestingly, when a stroke is induced or Notch signalling is disrupted, limited neurogenesis can be elicited from ependymal cells in the lateral ventricles of mice, but this leads to depletion of the ependymal cells (Carlen *et al.*, 2009). Hence, attenuating factors are needed to keep the balance between progenitor maintenance and neuronal differentiation in successful regenerative neurogenesis.

Microglia may signal directly to ERGs to attenuate regenerative neurogenesis. Both signal (*sema4ab*) and receptors (*plxnb1a/b*) were expressed with high selectivity in microglia and ERGs, respectively, as indicated by HCR-FISH. However, other cell types may also express low levels of these genes, as suggested by

scRNAseq. Direct signalling from BDMs to ERGs has also been shown for Tnfa, but with a promoting effect on neurogenesis (Cavone *et al.*, 2021). In mammals, microglia also attenuate regenerative neurogenesis in the subventricular zone and hippocampus, which is related to its pro-inflammatory status and may in part explain the poor regenerative outcome there (Matsuda *et al*, 2015; Monje *et al*, 2003; Nath *et al*, 2024).

Sema4ab/Plxn1a/b interactions inhibit proliferation of neural progenitor ERGs, but an additional effect on neuronal differentiation cannot be excluded. Interestingly, in mice, mutating *PlxnB1* and *PlxnB2* together decreased proliferative activity of progenitors and increased their differentiation in the developing cortex, leading to a net effect of reduced neurogenesis (Daviaud *et al.*, 2016). Our re-analysis of mouse scRNAseq data shows that microglia in a spinal injury site in mice selectively express *Sema4A* and spinal progenitors express *Plxnb1*. Hence, Sema4A could also contribute to inhibition of neurogenesis in the lesioned spinal cord of mice. A relatively stronger Sema4A signal in mice than in zebrafish could tip the balance to inhibition of neurogenesis after spinal injury.

In addition to potential direct signalling to ERGs, *sema4ab* also maintains the activation state of microglia. KEGG analysis in microglia clusters highlighted reduced activity of important activation pathways, related to bacterial (Toll-like receptors),viral (RIG-I) response, and initiation of the inflammatory response (Alhamdan *et al.*, 2024; Almeida-da-Silva *et al.*, 2023; Yoneyama *et al.*, 2024) to be changed after disruption of *sema4ab*. In addition, the top down-regulated genes, including activation markers such as *grn1* (Purrahman *et al*, 2023), confirm this change in activation state. In mammals, microglia cells also express Sema4A (Leitner *et al.*, 2015; Meda *et al.*, 2012), including in a spinal lesion site, as analysed here. In agreement with our

findings, injecting exogenous Sema4A into the mouse brain increased activation of microglia there (Chiou *et al*, 2019). Mammalian macrophages also increase *Sema4A* expression when activated by lipopolysaccharides (Meda *et al.*, 2012). Since the activation state of microglia affects cytokine signalling (Raziyeva *et al*, 2021), it was not surprising to detect significant changes in the abundance of different cytokines, in particular a reduction of pro-inflammatory ones, in the absence of *sema4ab.*

Changes in the cytokine milieu are the likely reason that disruption of *sema4ab* leads to global changes in the injury site environment. In scRNAseq, we could see profound changes in gene expression in many cell types, however, their abundance in the injury site did not change, as indicated by scRNAseq and histology. Even debris endocytosis by BDMs/microglia appeared unaltered. Hence, scRNAseq analysis reveals complex signalling interactions in a spinal injury site that depend on microglia activation. This data presents a resource for further analysis of the complex lesion site environment.

Combining scRNAseq with HCR-FISH, we here demonstrate that *sema4ab* signalling regulates expression of *tgfb3*, a crucial signalling molecule, in fibroblast-like cells. We find *tgfb3* expression only in fibroblasts by HCR-FISH and scRNAseq, and *sema4ab* mostly in microglia. Hence, changes of *tgfb3* expression after *sema4ab* disruption are most likely a consequence of perturbed microglia/fibroblast cross-talk. Interestingly, our re-analysis of mouse scRNAseq data shows expression of *Tgfb3* in fibroblasts, but not in microglia, and *Sema4A* in microglia, but not in fibroblasts in a spinal injury site, raising the possibility for similar microglia/fibroblast cross-talk in a non-regenerating system.

How microglia signal to fibroblasts is unclear. We tried to find evidence for direct involvement of *sema4ab* signalling. However, somatic mutations of a number of potential receptors for Sema4ab (*havcr1, havcr2, nrp1b, plxnd1*) (Alto & Terman, 2017; Rajabinejad *et al.*, 2020), could not replicate *tgfb3* upregulation or increased neurogenesis (*plxnb2a, plxnb2b*), or were not detectably expressed by HCR-FISH in non-ERG cells (*plxn1a/b*). It is most likely that fibroblasts react to changed levels of pro-inflammatory cytokines in the injury site. For example, responsiveness of fibroblasts to pro-inflammatory cytokines, such as TNF (Osei *et al*, 2020) and IL-1beta (Pilling *et al*, 2015) is well established and CellChat identified potentially altered *tnfb/tnfrsf1a* receptor/ligand signalling between microglia and fibroblasts in the absence of Sema4ab signalling.

Our data indicate that fibroblast-produced Tgfb3 promotes regenerative neurogenesis. In the adult zebrafish retina, Tgfb3 has been shown to increase pSmad levels in Müller glia, the retinal progenitor cells, and inhibit their injury-induced proliferation (Lee *et al*, 2020). However, there is also evidence for pro-regenerative functions of Tgfb3 in zebrafish retina regeneration, perhaps through indirect effects (Conedera *et al*, 2021; Lenkowski *et al*, 2013; Sharma *et al*, 2020). Exogenous TGFB3 has been shown to be a mitogen for retinal cells of the developing rat *in vitro* (Anchan & Reh, 1995). This indicates context-dependent functions for Tgfb3 in neural development and regeneration.

The altered cytokine environment is also likely to contribute to enhanced axonal regrowth in the absence of *sema4ab* function. Tgfb3 promotes axon regrowth after spinal cord injury in larval zebrafish (Keatinge *et al.*, 2021) and the increased axon regrowth after *sema4ab* disruption in our study fits well with the observed

increase in *tgfb3* expression. Hence, *tgfb3* is a pro-regenerative factor after spinal injury, expression levels of which are controlled by *sema4ab.*

Tgf signalling could act on axon growth via changing the ECM composition. We observed changed expression of ECM-related genes by fibroblasts after *sema4ab* disruption, as indicated by KEGG analysis. Interestingly, Tgfb3 signalling is associated with scar-free wound healing in mammalian models by modifying ECM composition (Shah *et al*, 1995; Weng *et al*, 2020). This may lead to a more favourable spinal ECM environment and could at least in part explain increased axon regeneration in *sema4ab* somatic mutants (Kolb *et al.*, 2023; Tsata *et al.*, 2021; Wehner *et al.*, 2017). Indeed, depleting BDMs/microglia in spinal cord injury in mammals can lead to a more favourable fibrotic response (Zhu *et al*, 2015). However, in another model of depleting BDMs, resident microglia were over-activated (Greenhalgh *et al*, 2018), leading to a worse outcome for recovery. This highlights the complexity of BDMs/microglia cross-talk with fibroblasts and other cell types in potential therapeutic interventions.

The reduced levels of *il1b* expression seen here may also be promoting axon regrowth. Increased levels of *il1b* signalling inhibit axon regeneration in an *irf8* mutant zebrafish, and direct targeting of *il1b* expression (Tsarouchas *et al.*, 2018) or reduction by drug treatment (Oprişoreanu *et al*, 2023) partially rescues axon regrowth in that mutant. This indicates that lower expression levels of *il1b* may be beneficial for axon growth. On the other hand, we also see reduced expression of *tnfa* after *sema4ab* disruption, which does not correlate with the observed increase in axon regrowth. As previously shown, *tnfa*-deficient larvae show reduced axon regrowth, identifying *tnfa* as a pro-regenerative factor (Tsarouchas *et al.*, 2018). This again stresses the complexity of signalling cross-talk in a spinal injury site.

It is interesting that the increased axon bridging observed after *sema4ab* disruption did not translate into improved behavioural recovery. A positive correlation between these read-outs has been observed previously in larval (Tsarouchas *et al.*, 2018; Wehner *et al.*, 2017) and adult (Cigliola *et al.*, 2023; Goldshmit *et al.*, 2012; Huang *et al.*, 2021; Mokalled *et al.*, 2016) lesioned zebrafish. A possible explanation for this apparent discrepancy is that *sema4ab* may have a role in re-establishing synapses, such that disruption of *sema4ab* prevents functionally meaningful re-connections. Indeed, the mammalian homolog Sema4A is important for synapse formation (McDermott *et al.*, 2018), as are other Sema4 family members, such as Sema4D (Raissi *et al*, 2013) and Sema4B (Burkhardt *et al*, 2005).

We conclude that the microglia activation state is crucial for the outcome of a spinal injury. The balance of pro- and anti-regenerative signals from multiple cell types determines the regenerative outcome. Single cell -omics approaches are well placed to unravel such complexity. Here, we identify microglia-derived *sema4ab* as a potentially evolutionarily conserved signal in the regulation of the cytokine milieu and as an inhibitor of regeneration of neurons and axons. Hence, *Sema4a* may present a potential therapeutic target in non-regenerating mammals.

MATERIALS AND METHODS

Animals

All zebrafish lines were raised and kept under standard conditions (Westerfield, 2000). Zebrafish experiments were performed under state of Saxony licenses TVV 36/2021, TVV 45/2018, and holding licenses DD24-5131/364/11, DD24-5131/364/12. For experimental conditions, larvae up to an age of 5 days post-fertilization (dpf) were used of the following lines: wild type (AB); Tg(*mnx1:GFP*)^{ml2tg} , abbreviated as *mnx1:GFP* (Flanagan-Steet *et al*, 2005); Tg(*Xla.Tubb:DsRed*)^{zf1826}, abbreviated as *tubb5:dsred* (Peri & Nusslein-Volhard, 2008); Tg(*her4.1:EGFP*)^{y83Tg}, abbreviated as *her4.1:EGFP*) (Yeo *et al*, 2007); Tg(*olig2:EGFP*), abbreviated as *olig2:EGFP* (Shin *et al*, 2003); Tg(*mpx:GFP*)^{uwm1}, abbreviated as *mpx:GFP* (Renshaw *et al.*, 2006); Tg(*mpeg1.1:mCherry*)^{gl23}, abbreviated as *mpeg:mCherry* (Ellett *et al.*, 2011); Tg(*pdgfrb:Gal4ff*)^{ncv24}; Tg(*UAS:GFP*), abbreviated as *pdgfrb:GFP* (Ando *et al*, 2016); Tg(*il1b:GFP*)^{sh445}, abbreviated as *il1b:GFP* (Nguyen-Chi *et al*, 2014); and Tg(*tnfa:EGFP*)^{ump5Tg}, abbreviated as *tnfa:EGFP* (Nguyen-Chi *et al*, 2015).

Spinal cord lesion

Lesions of larvae were performed as previously described (Ohnmacht et al., 2016). Briefly, at 3 dpf, zebrafish larvae were deeply anaesthetized in E3 medium (Nüsslein-Volhard & Dahm, 2002) containing 0,02 % of MS-222 (Sigma). Larvae were then transferred to an agarose plate. After removal of excess water, larvae were placed in lateral positions. A transection of the entire spinal cord was made

using a 30G syringe needle at the level of the 15th myotome, without injuring the notochord.

Generation of somatic mutants

Somatic mutations were generated mainly following a previous protocol (Keatinge et al., 2021). CRISPR gRNAs were selected using the CRISPRscan website (www.crisprscan.org/gene) webtools. gRNAs were chosen based on the CRISPRScan score (preferentially > 60), and on the availability of a suitable restriction enzyme recognition site (www.snapgene.com) that would be destroyed by the gRNA. Additional criteria were to avoid the first exon and to target functional domains. 1 nL of gRNA mix (1 µl of Tracer (5nM, TRACRRNA05N, Sigma-Aldrich), 1 µl of gRNA (20µM, Sigma-Aldrich), 1 µL of phenol red (P0290, Sigma-Aldrich) and 1 µL of Cas9 (20µM, M0386M, New England Biolabs) was injected into one-cell stage embryos. gRNA efficiency was tested by restriction fragment length polymorphism analysis (RFLP) in a proportion of larvae for each experiment as an internal experimental control (Keatinge et al., 2021). Sequences for gRNAs, primers for RFLPs and RFLPs can be found in Suppl. Table 5 and Suppl. Fig. 14. All experiments conducted with somatic mutants were carried out with a control injected group with a non-targeting gRNA.

Generation of s*ema4ab* germline mutant and *Tg(mfap4:mCherry-CAAX;myl7:mCerulean)* line.

The *sema4ab* mutant stable line was generated by raising somatic mutants as potential founders, as described (Keatinge et al., 2021). The founder selected to

generate the stable line carried a 14 bp insertion in exon 6 that generated a frame shift with a premature stop codon. Sequencing primers were the same as for RFLP.

BDMs/microglia selectively express *mfap4 (Walton et al, 2015).* To generate the *Tg(mfap4:mCherry-CAAX;myl7:mCerulean)* line (abbreviated as *mfap4:mCherry)*, pDEST *mfap4:turquoise2* vector purchased from Addgene (#135218) was used to PCR-amplify the *mfap4* promoter sequence with primers designed to introduce 5´ SacI and 3´ AscI. In parallel, a second plasmid backbone containing *ins:nls-mCerulean; cryaa:mCherry* (previously generated in the group) was digested with SacI/AscI and ligated with mfap4 using SacI/AscI sites *(mfap4:nls-mCerulean; cryaa:mCherry).* Subsequently, mCherry was PCR amplified by using primers designed to introduce 5´ EcoRI and 3´ CAAX box followed by a stop codon and PacI. Then *mfap4:nls-mCerulean; cryaa:mCherry* were digested and ligated using EcoRI/PacI to mCherry-CAAX fragment *(mfap4:mCherry-CAAX; cryaa:mCherry).* Finally, the newly generated *mfap4:mCherry-CAAX; cryaa:mCherry* construct and *ins1.1:ins-sepHLourin; myl7:NLS-mCerulean* construct (previously generated in the lab) were digested with EcoRI/PacI to yield compatible fragments which were ligated together to generate the final construct *(mfap4:mCherry-CAAX;myl7:mCerulean).*The entire construct was flanked with I-Sce sites to facilitate transgenesis and was injected in wild type AB eggs. Several founders were selected based on mCerulean (blue) expression in the heart and mCherry (red) expression in BDMs and the founder with Mendelian segregation in the F1 was selected. Primers are described in Suppl. Table 6.

In situ **hybridization chain reaction (HCR-FISH)**

Larvae were collected in E3 medium and incubated with 0.003 % 1-phenyl 2-thiourea (PTU) at 6 hpf to suppress melanocyte development. Larvae were fixed overnight in 4 % paraformaldehyde (PFA) at 4 ºC and then transferred to 100 % Methanol (MeOH) at -20 °C overnight for permeabilization. The next day, larvae were rehydrated in a graded series of MeOH at room temperature (RT) and subsequent washes in phosphate buffered saline with 0.1 % Tween (PBST). Thereafter, larvae were treated with 500 µL proteinase K (Roche) at a concentration of 30 µg/mL for 45 min at RT, followed by post-fixation in 4 % PFA for 20 min RT and washes with PBST (3 x 5 min). Pre-hybridisation was performed using 500 µL of pre-warmed probe hybridisation buffer (Molecular Instruments (Choi et al., 2018)) for 30 min at 37 °C. The probe sets, which were designed based on the NCBI sequence by Molecular Instruments (Choi et al., 2018), were prepared using 2 pmol of each probe set in 500 µL of pre-warmed hybridisation buffer. Then, buffer was replaced with probe sets and incubated for 16 h at 37 °C. On the following day, samples were washed 4 x 15 min with pre-warmed probe washing buffer (Molecular Instruments) at 37 °C followed by 2 x 5 min in 5x sodium chloride sodium citrate with 0.1 % Tween (SSCT) at RT. Larvae were then treated with 500 µL of room temperature equilibrated amplification buffer (Molecular Instruments, LA, USA) for 30 min at RT. Hairpin RNA preparation was performed following the manufacturer's instructions. Samples were incubated with Hairpin RNAs for 16 h in the dark at RT. Finally, samples were washed for 3 x 30 min in 5 x SSCT at RT and immersed in 70 % glycerol for imaging on a Zeiss LSM980 confocal microscope.

For HCR-FISH on adult animal, fish were killed, perfusion-fixed with 4% para-formaldehyde, and tissue slices of 50 µm thickness were obtained from dissected unlesioned spinal cord using a vibrating blade microtome (VT1200S, Leica, Wetzlar,

Germany), as described (Becker *et al*, 1997). HCR was performed right away following the protocol described above for larvae, with the exception that no permeabilization steps were applied (starting directly with hybridization blocking buffer step).

Combining EdU with motor neuron and ERG labelling

Labelling newly generated motor neurons followed previous protocols (Ohnmacht et al., 2016). Briefly, lesioned and unlesioned larvae were incubated in E3 medium containing 1 % dimethylsulfoxide (DMSO, Sigma-Aldrich, Taufkirchen, Germany) and 1:100 EdU (Thermo-Fisher, Schwerte, Germany) for 48 h. Samples were fixed in 4 % PFA for 3h at RT and permeabilised in 100 % MeoH at -20 ºC for at least overnight. Larvae were then rehydrated, tails were dissected and incubated in proteinase K (Roche, Sigma-Aldrich) for 45 min at RT at a concentration of 10 µg/mL and then postfixed at RT in 4 % PFA for 15 min. Then, larvae were incubated for 20 min at RT in 0.5 % DMSO-PBST and incubated for 2 h at RT with the Click-it Chemistry Edu Alexa 647 kit (Thermo-Fisher, Waltham, USA) as described by the manufacturer. Subsequently, tails were washed in PBST and incubated with blocking buffer solution (2 %BSA, 1 % DMSO, 1 % Triton, 10 % Normal donkey serum, in PBST) for 1 h at RT and then with a chicken anti-GFP antibody, (1:200, Abcam, Cambridge, UK) at 4 ºC for 48 hours. Secondary antibody (alexa-488 anti-chicken, 1:200, Jackson Immuno) incubation took place overnight at 4 ºC. Finally, samples were washed in PBST and transferred to 70 % glycerol in PBST, mounted and imaged. Imaging was performed using a Widefield Axio Observer (Inverted) with ApoTome 2 Unit (Zeiss). Images were analysed using Fiji (Rueden *et al*, 2017;

Schindelin *et al*, 2012). Newly generated motor neurons were counted by assessing the number of double-positive cells for GFP and EdU. Cells were counted manually along the Z-stack, ensuring counting individual cells in single optical sections, in 50 µm windows located at both sides of the injury site (100 µm in total). Experimental conditions were occluded for the analysis. At least two independent experiments were performed. Individual experiments were merged and analysed for statistical significance.

To label proliferating ERGs, we followed the same experimental procedure, imaging and cell counting analysis as for newly generated motor neurons using the ERG reporter line her4.1:EGFP instead of the mnx1:GFP transgenic line.

Generation of Heat shock plasmid and treatment

To create the pTol:sema4ab-T2a-mcherry plasmid, we modified the pTol-hsp70l:mCherry-T2A-atho1b vector (Ezhkova *et al*, 2023). We PCR-amplified the *sema4ab* coding sequence from genomic cDNA and PCR-amplified T2a-mcherry with specific primers (Suppl. Table 7). Then, we performed a simultaneous multiple fragment ligation in the opened backbone vector. The final construct pTol-hsp70l:sema4ab-T2a:mcherry was verified by sequencing, qRT-PCR for over-expression and mCherry fluorescence after injection.

Measurement of axonal regrowth

As an indicator for successful axon regrowth, we determined the extent of continuous labelling of axons across the spinal cord injury site, termed axonal

bridging. As a refinement of previous scoring protocols, we here determined the cross-sectional area of the axonal bridge at its narrowest point. Spinal lesion was performed at 3 dpf as described in larvae that were kept into 0.003 % PTU in E3 water from 72 hpf. The *tubb5:dsred* transgenic line was chosen for this experiment, because neuronal cell bodies and axons are labelled by fluorescence in that line. At 2 hpl, larvae were inspected under a fluorescence stereo-microscope and those larvae with incomplete spinal cord transection and those in which the notochord was inadvertently injured (over-lesioned) were excluded from the experiment. At 48 hpl, larvae were fixed for 1 h in 4 % PFA and afterwards washed 3 x 5 min with PBST. For microscopy, the larvae were mounted in 70 % glycerol in PBST and imaged right away. Images were taken with a Dragonfly Spinning Disk microscope (Andor/Oxford Instruments, Belfast, UK) with a step size of 1 µm with overall 41 optical sections.

The bridge thickness was determined by calculating the cross-sectional area of the neuronal tissue bridge using a custom script in Fiji (Rueden *et al.*, 2017; Schindelin *et al.*, 2012). Measures were taken at the narrowest point of the axonal bridge, automatically detected by using a maximum projection of the z-stack and a binary segmentation. Measurements of three independent experiments were obtained and merged for statistical analysis (see below and figure legends).

Analysis of swimming behaviour

The swimming behaviour was assessed using the ZebraBox (View Point, Lyon, France). As above, under- and over-lesioned larvae were excluded from the experiment at 2 hpl. Subsequently, the larvae were individually arranged in 24-well plates, ensuring representation of all groups on each plate, and kept in the incubator

at 28 ºC until 48 hpl. Larval movements were automatically tracked during three repetitions of the same protocol. The protocol comprised 1 min of rest, a 1 second vibration stimulus (frequency set at 1000 Hz [target power 100]), followed by 59 seconds of no stimulus. The analysis focused on the time-period of 1 minute encompassing the vibration stimulus (including the 1-second stimulus and the subsequent 59 seconds). For each larva, the mean of their swimming distances over the three repeats was computed. Two independent experiments with an average of 30 larvae per condition were performed and the results were merged for statistical analysis (see below and figure legends).

Quantitative RT-PCR

Following spinal cord lesion of 3 dpf, RNA extraction was performed at 1 dpl using the RNeasy Mini Kit (Qiagen) according to the manufacturer's instructions (50 larvae/condition). The injury site was enriched by cutting away rostral and caudal parts from the larvae at positions approximately 3 somites away from the lesion site in either direction. cDNA was synthesized using the iScript™ cDNA Synthesis Kit (BioRad, cat #. 1708890) according to the manufacturer's instructions. qRT-PCR was performed using the SsoAdvanced Universal SYBR Green Supermix kit (BioRad) according to the manufacturer's instructions and run in triplicates on a LightCycler 480SW instrument (Roche). For gene-specific primers see Suppl. Table 8. Each condition was normalized to a housekeeping gene and the experimental group was compared to controls by normalizing to the control group. At least three individual experiments were run. For statistical analysis, a One-Sample T-test was used.

Immune cell counting in whole-mounted larvae.

Larvae were lesioned at 3 dpf and fixed for 1 h in 4 % PFA at different time points. Larvae were washed in PBST and transferred to glycerol (70 % in PBST), mounted and imaged immediately using a Widefield Axio Observer (Inverted) with an ApoTome 2 Unit. Images were analysed using Fiji with the experimental condition unknown to the observer. A window of 200 µm width and 75 µm height was placed in the centre of the injury site of individual images, right above the notochord. Cells were counted manually inside the window along the Z-stack with the experimental condition occluded. At least two individual experiments were carried out and merged.

Acridine Orange labelling

Larvae of the *mpeg:mCherry* line were incubated after a lesion in 1 µg/ml of Acridine Orange (stock solution 10 mg/ml in water) in E3 for 24 h. Then, fish were washed for 3 x 10 min in E3. Larvae were then mounted in 0.5 % agarose in E3 for live imaging on the Dragonfly Spinning Disk microscope (Andor). To estimate total debris, GFP mean intensity was analysed using a 250x100 µm counting window placed in the centre of the injury site. To determine the number of BDMs/microglia that ingested debris, cells positive for both mCherry and GFP were counted in the injury site using same window as before.

Fluorescence intensity/area measurements

Images were analysed with Fiji ImageJ (http:// https://imagej.net/ij/). The region of interest was defined as a rectangle of 400 x 100 µm, centred on the injury site and located right above the notochord. Z-stacks were collapsed in sum intensity projections and then background subtraction was performed before analysing the mean intensity with a custom Fiji macro to automatize the process (Rueden *et al.*, 2017; Schindelin *et al.*, 2012). Mean intensity was represented by normalizing each value to the control average value.

Drug treatment of larvae

SB431542 (Fisher Scientific) was dissolved in DMSO to a stock concentration of 10 mM. The working concentration was 50 µM prepared by a dilution of the stock solution in E3. Larvae were pre-treated for 2 h before injury and then incubated for 48 hpl. Control larvae were treated with DMSO at the same concentration.

Cell dissociation and fluorescence-activated sorting

50 larvae per sample were used. Lesion-site tissue was neriched by dissecting 3 somites rostral and caudal of the injury site and collecting them in cold 1 x PBS. The tissue was dissociated using the Miltenyi Neural Tissue Dissociation Kit (P) with addition of collagenase. In brief, we removed excess 1x PBS and added 950 µL Buffer X. 6 µL of 1/1000 diluted β-mercaptoethanol, 50 µL Enzyme P and 8 µL collagenase (50 mg/mL) were added. The tissue was pipetted 10 times with 1 mL pipette tips and let it rotate at RT (~22-23 °C) for approximately 1 min. In the meantime, 10 µL of Buffer Y and 10 µL of Enzyme A were mixed and added this to

the dissociation mix. Tissue was triturated slowly using fire polished small-orifice glass Pasteur pipette. Each trituration was performed 10 times (6 seconds each) for 1 min and we let the sample rotate for 1 min. This step was repeaed until complete dissociation was achieved. The reaction was stopped after ~14 mins by adding 1 mL of DMEM + FBS (1 %) + Protease Inhibitor (1 x) mix (DFP), followed by centrifugation at + 4 °C at 500 g for 5 mins. The supernatant was removed and the pellet was resuspended in 1 mL of HBSS (Mg2+/Ca+) + Protease Inhibitor (1x) and then passed through a 40 µm filter equilibrated with 200 µL of DFP. Cells were recentrifuged at +4 °C at 500 g for 5 mins. The pellet was resuspended in 300 µL of DFP. Just before cell sorting, 0.5 µL of propidium iodide (100 µg/mL) was added and mixed well by pipetting. Viable, propidium iodide-negative cells were sorted using FACS Aria (BD Biosciences) using a 100 µm nozzle at flow rate 1. 100,000 cells per sample were sorted into BSA coated 1.5 mL Eppendorf tubes with 500 µL of a 0.4 % BSA solution in 1x PBS. The sorted cells volume was around 200 µL and the final concentration of BSA was 0.28 %. One control gRNA and two *sema4ab* gRNA samples were processed by the Dresden Concept Genome Center for cell encapsulation using the 10X Genomic V3.

Droplet encapsulation and single-cell RNA sequencing

Cells were pelleted at 500 g for 5 minutes at 4°C, leaving 20 µL of suspension. Cell viability was assessed with trypan blue, and samples with > 80 % viability were prepared for encapsulation. Single-cell RNA sequencing followed the 10x Genomics (Chromium Single-cell Next GEM 3' Library Kit V3.1) workflow (Zheng *et al*, 2017). In brief, cells were mixed with Reverse Transcription Reagent and

loaded onto a Chromium Single Cell G Chip, targeting 10,000 cells per sample. GEM generation, barcoding, reverse transcription, cDNA amplification, fragmentation, and purification were performed according to the manufacturer's protocol. Libraries were prepared using 25 % of cDNA, quantified, and sequenced on an Illumina NovaSeq 6000 in 100 bp paired-end mode.

Alignment to zebrafish genome

The raw sequencing data were processed with the 'count' command of the Cell Ranger software (v7.1) provided by 10x Genomics. To build the reference, the zebrafish genome (GRCz11) and gene annotation (Ensembl 109), were downloaded from Ensembl (https://www.ensembl.org/). The 'count' command was used to generate count matrices that were further used by Seurat V5 for downstream analyses.

Quality Control and Doublet Removal

For data analyses, cells were kept based on the following conditions: (i) nFeature_RNA >= 200 (number of genes detected per cell), 500 < nCount_RNA < 50000 (number of total reads detected per cell), (ii) percent.mt > 20 % (mitochondrial RNA percentage), (iii) nCount_RNA/nFeature_RNA > 20-fold (an indication of possible doublets), (iv) genes found in fewer than 3 cells were removed from the analyses. Additionally, doublets were determined using scDblFinder V1.18.0 (Germain *et al*, 2021). However, rare cells expressing markers for cell types distinct from the clusters they were allocated to remained and were possible doublets. Cells were removed, if cells other than neurons expressed *elavl3* or *elavl4*, if cells other

than red blood cells expressed *hbbe1.3/hbbe2*, if cells other than muscle, fibroblast-like cells or keratinocytes expressed *col12a1a*, *col12a1b*, or if cells other than muscle or fibroblast-like cells expressed *fgl1,* or *vwde*. Using this method an additional ~5% of cells per sample were removed.

Seurat Data Analyses

After filtering out low-quality cells and doublets, we utilized Seurat V5 for data integration using the CCAIntegration method, following the standard pipeline. A Seurat object was created, and the data were normalized. The top 2,000 variable genes were identified, and the data were scaled using all genes, with nCount_RNA regressed out. Clustering was performed at a resolution of 1.0, yielding 44 distinct clusters (0–43).

After removing low-quality cells and doublets, we utilized Seurat V5 for data integration using CCAIntegration method and followed its standard pipeline. Briefly, a Seurat object was created and the data were normalized. The top 2000 variable genes were identified, and the data were scaled using all genes, with nCount_RNA regressed out. Clustering was performed at resolution 1, yielding 44 distinct clusters (numbered as 0-43).

Finding Marker Genes and annotation of clusters

To identify marker genes (the genes which are specific to a cluster compared to the remaining all other cell types), the FindAllMarkers function from Seurat, using the default options was used. The “Wilcoxon rank sum test”, and p_val_adj (p-value

adjusted) < 0.1 and avg_log2FC >= 0.25 (average log2 fold change) was used for selecting significantly expressed marker genes. Additionally, genes were selected using pct.1 (percentage in the cluster) > 0.2 and ordered, based on their agvg_log2FC in descending order for each cell cluster. Based on the literature, known cell type marker genes were selected from the top ranked genes and used to annotate the main cell types accordingly.

The main cell types were annotated using the following marker genes and the top-ranked genes for each cluster (Cavone *et al.*, 2021; Chen *et al*, 2023; Farrell *et al*, 2018): Ependymoradial Glia (ERG; *fabp7a, sox2*), Enteric Nervous System (ENS; phox2aa, phox2b), Fibroblast-Like Cells (FBL; 3 main clusters, *col12a1a*, *col12a1b*, *pdgfrb*+), Keratinocytes (KC; *pfn1, krt4*), Peridermis (PD; *krt5, krt91, icn2)*, Muscle Cells (MC; m*eox1, mylz3*), Xanthophores (XP; *gch2, aox5)*, Oligodendrocyte (OD; *cldnk, mbpb, mpz*), Kolmer-Agduhr Cells (KA; *npcc, sst1.1*), neutrophils (NP; *lcp1, mpx, lyz*), BDMs/microglia (MM; *lcp1, mfap4, mpeg1.1*), Neurons (NN; *elavl3, elavl4*), Endothelia Cells (EC; *kdrl, cldn5b*), Notochord (NC; s*hha, gas2b*), Red Blood Cells (RBC; *hbbe1.3, hbbe2*) and 5 clusters that remained not annotated (c#28, c#31, c#32, c#34 and c#36).

Differentially Expressed Gene Analysis (DEG)

The FindMarkers function in Seurat was used to determine the differentially expressed genes using “Wilcoxon rank sum test”. p_val_adj < 0.1 and abs(avg log2FC) >= 0.25 were used for selecting significantly expressed genes.

Gene Ontology term and KEGG Analyses

For KEGG (Kyoto Encyclopedia of Genes and Genomes) analyses, GOstats (Falcon & Gentleman, 2007), giving all differentially expressed genes (over- or under-represented) using 0.25 log2FC and p_value < 0.05 as input, were used. Enriched terms were selected with a p-value < 0.05.

Cell-Cell Interaction

CellChat V2.1.0 (Jin *et al.*, 2021) was used for cell-cell interaction and a custom cell-cell interaction as described (Cosacak et al. 2019). In brief, the CellChat Database was modified by adding *sema4ab* as ligand and *plxnb1a, plxnb1b, plxnb2a, plxnb2b, plxnd1, havcr1, havcr2, nrp1a and nrp1b* as its receptors. As there was a pathway named SEMA4, the pathway was renamed to “SEMA4AB” for *sema4ab* and to “SEMA4other” for *sema4c/sema4g*. Then, CellChat objects were created for each data set using normalized data from the integrated Seurat object. Finally, the CellChat objects were merged for comparative analyses.

Cell cycle scoring analysis (for materials and methods)

Cell cycle scoring analysis was performed using the “Cell-Cycling Scoring and Regression” code for Seurat in R (Satija *et al.*, 2015) (https://github.com/satijalab/seurat/blob/HEAD/vignettes/cell_cycle_vignette.Rmd; compiled: 2023-10-31) based in a published gene list (Tirosh *et al*, 2016) (loaded in Seurat) and adapted to zebrafish orthologues manually using ZFIN (Sprague *et al*, 2003).

Time-lapse microscopy

Zebrafish larvae were prepared for time lapse microscopy based on our established protocol (https://ibidi.com/img/cms/support/UP/UP12_Zebrafish_Co_Culture.pdf). Briefly, double transgenic zebrafish larvae (*pdgfrb:GFP*; *mfap4:mCherry*) were lesioned at 3 dpf and anaesthetized with MS-222 (160 mg/L in E3 medium). Low melting point agarose (0.5 %, Biozym Plaque Agarose - Low melting Agarose #840100) was prepared in E3 medium and allowed to cool down to 38 °C before adding MS-222 (final concentration 80 mg/L). Anaesthetized zebrafish larvae were transferred to the agarose and one by one positioned into individual wells of the chambered coverslip. Six larvae were used in total; three control gRNA-injected and three *sema4ab* haCR-injected ones. Microscopy was performed with a Dragonfly Spinning Disk microscope (Andor/Oxford Instruments, Belfast, UK) with a temperature-controlled stage at 28 °C using a 20x objective (20x/0.75 U Plan SApo, Air, DIC, OLYMPUS, Tokyo, Japan). The GFP fluorophore was excited with a 488 nm laser (laser power 20 %) with an exposure time of 180 ms and the mCherry flourophore was excited with a 561 nm laser (laser power 50 %) with an exposure time of 900 ms. We acquired z-stacks of 43 optical sections, with a step size of 1 µm. The interval between single frames of the time-lapse movies was 6 minutes. Time-lapse was performed from 10 hpl until 25 hpl.

Bias mitigation and statistical analysis

The experimental conditions were occluded before manual counting and analysis and processing was automated where possible (e. g. measurements of

axonal regrowth and intensity measurements). For manual counts of EdU+ cells, pilot experiments were performed by two independent experimenters, both showing comparable effect sizes. Experiments were performed in duplicate, if not indicated differently.

Statistical methods to analyse scRNAseq data are described above. For all other experiments, quantitative data was tested for normality using Shapiro-Wilk's W-test. Then, parametric (unpaired Student's t-test or one-way ANOVA) and non-parametric (Mann-Whitney U test or Kruskal-Wallis test) were applied as appropriate. Error bars in figures indicate standard error of the mean (SEM), p-values were represented as asterisks in the figures (*$p < 0.05$; **$p < 0.01$; *** $p < 0.001$) and exact p-values are given in figure legends. To generate graphs and for statistical analysis we used GraphPad Prism 8 (GraphPad Software, Boston, USA).

Figure preparation

Images were adjusted for brightness, contrast and intensity. Drawings were made using CorelDraw X8 (Corel/Alludo, Ottawa, Canada). Figure plates were prepared using CorelDraw X8 (Corel/Alludo, Ottawa, Canada) and Adobe Photoshop 2024 (Adobe, CA, USA).

Data availability

The scRNA-seq raw data of zebrafish larvae generated in this study can be accessed at NCBI GEO accession no. xx. Additional datasets used in this are publicly accessible at NCBI GEO accession numbers; GSE213435 (adult zebrafish),

GSE218584 (adult mouse). The R-source codes for single-cell analyses are available on GitHub; https://github.com/micosacak/scRNA_seq_zebrafish_sema4ab.

ACKNOWLEDGEMENTS

We thank Dr. Stefan Hans for reagents; Drs Hella Hartmann and Ruth Hans for imaging advice; Dr. Daniel Wehner for critical reading; and Dr. Judith Konantz, Marika Fischer, and Silvio Kunadt for fish care. This work was supported by the Light Microscopy Facility, the DRESDEN-concept Genome Center, the Flow Cytometry Facility, and the Zebrafish Facility, all core facilities of the Center for Molecular and Cellular Bioengeneering (CMCB) at the Technische Universität (TU) Dresden. Funding was provided by the BBSRC (BB/T015594/1 to TB, CGB), an Alexander von Humboldt Stiftung Professorship award (to CGB), and TU Dresden core funding (to CGB).

AUTHOR CONTRIBUTIONS (CRediT nomenclature)

ADS: conceptualization, methodology, validation, formal analysis, investigation, writing - original draft, writing - review and editing, visualisation, supervision; MIC: methodology, validation, formal analysis, investigation, writing - review and editing; KH: methodology, validation, formal analysis, investigation, visualization; FK: software; methodology; AMO: investigation; MW: investigation; ÖC: investigation, DZ: investigation; JA: investigation, AB: investigation; formal analysis; AH: resources; NN: resources; CGB: conceptualization, writing - original draft, writing - review and editing, visualisation, supervision, funding acquisition; TB:

conceptualization, writing - original draft, writing - review and editing, visualisation, supervision, funding acquisition.

REFERENCES

Alhamdan F, Bayarsaikhan G, Yuki K (2024) Toll-like receptors and integrins crosstalk. *Front Immunol* 15: 1403764

Almeida-da-Silva CLC, Savio LEB, Coutinho-Silva R, Ojcius DM (2023) The role of NOD-like receptors in innate immunity. *Front Immunol* 14: 1122586

Alto LT, Terman JR (2017) Semaphorins and their Signaling Mechanisms. *Methods in molecular biology (Clifton, NJ)* 1493: 1-25

Anchan RM, Reh TA (1995) Transforming growth factor-beta-3 is mitogenic for rat retinal progenitor cells in vitro. *J Neurobiol* 28: 133-145

Anderson MA, Burda JE, Ren Y, Ao Y, O'Shea TM, Kawaguchi R, Coppola G, Khakh BS, Deming TJ, Sofroniew MV (2016) Astrocyte scar formation aids central nervous system axon regeneration. *Nature* 532: 195-200

Ando K, Fukuhara S, Izumi N, Nakajima H, Fukui H, Kelsh RN, Mochizuki N (2016) Clarification of mural cell coverage of vascular endothelial cells by live imaging of zebrafish. *Development* 143: 1328-1339

Becker CG, Becker T (2015) Neuronal regeneration from ependymo-radial glial cells: cook, little pot, cook! *Dev Cell* 32: 516-527

Becker CG, Lieberoth BC, Morellini F, Feldner J, Becker T, Schachner M (2004) L1.1 is involved in spinal cord regeneration in adult zebrafish. *J Neurosci* 24: 7837-7842

Becker T, Becker CG (2001) Regenerating descending axons preferentially reroute to the gray matter in the presence of a general macrophage/microglial reaction caudal to a spinal transection in adult zebrafish. *J Comp Neurol* 433: 131-147

Becker T, Becker CG (2022) Regenerative neurogenesis: the integration of developmental, physiological and immune signals. *Development* 149

Becker T, Wullimann MF, Becker CG, Bernhardt RR, Schachner M (1997) Axonal regrowth after spinal cord transection in adult zebrafish. *J Comp Neurol* 377: 577-595

Briona LK, Dorsky RI (2014) Radial glial progenitors repair the zebrafish spinal cord following transection. *Exp Neurol* 256: 81-92

Briona LK, Poulain FE, Mosimann C, Dorsky RI (2015) Wnt/beta-catenin signaling is required for radial glial neurogenesis following spinal cord injury. *Dev Biol* 403: 15-21

Burkhardt C, Muller M, Badde A, Garner CC, Gundelfinger ED, Puschel AW (2005) Semaphorin 4B interacts with the post-synaptic density protein PSD-95/SAP90 and is recruited to synapses through a C-terminal PDZ-binding motif. *FEBS Lett* 579: 3821-3828

Carlen M, Meletis K, Goritz C, Darsalia V, Evergren E, Tanigaki K, Amendola M, Barnabe-Heider F, Yeung MS, Naldini L *et al* (2009) Forebrain ependymal cells are Notch-dependent and generate neuroblasts and astrocytes after stroke. *Nat Neurosci* 12: 259-267

Carvalheiro T, Affandi AJ, Malvar-Fernandez B, Dullemond I, Cossu M, Ottria A, Mertens JS, Giovannone B, Bonte-Mineur F, Kok MR *et al* (2019) Induction of Inflammation and Fibrosis by Semaphorin 4A in Systemic Sclerosis. *Arthritis Rheumatol* 71: 1711-1722

Cavone L, McCann T, Drake LK, Aguzzi EA, Oprişoreanu AM, Pedersen E, Sandi S, Selvarajah J, Tsarouchas TM, Wehner D *et al* (2021) A unique macrophage

subpopulation signals directly to progenitor cells to promote regenerative neurogenesis in the zebrafish spinal cord. *Dev Cell* 56: 1617-1630.e1616

Chang W, Pedroni A, Bertuzzi M, Kizil C, Simon A, Ampatzis K (2021) Locomotion dependent neuron-glia interactions control neurogenesis and regeneration in the adult zebrafish spinal cord. *Nat Commun* 12: 4857

Chen F, Kohler M, Cucun G, Takamiya M, Kizil C, Cosacak MI, Rastegar S (2023) sox1a:eGFP transgenic line and single-cell transcriptomics reveal the origin of zebrafish intraspinal serotonergic neurons. *iScience* 26: 107342

Chiou B, Neely E, Kallianpur A, Connor JR (2019) Semaphorin4A causes loss of mature oligodendrocytes and demyelination in vivo. *J Neuroinflammation* 16: 28

Cigliola V, Shoffner A, Lee N, Ou J, Gonzalez TJ, Hoque J, Becker CJ, Han Y, Shen G, Faw TD *et al* (2023) Spinal cord repair is modulated by the neurogenic factor Hb-egf under direction of a regeneration-associated enhancer. *Nat Commun* 14: 4857

Conedera FM, Quintela Pousa AM, Presby DM, Mercader N, Enzmann V, Tschopp M (2021) Diverse Signaling by TGFβ Isoforms in Response to Focal Injury is Associated with Either Retinal Regeneration or Reactive Gliosis. *Cell Mol Neurobiol* 41: 43-62

Daviaud N, Chen K, Huang Y, Friedel RH, Zou H (2016) Impaired cortical neurogenesis in plexin-B1 and -B2 double deletion mutant. *Dev Neurobiol* 76: 882-899

de Sena-Tomas C, Rebola Lameira L, Rebocho da Costa M, Naique Taborda P, Laborde A, Orger M, de Oliveira S, Saude L (2024) Neutrophil immune profile

guides spinal cord regeneration in zebrafish. *Brain Behav Immun* 120: 514-531

Dias DO, Kim H, Holl D, Werne Solnestam B, Lundeberg J, Carlen M, Goritz C, Frisen J (2018) Reducing Pericyte-Derived Scarring Promotes Recovery after Spinal Cord Injury. *Cell* 173: 153-165 e122

Dias TB, Yang YJ, Ogai K, Becker T, Becker CG (2012) Notch signaling controls generation of motor neurons in the lesioned spinal cord of adult zebrafish. *J Neurosci* 32: 3245-3252

Dusart I, Schwab ME (1994) Secondary cell death and the inflammatory reaction after dorsal hemisection of the rat spinal cord. *Eur J Neurosci* 6: 712-724

Ellett F, Pase L, Hayman JW, Andrianopoulos A, Lieschke GJ (2011) mpeg1 promoter transgenes direct macrophage-lineage expression in zebrafish. *Blood* 117: e49-56

Emmerich K, Hageter J, Hoang T, Lyu P, Sharrock AV, Ceisel A, Thierer J, Chunawala Z, Nimmagadda S, Palazzo I *et al* (2024) A large-scale CRISPR screen reveals context-specific genetic regulation of retinal ganglion cell regeneration. *Development* 151

Ezhkova D, Schwarzer S, Spiess S, Geffarth M, Machate A, Zoller D, Stucke J, Alexopoulou D, Lesche M, Dahl A *et al* (2023) Transcriptome analysis reveals an Atoh1b-dependent gene set downstream of Dlx3b/4b during early inner ear development in zebrafish. *Biol Open* 12

Falcon S, Gentleman R (2007) Using GOstats to test gene lists for GO term association. *Bioinformatics* 23: 257-258

Farrell JA, Wang Y, Riesenfeld SJ, Shekhar K, Regev A, Schier AF (2018) Single-cell reconstruction of developmental trajectories during zebrafish embryogenesis. *Science* 360

Flanagan-Steet H, Fox MA, Meyer D, Sanes JR (2005) Neuromuscular synapses can form in vivo by incorporation of initially aneural postsynaptic specializations. *Development* 132: 4471-4481

Francos-Quijorna I, Sánchez-Petidier M, Burnside ER, Badea SR, Torres-Espin A, Marshall L, de Winter F, Verhaagen J, Moreno-Manzano V, Bradbury EJ (2022) Chondroitin sulfate proteoglycans prevent immune cell phenotypic conversion and inflammation resolution via TLR4 in rodent models of spinal cord injury. *Nat Commun* 13: 2933

Germain PL, Lun A, Garcia Meixide C, Macnair W, Robinson MD (2021) Doublet identification in single-cell sequencing data using scDblFinder. *F1000Research* 10: 979

Goldshmit Y, Sztal TE, Jusuf PR, Hall TE, Nguyen-Chi M, Currie PD (2012) Fgf-dependent glial cell bridges facilitate spinal cord regeneration in zebrafish. *J Neurosci* 32: 7477-7492

Greenhalgh AD, Zarruk JG, Healy LM, Baskar Jesudasan SJ, Jhelum P, Salmon CK, Formanek A, Russo MV, Antel JP, McGavern DB *et al* (2018) Peripherally derived macrophages modulate microglial function to reduce inflammation after CNS injury. *PLoS Biol* 16: e2005264

Griffin JM, Bradke F (2020) Therapeutic repair for spinal cord injury: combinatory approaches to address a multifaceted problem. *EMBO Mol Med* 12: e11505

Huang CX, Zhao Y, Mao J, Wang Z, Xu L, Cheng J, Guan NN, Song J (2021) An injury-induced serotonergic neuron subpopulation contributes to axon

regrowth and function restoration after spinal cord injury in zebrafish. *Nat Commun* 12: 7093

Jin S, Guerrero-Juarez CF, Zhang L, Chang I, Ramos R, Kuan CH, Myung P, Plikus MV, Nie Q (2021) Inference and analysis of cell-cell communication using CellChat. *Nat Commun* 12: 1088

Keatinge M, Tsarouchas TM, Munir T, Porter NJ, Larraz J, Gianni D, Tsai HH, Becker CG, Lyons DA, Becker T (2021) CRISPR gRNA phenotypic screening in zebrafish reveals pro-regenerative genes in spinal cord injury. *PLoS Genet* 17: e1009515

Kolb J, Tsata V, John N, Kim K, Mockel C, Rosso G, Kurbel V, Parmar A, Sharma G, Karandasheva K *et al* (2023) Small leucine-rich proteoglycans inhibit CNS regeneration by modifying the structural and mechanical properties of the lesion environment. *Nat Commun* 14: 6814

Kyritsis N, Kizil C, Zocher S, Kroehne V, Kaslin J, Freudenreich D, Iltzsche A, Brand M (2012) Acute inflammation initiates the regenerative response in the adult zebrafish brain. *Science* 338: 1353-1356

Lee MS, Wan J, Goldman D (2020) Tgfb3 collaborates with PP2A and notch signaling pathways to inhibit retina regeneration. *eLife* 9

Leitner DF, Todorich B, Zhang X, Connor JR (2015) Semaphorin4A Is Cytotoxic to Oligodendrocytes and Is Elevated in Microglia and Multiple Sclerosis. *ASN Neuro* 7

Lenkowski JR, Qin Z, Sifuentes CJ, Thummel R, Soto CM, Moens CB, Raymond PA (2013) Retinal regeneration in adult zebrafish requires regulation of TGFbeta signaling. *Glia* 61: 1687-1697

Liu XZ, Xu XM, Hu R, Du C, Zhang SX, McDonald JW, Dong HX, Wu YJ, Fan GS, Jacquin MF *et al* (1997) Neuronal and glial apoptosis after traumatic spinal cord injury. *J Neurosci* 17: 5395-5406

Llorens-Bobadilla E, Chell JM, Le Merre P, Wu Y, Zamboni M, Bergenstråhle J, Stenudd M, Sopova E, Lundeberg J, Shupliakov O *et al* (2020) A latent lineage potential in resident neural stem cells enables spinal cord repair. *Science* 370: DOI: 10.1126/science.abb8795

Matsuda T, Murao N, Katano Y, Juliandi B, Kohyama J, Akira S, Kawai T, Nakashima K (2015) TLR9 signalling in microglia attenuates seizure-induced aberrant neurogenesis in the adult hippocampus. *Nat Commun* 6: 6514

McDermott JE, Goldblatt D, Paradis S (2018) Class 4 Semaphorins and Plexin-B receptors regulate GABAergic and glutamatergic synapse development in the mammalian hippocampus. *Mol Cell Neurosci* 92: 50-66

Meda C, Molla F, De Pizzol M, Regano D, Maione F, Capano S, Locati M, Mantovani A, Latini R, Bussolino F *et al* (2012) Semaphorin 4A exerts a proangiogenic effect by enhancing vascular endothelial growth factor-A expression in macrophages. *J Immunol* 188: 4081-4092

Mokalled MH, Patra C, Dickson AL, Endo T, Stainier DY, Poss KD (2016) Injury-induced ctgfa directs glial bridging and spinal cord regeneration in zebrafish. *Science* 354: 630-634

Monje ML, Toda H, Palmer TD (2003) Inflammatory blockade restores adult hippocampal neurogenesis. *Science* 302: 1760-1765

Nath S, Martinez Santamaria JC, Chu YH, Choi JS, Conforti P, Lin JD, Sankowski R, Amann L, Galanis C, Wu K *et al* (2024) Interaction between subventricular

zone microglia and neural stem cells impacts the neurogenic response in a mouse model of cortical ischemic stroke. *Nat Commun* 15: 9095

Nguyen-Chi M, Laplace-Builhe B, Travnickova J, Luz-Crawford P, Tejedor G, Phan QT, Duroux-Richard I, Levraud JP, Kissa K, Lutfalla G *et al* (2015) Identification of polarized macrophage subsets in zebrafish. *eLife* 4: e07288

Nguyen-Chi M, Phan QT, Gonzalez C, Dubremetz JF, Levraud JP, Lutfalla G (2014) Transient infection of the zebrafish notochord with E. coli induces chronic inflammation. *Dis Model Mech* 7: 871-882

Nüsslein-Volhard C, Dahm R (2002) *Zebrafish: a practical approach*. Oxford University Press, Oxford, UK

Ohnmacht J, Yang Y, Maurer GW, Barreiro-Iglesias A, Tsarouchas TM, Wehner D, Sieger D, Becker CG, Becker T (2016) Spinal motor neurons are regenerated after mechanical lesion and genetic ablation in larval zebrafish. *Development* 143: 1464-1474

Oprişoreanu AM, Ryan F, Richmond C, Dzekhtsiarova Y, Carragher NO, Becker T, David S, Becker CG (2023) Drug screening in zebrafish larvae reveals inflammation-related modulators of secondary damage after spinal cord injury in mice. *Theranostics* https://www.thno.org/v13p2531

Osei ET, L BM-G, Hsieh A, Warner SM, Al-Fouadi M, Wang M, Cole DJ, Maksym GN, T SH, Timens W *et al* (2020) Epithelial-interleukin-1 inhibits collagen formation by airway fibroblasts: Implications for asthma. *Sci Rep* 10: 8721

Pataskar A, Jung J, Smialowski P, Noack F, Calegari F, Straub T, Tiwari VK (2016) NeuroD1 reprograms chromatin and transcription factor landscapes to induce the neuronal program. *EMBO J* 35: 24-45

Peri F, Nusslein-Volhard C (2008) Live imaging of neuronal degradation by microglia reveals a role for v0-ATPase a1 in phagosomal fusion in vivo. *Cell* 133: 916-927

Pilling D, Vakil V, Cox N, Gomer RH (2015) TNF-alpha-stimulated fibroblasts secrete lumican to promote fibrocyte differentiation. *Proc Natl Acad Sci U S A* 112: 11929-11934

Purrahman D, Shojaeian A, Poniatowski LA, Piechowski-Jozwiak B, Mahmoudian-Sani MR (2023) The Role of Progranulin (PGRN) in the Pathogenesis of Ischemic Stroke. *Cell Mol Neurobiol* 43: 3435-3447

Raissi AJ, Staudenmaier EK, David S, Hu L, Paradis S (2013) Sema4D localizes to synapses and regulates GABAergic synapse development as a membrane-bound molecule in the mammalian hippocampus. *Mol Cell Neurosci* 57: 23-32

Rajabinejad M, Asadi G, Ranjbar S, Afshar Hezarkhani L, Salari F, Gorgin Karaji A, Rezaiemanesh A (2020) Semaphorin 4A, 4C, and 4D: Function comparison in the autoimmunity, allergy, and cancer. *Gene* 746: 144637

Raziyeva K, Kim Y, Zharkinbekov Z, Kassymbek K, Jimi S, Saparov A (2021) Immunology of Acute and Chronic Wound Healing. *Biomolecules* 11

Reimer MM, Sorensen I, Kuscha V, Frank RE, Liu C, Becker CG, Becker T (2008) Motor neuron regeneration in adult zebrafish. *J Neurosci* 28: 8510-8516

Renshaw SA, Loynes CA, Trushell DM, Elworthy S, Ingham PW, Whyte MK (2006) A transgenic zebrafish model of neutrophilic inflammation. *Blood* 108: 3976-3978

Rueden CT, Schindelin J, Hiner MC, DeZonia BE, Walter AE, Arena ET, Eliceiri KW (2017) ImageJ2: ImageJ for the next generation of scientific image data. *BMC Bioinformatics* 18: 529

Satija R, Farrell JA, Gennert D, Schier AF, Regev A (2015) Spatial reconstruction of single-cell gene expression data. *Nat Biotechnol* 33: 495-502

Schindelin J, Arganda-Carreras I, Frise E, Kaynig V, Longair M, Pietzsch T, Preibisch S, Rueden C, Saalfeld S, Schmid B *et al* (2012) Fiji: an open-source platform for biological-image analysis. *Nat Methods* 9: 676-682

Shah M, Foreman DM, Ferguson MW (1995) Neutralisation of TGF-beta 1 and TGF-beta 2 or exogenous addition of TGF-beta 3 to cutaneous rat wounds reduces scarring. *J Cell Sci* 108 (Pt 3): 985-1002

Sharma P, Gupta S, Chaudhary M, Mitra S, Chawla B, Khursheed MA, Saran NK, Ramachandran R (2020) Biphasic Role of Tgf-β Signaling during Müller Glia Reprogramming and Retinal Regeneration in Zebrafish. *iScience* 23: 100817

Sharp KG, Yee KM, Steward O (2014) A re-assessment of long distance growth and connectivity of neural stem cells after severe spinal cord injury. *Exp Neurol* 257: 186-204

Shihabuddin LS, Horner PJ, Ray J, Gage FH (2000) Adult spinal cord stem cells generate neurons after transplantation in the adult dentate gyrus. *J Neurosci* 20: 8727-8735

Shin J, Park HC, Topczewska JM, Mawdsley DJ, Appel B (2003) Neural cell fate analysis in zebrafish using olig2 BAC transgenics. *Methods Cell Sci* 25: 7-14

Song C, Hsu K, Yamen E, Yan W, Fock J, Witting PK, Geczy CL, Freedman SB (2009) Serum amyloid A induction of cytokines in monocytes/macrophages and lymphocytes. *Atherosclerosis* 207: 374-383

Sprague J, Clements D, Conlin T, Edwards P, Frazer K, Schaper K, Segerdell E, Song P, Sprunger B, Westerfield M (2003) The Zebrafish Information Network

(ZFIN): the zebrafish model organism database. *Nucleic Acids Res* 31: 241-243

Stenudd M, Sabelström H, Llorens-Bobadilla E, Zamboni M, Blom H, Brismar H, Zhang S, Basak O, Clevers H, Göritz C *et al* (2022) Identification of a discrete subpopulation of spinal cord ependymal cells with neural stem cell properties. *Cell Rep* 38: 110440

Sun H, Kawahara Y, Ito K, Kanazawa I, Kwak S (2006) Slow and selective death of spinal motor neurons in vivo by intrathecal infusion of kainic acid: implications for AMPA receptor-mediated excitotoxicity in ALS. *J Neurochem* 98: 782-791

Tirosh I, Izar B, Prakadan SM, Wadsworth MH, 2nd, Treacy D, Trombetta JJ, Rotem A, Rodman C, Lian C, Murphy G *et al* (2016) Dissecting the multicellular ecosystem of metastatic melanoma by single-cell RNA-seq. *Science* 352: 189-196

Toyofuku T, Nojima S, Ishikawa T, Takamatsu H, Tsujimura T, Uemura A, Matsuda J, Seki T, Kumanogoh A (2012) Endosomal sorting by Semaphorin 4A in retinal pigment epithelium supports photoreceptor survival. *Genes Dev* 26: 816-829

Tran AP, Warren PM, Silver J (2018) The Biology of Regeneration Failure and Success After Spinal Cord Injury. *Physiol Rev* 98: 881-917

Tsarouchas TM, Wehner D, Cavone L, Munir T, Keatinge M, Lambertus M, Underhill A, Barrett T, Kassapis E, Ogryzko N *et al* (2018) Dynamic control of proinflammatory cytokines Il-1β and Tnf-α by macrophages in zebrafish spinal cord regeneration. *Nat Commun* 9: 4670

Tsata V, Möllmert S, Schweitzer C, Kolb J, Möckel C, Böhm B, Rosso G, Lange C, Lesche M, Hammer J *et al* (2021) A switch in pdgfrb(+) cell-derived ECM

composition prevents inhibitory scarring and promotes axon regeneration in the zebrafish spinal cord. *Dev Cell* 56: 509-524.e509

Tsata V, Wehner D (2021) Know How to Regrow-Axon Regeneration in the Zebrafish Spinal Cord. *Cells* 10

Vandestadt C, Vanwalleghem GC, Khabooshan MA, Douek AM, Castillo HA, Li M, Schulze K, Don E, Stamatis SA, Ratnadiwakara M *et al* (2021) RNA-induced inflammation and migration of precursor neurons initiates neuronal circuit regeneration in zebrafish. *Dev Cell* 56: 2364-2380.e2368

Walton EM, Cronan MR, Beerman RW, Tobin DM (2015) The Macrophage-Specific Promoter mfap4 Allows Live, Long-Term Analysis of Macrophage Behavior during Mycobacterial Infection in Zebrafish. *PLoS One* 10: e0138949

Wehner D, Tsarouchas TM, Michael A, Haase C, Weidinger G, Reimer MM, Becker T, Becker CG (2017) Wnt signaling controls pro-regenerative Collagen XII in functional spinal cord regeneration in zebrafish. *Nat Commun* 8: 126

Weng L, Funderburgh JL, Khandaker I, Geary ML, Yang T, Basu R, Funderburgh ML, Du Y, Yam GH (2020) The anti-scarring effect of corneal stromal stem cell therapy is mediated by transforming growth factor beta3. *Eye Vis (Lond)* 7: 52

Westerfield M (2000) *The zebrafish book: a guide for the laboratory use of zebrafish (Danio rerio)*. University of Oregon Press, Eugene

Woodcock T, Morganti-Kossmann MC (2013) The role of markers of inflammation in traumatic brain injury. *Front Neurol* 4: 18

Xue X, Wu X, Fan Y, Han S, Zhang H, Sun Y, Yin Y, Yin M, Chen B, Sun Z *et al* (2024) Heterogeneous fibroblasts contribute to fibrotic scar formation after spinal cord injury in mice and monkeys. *Nat Commun* 15: 6321

Yeo SY, Kim M, Kim HS, Huh TL, Chitnis AB (2007) Fluorescent protein expression driven by her4 regulatory elements reveals the spatiotemporal pattern of Notch signaling in the nervous system of zebrafish embryos. *Dev Biol* 301: 555-567

Yoneyama M, Kato H, Fujita T (2024) Physiological functions of RIG-I-like receptors. *Immunity* 57: 731-751

Yu F, Wang Y, Stetler AR, Leak RK, Hu X, Chen J (2022) Phagocytic microglia and macrophages in brain injury and repair. *CNS Neurosci Ther* 28: 1279-1293

Zambusi A, Novoselc KT, Hutten S, Kalpazidou S, Koupourtidou C, Schieweck R, Aschenbroich S, Silva L, Yazgili AS, van Bebber F *et al* (2022) TDP-43 condensates and lipid droplets regulate the reactivity of microglia and regeneration after traumatic brain injury. *Nat Neurosci* 25: 1608-1625

Zheng GX, Terry JM, Belgrader P, Ryvkin P, Bent ZW, Wilson R, Ziraldo SB, Wheeler TD, McDermott GP, Zhu J *et al* (2017) Massively parallel digital transcriptional profiling of single cells. *Nat Commun* 8: 14049

Zhu Y, Soderblom C, Krishnan V, Ashbaugh J, Bethea JR, Lee JK (2015) Hematogenous macrophage depletion reduces the fibrotic scar and increases axonal growth after spinal cord injury. *Neurobiol Dis* 74: 114-125

FIGURES

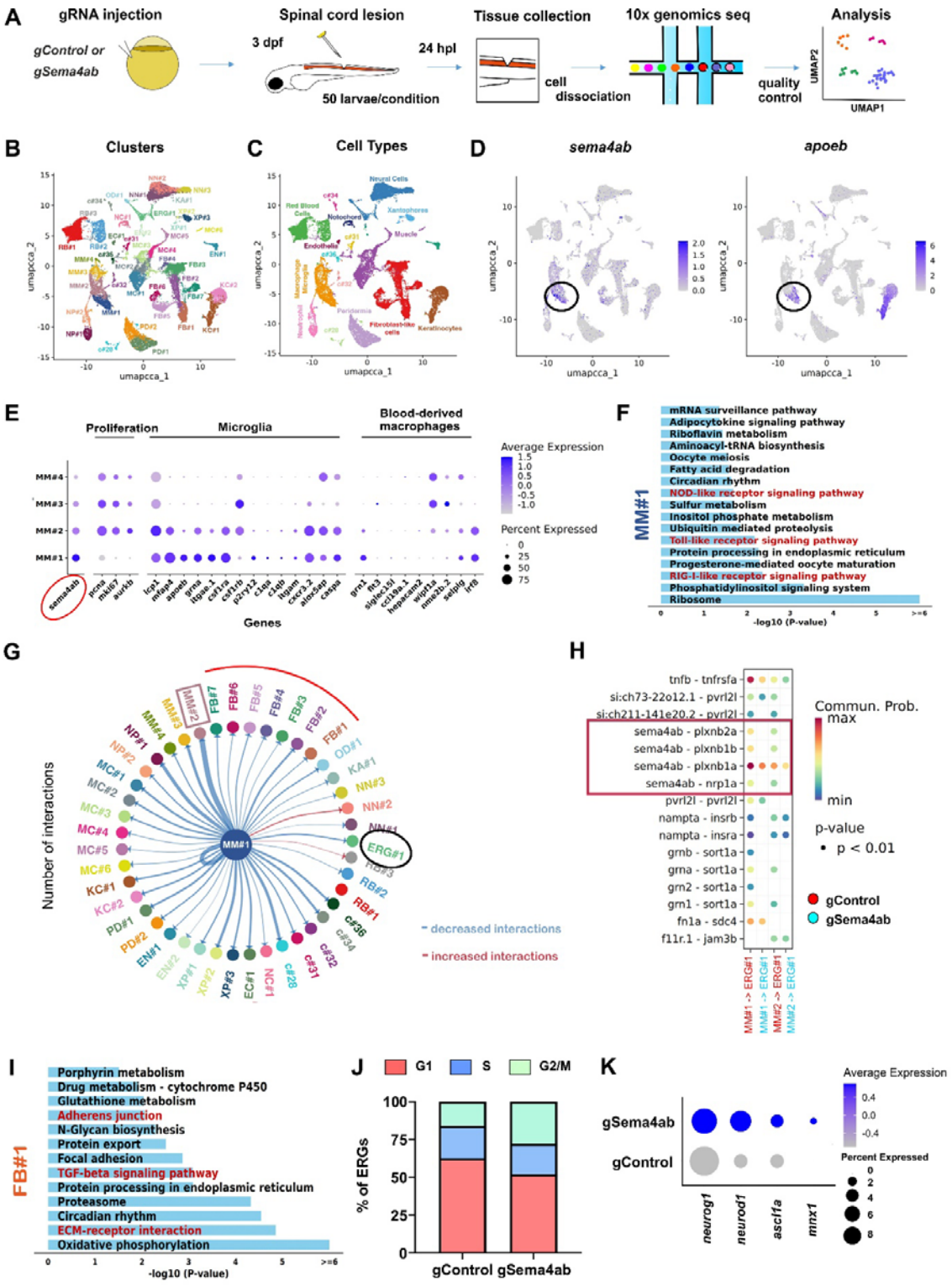
A
gRNA injection
gControl or
gSema4ab
Spinal cord lesion
3 dpf
24 hpl
50 larvae/condition
Tissue collection
cell
dissociation
10x genomics seq
quality
control
Analysis
UMAP2
UMAP1
B
Clusters
C
Cell Types
D
sema4ab
apoeb
umapcca_1
umapcca_2
E
Proliferation
Microglia
Blood-derived
macrophages
MM#4
MM#3
MM#2
MM#1
Genes
Average Expression
Percent Expressed
F
MM#1
mRNA surveillance pathway
Adipocytokine signaling pathway
Riboflavin metabolism
Aminoacyl-tRNA biosynthesis
Oocyte meiosis
Fatty acid degradation
Circadian rhythm
NOD-like receptor signaling pathway
Sulfur metabolism
Inositol phosphate metabolism
Ubiquitin mediated proteolysis
Toll-like receptor signaling pathway
Protein processing in endoplasmic reticulum
Progesterone-mediated oocyte maturation
RIG-I-like receptor signaling pathway
Phosphatidylinositol signaling system
Ribosome
-log10 (P-value)
G
Number of interactions
MM#1
ERG#1
decreased interactions
increased interactions
H
tnfb - tnfrsfa
si:ch73-22o12.1 - pvrl2l
si:ch211-141e20.2 - pvrl2l
sema4ab - plxnb2a
sema4ab - plxnb1b
sema4ab - plxnb1a
sema4ab - nrp1a
pvrl2l - pvrl2l
nampta - insrb
nampta - insra
grnb - sort1a
grna - sort1a
grn2 - sort1a
grn1 - sort1a
fn1a - sdc4
f11r.1 - jam3b
MM#1 -> ERG#1
MM#1 -> ERG#1
MM#2 -> ERG#1
MM#2 -> ERG#1
Commun. Prob.
max
min
p-value
p < 0.01
gControl
gSema4ab
I
FB#1
Porphyrin metabolism
Drug metabolism - cytochrome P450
Glutathione metabolism
Adherens junction
N-Glycan biosynthesis
Protein export
Focal adhesion
TGF-beta signaling pathway
Protein processing in endoplasmic reticulum
Proteasome
Circadian rhythm
ECM-receptor interaction
Oxidative phosphorylation
-log10 (P-value)
J
G1
S
G2/M
% of ERGs
gControl
gSema4ab
K
Average Expression
gSema4ab
gControl
neurog1
neurod1
ascl1a
mnx1
Percent Expressed

Figure 1. scRNAseq indicates changes in cell interactions between microglia and other cell types after sema4ab ablation. (A) Schematic showing the experimental design for scRNAseq. **(B, C)** Cluster analysis identifies 44 cell clusters (B) that represent the main expected cell types (C) in the injury site at 24 hpl. **(D)** Feature plots for *sema4ab* and *apoeb* (microglia) showing overlap (black circle). **(E)** A dot plot of the four BDMs/microglia clusters showing that *sema4ab*-enriched clusters align with the expression of microglia marker genes. **(F)** KEGG analysis of the main cluster that expresses *sema4ab* (MM#1) shows changes in immune activation pathways (highlighted in red). **(G)** CellChat analysis for MM#1 shows interactions with all cell types and a general decrease in these interactions (blue lines) when *sema4ab* is disrupted. Interactions of MM#1 with ERGs (circle), fibroblasts (red curved line) and MM#2 (box) are highlighted. **(H)** Dot plot illustrating the communication probabilities of all ligand-receptor interactions identified by CellChat between MM#1 and MM#2 and ERGs. Potential direct interactions of *sema4ab* are highlighted (red box). **(I)** KEGG analysis of the signalling pathways most affected by *sema4ab* disruption in fibroblast-like cell cluster FB#1 is shown. *tgfb* signalling and ECM receptor interactions are highlighted in red. **(J)** Graph shows the proportions of ERGs in each cell cycle phase in control gRNA-injected larvae and *sema4ab* gRNA-injected larvae. Note that the proportion of cells in M/G2 phase is increased in *sema4ab* somatic mutants (gControl: 16% vs gSema4ab: 28%). **(K)** Dot plot showing an increase in differentiation marker gene expression in ERG progenitors when *sema4ab* is disrupted.

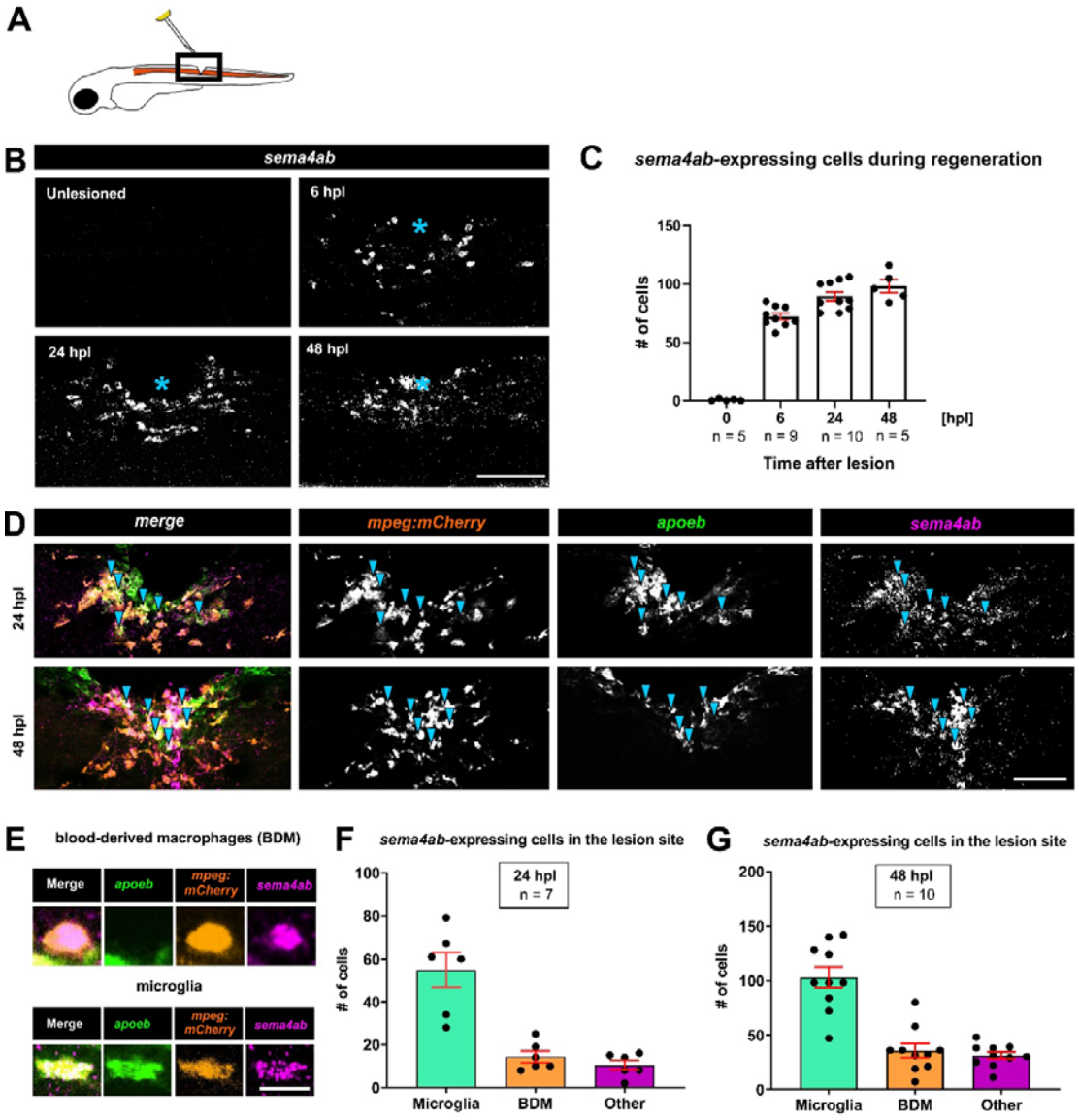
A
B
sema4ab
Unlesioned
6 hpl
24 hpl
48 hpl
C
sema4ab-expressing cells during regeneration
# of cells
150
100
50
0
0
6
24
48
[hpl]
n = 5
n = 9
n = 10
n = 5
Time after lesion
D
merge
mpeg:mCherry
apoeb
sema4ab
24 hpl
48 hpl
E
blood-derived macrophages (BDM)
Merge
apoeb
mpeg: mCherry
sema4ab
microglia
F
sema4ab-expressing cells in the lesion site
24 hpl
n = 7
# of cells
Microglia
BDM
Other
G
sema4ab-expressing cells in the lesion site
48 hpl
n = 10
# of cells
Microglia
BDM
Other

Fig. 2. *Sema4ab* is expressed mainly in microglia in the spinal injury site. (A) Schematic of a zebrafish larva indicating the lateral view of the spinal injury site shown throughout the article, unless specified differently. **(B,C)** A time-course analysis of HCR-FISH indicates increased expression of *sema4ab* during spinal cord repair (B), quantified in (C). **(D)** Triple-multiplexed HCR-FISH at 24 hpl shows co-localisation of *sema4ab, mpeg:mCherry, and apoeb* at 24 hpl and 48 hpl (blue arrowheads). **(E)** High magnifications of *apoeb/mpeg:mCherry/sema4ab* double- and triple-positive cells used for cell counting to differentiate blood-derived macrophages (BDMs; *apoeb-*) from microglia (*apoeb+*). **(F-G)** Quantifications at 24 and 48 hpl show that most *sema4ab+* cells are microglial cells (*apoeb+/mpeg:mCherry+*). Error bars show SEM. Asterisks indicate the injury site. Scale bars: 100 µm (B, D), 15 µm (E).

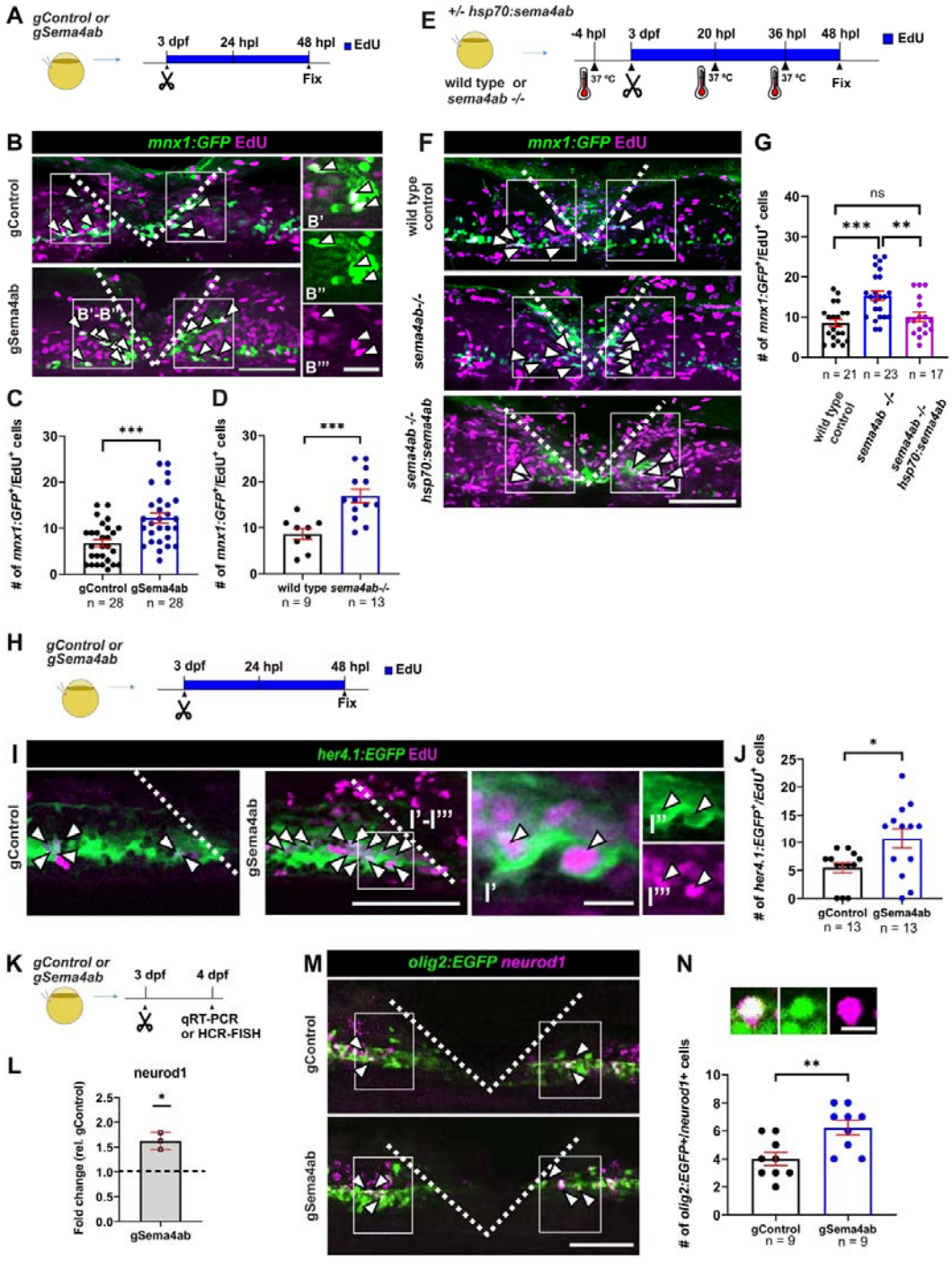
A
gControl or gSema4ab
3 dpf
24 hpl
48 hpl
EdU
Fix
E
+/- hsp70:sema4ab
wild type or sema4ab -/-
-4 hpl
3 dpf
20 hpl
36 hpl
48 hpl
EdU
37 °C
Fix
B
mnx1:GFP EdU
gControl
gSema4ab
B'-B'''
B'
B''
B'''
C
# of mnx1:GFP+/EdU+ cells
***
gControl
gSema4ab
n = 28
n = 28
D
# of mnx1:GFP+/EdU+ cells
***
wild type
sema4ab-/-
n = 9
n = 13
F
mnx1:GFP EdU
wild type control
sema4ab-/-
sema4ab -/- hsp70:sema4ab
G
# of mnx1:GFP+/EdU+ cells
ns
***
**
n = 21
n = 23
n = 17
wild type control
sema4ab -/-
sema4ab -/- hsp70:sema4ab
H
gControl or gSema4ab
3 dpf
24 hpl
48 hpl
EdU
Fix
I
her4.1:EGFP EdU
gControl
gSema4ab
I'-I'''
I'
I''
I'''
J
# of her4.1:EGFP+/EdU+ cells
*
gControl
gSema4ab
n = 13
n = 13
K
gControl or gSema4ab
3 dpf
4 dpf
qRT-PCR or HCR-FISH
L
neurod1
Fold change (rel. gControl)
*
gSema4ab
M
olig2:EGFP neurod1
gControl
gSema4ab
N
# of olig2:EGFP+/neurod1+ cells
**
gControl
gSema4ab
n = 9
n = 9

Fig. 3. *Sema4ab* loss of function increases regenerative neurogenesis. Photomicrographs are oriented as in Fig. 1. Arrowheads indicate double-labelled cells; dotted lines indicate the injury zone; white boxes indicate regions of analysis. **(A-C)** (A) shows schematic of the experiment. Lesion-induced generation of motor neurons (*mnx1:GFP*+/EdU+) is increased in somatic mutants for *sema4ab* (arrowheads in B and B'-B'''), quantified in (C) (gControl: 6.9 cells per larva ± 0.8; gSema4ab: 12.9 cells per larva ± 1.1; Mann-Whitney U-test: p = 0.0001). (**D)** Quantifications in germline mutants for *sema4ab* show a similar increase in generation of motor neurons after lesion (wild type: 8.7 cells per larva ± 1.2; sema4ab-/-: 16.9 cells per larva ± 1.5; Mann-Whitney U-test: p = 0.0001). Lesion and EdU application paradigm was as for (A-C). **(E-G)** E shows a schematic of the experiments. Overexpression of *sema4ab* driven by a heat-shock promotor (*hsp70:sema4ab*) reduces over-production of motor neurons (*mnx1:GFP*+/EdU+) back to wild type levels in *sema4ab* germline mutants, imaged in (F) and quantified in (G); (wild type: 8.5 cells per larva ± 0.95; *sema4ab* -/-: 15.4 cells per larva ± 1.2; *sema4ab*-/- + *hsp70:sema4ab*: 10 cells per larva ± 1.15; Kruskal-Wallis test: p = 0.0004; Dunn's multiple comparisons test: ***p = 0.006; n.s > 0.9999, **p = 0.0168). All conditions shown were heat-shocked. **(H-J)** (H) shows a schematic of the experiment. Lesion-induced generation of ERGs (*her4.1:EGFP*+/*EdU*+) is increased in somatic mutants for *sema4ab* (gControl: 5.4 cells per larva ± 0.9; gSema4ab: 10.77 cells per larva ± 1.8; Mann-Whitney U-test: p = 0.0219). **(K-N)** (K) shows a schematic of the experimental design. (L) Expression of *neurod1* is increased in qRT-PCR (1.62-fold increase) after *sema4ab* mutation. (M) An example of a double-labelled cell is shown. The number of *neurod1*-labelled motor neuron progenitor cells (*olig2:EGFP+/neurod1+*) is increased after *sema4ab* disruption (gControl: 4.0 cells

per larvae ± 0.4714; gSema4ab: 6.2 ± 0.5212 cells per larvae; Unpaired t-test: p= 0.0060). Error bars show SEM. Scale bars: 50 µm (B, F, I, M), 15 µm (B'-B'''), 10 µm (N).

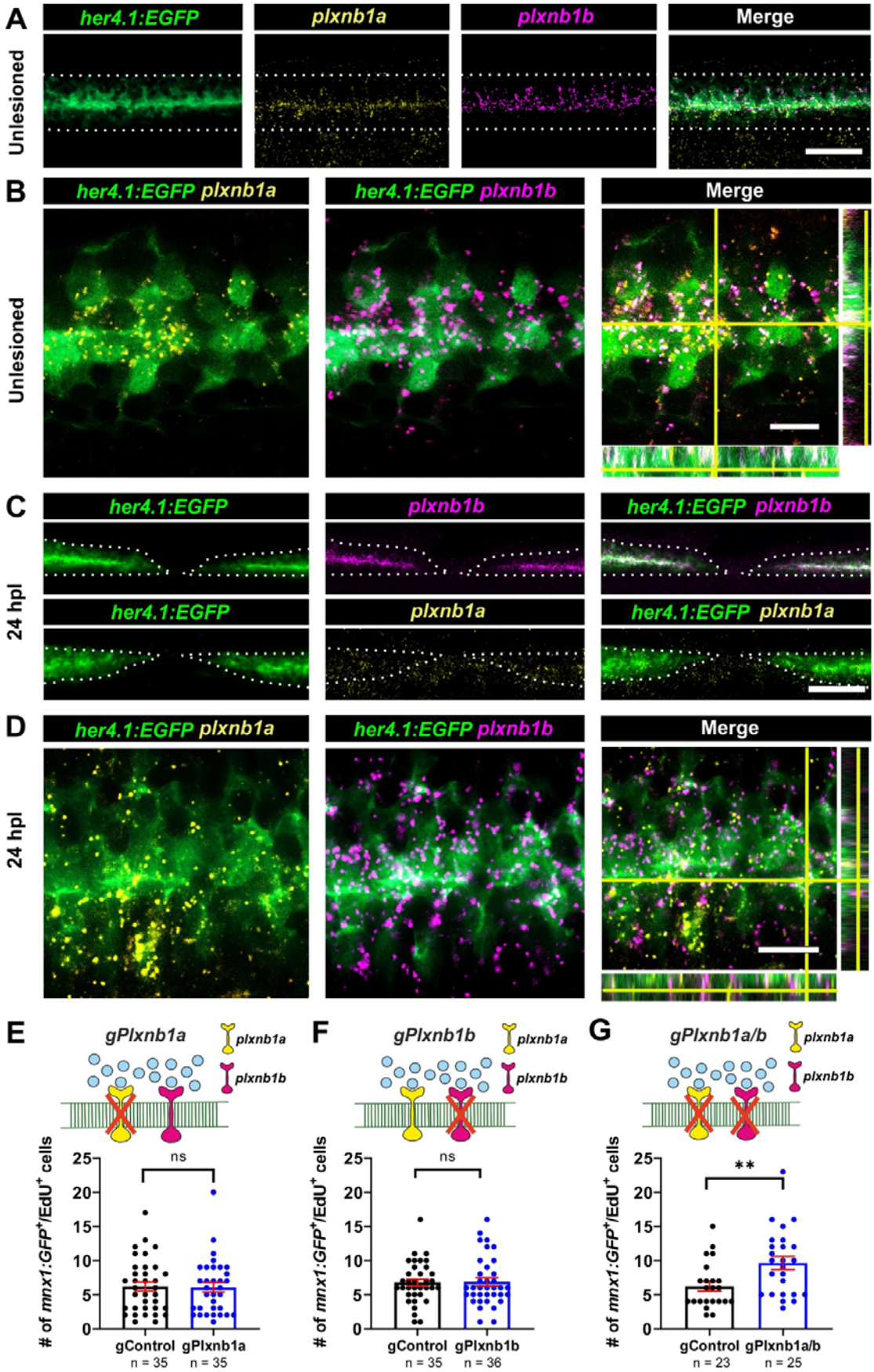
A
her4.1:EGFP
plxnb1a
plxnb1b
Merge
Unlesioned
B
her4.1:EGFP plxnb1a
her4.1:EGFP plxnb1b
Merge
Unlesioned
C
her4.1:EGFP
plxnb1b
her4.1:EGFP plxnb1b
her4.1:EGFP
plxnb1a
her4.1:EGFP plxnb1a
24 hpl
D
her4.1:EGFP plxnb1a
her4.1:EGFP plxnb1b
Merge
24 hpl
E
gPlxnb1a
plxnb1a
plxnb1b
ns
# of mnx1:GFP+/EdU+ cells
gControl
gPlxnb1a
n = 35
n = 35
F
gPlxnb1b
plxnb1a
plxnb1b
ns
# of mnx1:GFP+/EdU+ cells
gControl
gPlxnb1b
n = 35
n = 36
G
gPlxnb1a/b
plxnb1a
plxnb1b
**
# of mnx1:GFP+/EdU+ cells
gControl
gPlxnb1a/b
n = 23
n = 25

Fig. 4. *plxnb1a* and *plxnb1b* are selectively expressed by spinal progenitors and attenuate regenerative neurogenesis. Photomicrographs are oriented as in Fig. 2. **(A)** HCR-FISH in the *her4.1:EGFP* line indicate expression of *plxnb1a* and *plxnb1b* in spinal progenitor cells (*her4.1:EGFP*+) before injury**.** Dotted lines indicate the spinal cord boundaries. **(B)** High magnification showing co-localization of *plxnb1a* and *plxb1b* in *her4.1:EGFP*+ cells. **(C)** HCR-FISH in the *her4.1:EGFP* line indicates expression of *plxnb1a* and *plxnb1b* in spinal progenitor cells (*her4.1:EGFP*+) after injury**.** Dotted lines define the spinal cord extension. **(D)** High magnification showing co-localization of *plxnb1a* and *plxb1b* in *her4.1:EGFP*+ cells after injury. **(E-F)** Regenerative neurogenesis is not changed in single somatic mutants for *plxnb1a* (**E**, gControl: 6.2 cells per larva ± 0.66 ; gPlxnb1a: 6.1 cells per larva ± 0.71; Mann-Whitney U-test: p = 0.8371) and *plxnb1b* (**F**, gControl: 6.8 cells per larva ± 0.52 ; gPlxnb1b: 6.9 cells per larva ± 0.60; Mann-Whitney U-test: p = 0.6511). **(G)** Regenerative neurogenesis is increased in double somatic mutants of *plxnb1a and plxnb1b* by 55 % compared to lesioned control gRNA-injected larvae (gControl: 6.2 cells per larva ± 0.71 cells per larva; gPlxnb1a+b: 9.6 cells per larva ± 0.96; Mann-Whitney U-test: p = 0.0057). Error bars show SEM. Scale bars: 50 µm (A) 10 µm (B).

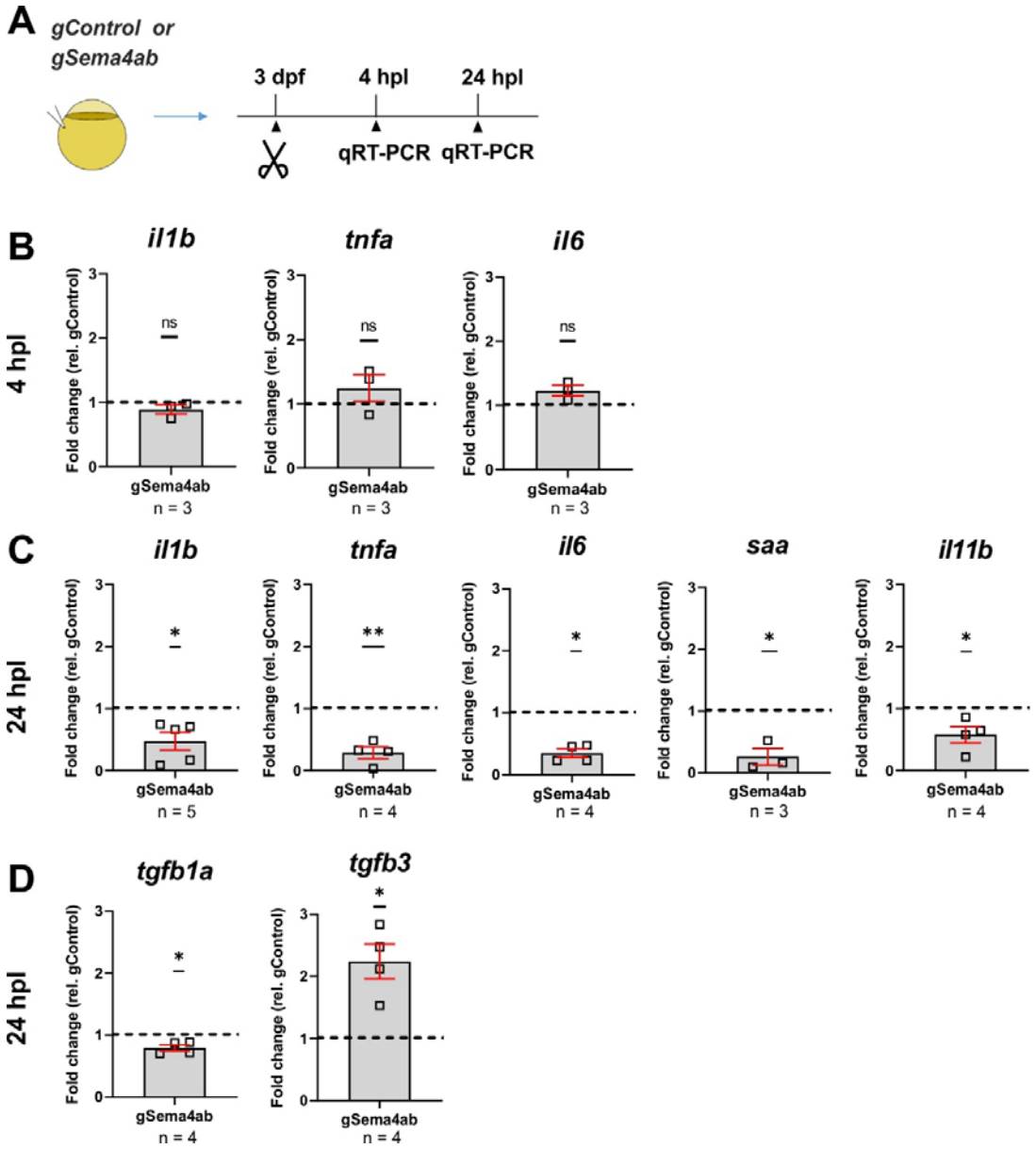
A
gControl or
gSema4ab
3 dpf
4 hpl
24 hpl
qRT-PCR
qRT-PCR
B
4 hpl
il1b
tnfa
il6
Fold change (rel. gControl)
ns
gSema4ab
n = 3
C
24 hpl
il1b
tnfa
il6
saa
il11b
*
**
gSema4ab
n = 5
n = 4
n = 3
D
24 hpl
tgfb1a
tgfb3
n = 4

Fig. 5. Loss of *sema4ab* function changes the cytokine profile of the injury site. **(A)** A schematic indicating the experimental design for cytokine quantification by qRT-PCR is shown. **(B)** qRT-PCR analyses of major pro-inflammatory cytokines in *sema4ab* somatic mutants show no differences to injured control gRNA-injected larvae at 4 hpl (peak of neutrophil response; *il1b*: p = 0.2526; *tnfa*: p = 0.3623; *il6*: p = 0.1028)**.** **(C)** At 24 hpl, *sema4ab* somatic mutants show decreased expression levels of pro-inflammatory cytokines (*il1b*: -2.12 fold-change, p = 0.0212; *tnfa*: -3.58 fold-change, p = 0.0047; *il6*: -2.94 fold-change, p = 0.0024; *saa*: -3.84 fold-change, p = 0.0311; *il11b*: -1.73 fold-change, p = 0.0495). **(D)** While the anti-inflammatory cytokine *tgfb1a* shows a slight decrease (-1.26 fold-change, p = 0.0251), *tgfb3* is substantially increased in expression in *sema4ab* somatic mutants (+2.24 fold-change, p = 0.0210). Statistical tests: One-sample t-test. Each dot represents a pool of 50 larvae. Error bars show SEM.

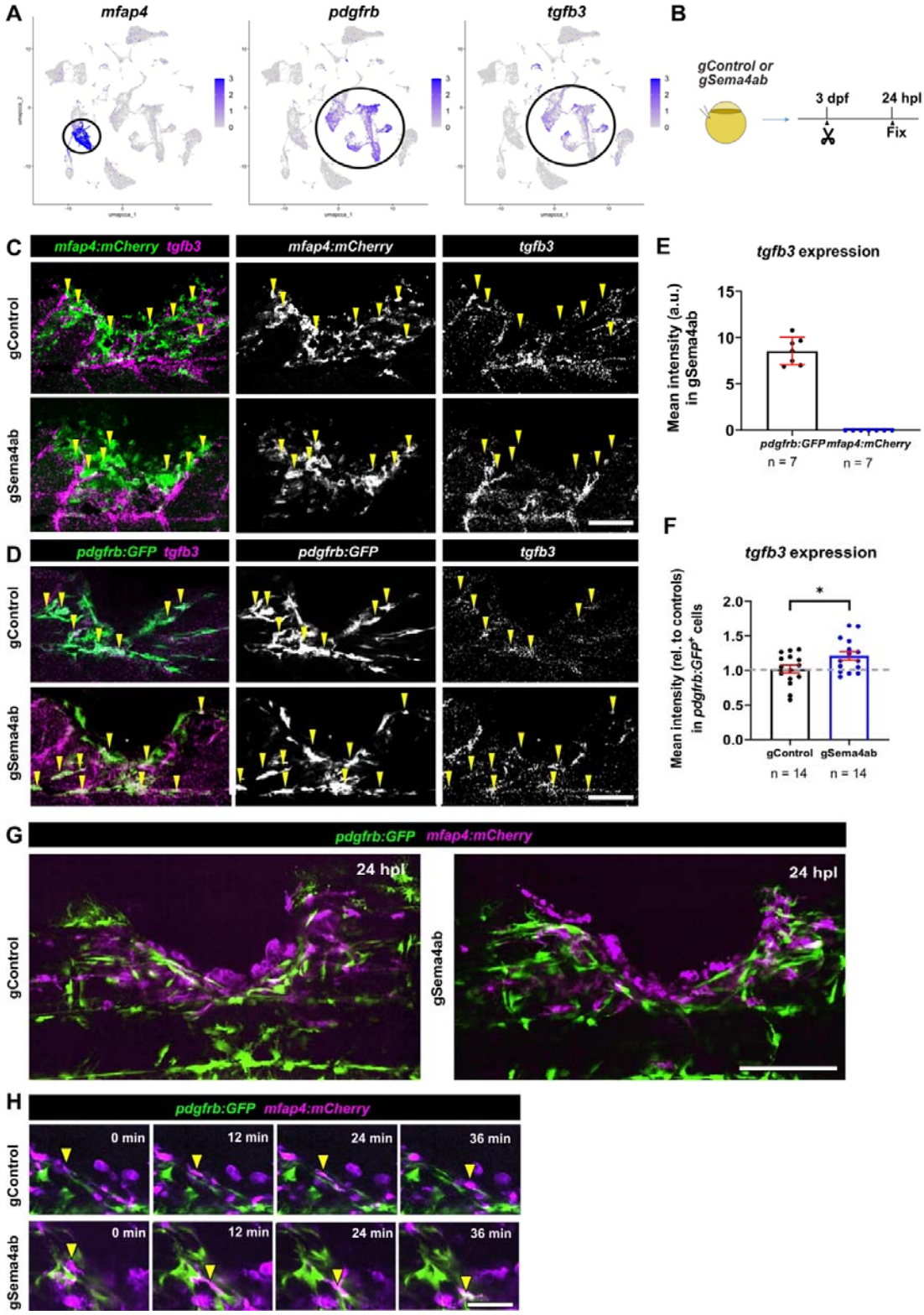
A
mfap4
pdgfrb
tgfb3
B
gControl or gSema4ab
3 dpf
24 hpl
Fix
C
mfap4:mCherry tgfb3
mfap4:mCherry
tgfb3
gControl
gSema4ab
D
pdgfrb:GFP tgfb3
pdgfrb:GFP
tgfb3
gControl
gSema4ab
E
tgfb3 expression
Mean intensity (a.u.) in gSema4ab
pdgfrb:GFP
mfap4:mCherry
n = 7
n = 7
F
tgfb3 expression
Mean intensity (rel. to controls) in pdgfrb:GFP+ cells
gControl
gSema4ab
n = 14
n = 14
G
pdgfrb:GFP mfap4:mCherry
24 hpl
24 hpl
gControl
gSema4ab
H
pdgfrb:GFP mfap4:mCherry
0 min
12 min
24 min
36 min
gControl
gSema4ab

Fig. 6. Fibroblasts increase *tgfb3* expression in the absence of *sema4ab* function. (A) Feature plot shows the expression of *tgfb3* in fibroblasts (*pdgfrb*+), but not in BDMs or microglia (*mfap4*+)**. (B)** A schematic indicating the experimental design for B-E is shown. **(C)** Multiplexed HCR-FISH at 24 hpl shows no detectable *tgfb3* signal in microglia or BdMs (*mfap4:mCherry*$^+$; arrowheads) in lesioned animals with or without *sema4ab* disruption. **(D)** Multiplexed HCR-FISH at 24 hpl shows *tgfb3* expression in fibroblast-like cells (*pdgfrb:GFP*$^+$; arrowheads) with or without *sema4ab* disruption. **(E)** Quantification of mean intensity of the *tgfb3* signal shows expression in *pdgfrb:GFP*+ cells but no detectable signal in *mfap4:mCherry*+ cells in *sema4ab* haCR-injected larvae. **(F)** Comparing mean intensity of the relative fluorescence for the *tgfb3* signal in *pdgfrb:GFP*$^+$ cells between control gRNA-injected and *sema4ab* haCR-injected larvae shows an increase of the *tgfb3* signal in fibroblasts in *sema4ab* haCR-injected larvae at 24 hpl (gControl: 1.01 a.u. ± 0.058; gSema4ab: 1.22 ± 0.063; t-test: $p = 0.0322$). **(G)** Individual frames of time-lapse movies show *mfap4:mCherry*+ cells in close contact to *pdgfrb:GFP*+ cells in both control gRNA injected and in *sema4ab* somatic mutants. **(H)** Time series of movie frames show that *mfap4:mCherry*+ cells (arrowheads) migrate along fibroblast processes in both conditions. Error bars show SEM. Scale bars: 50 µm (C,D), 100 µm (G), 15 µm (H).

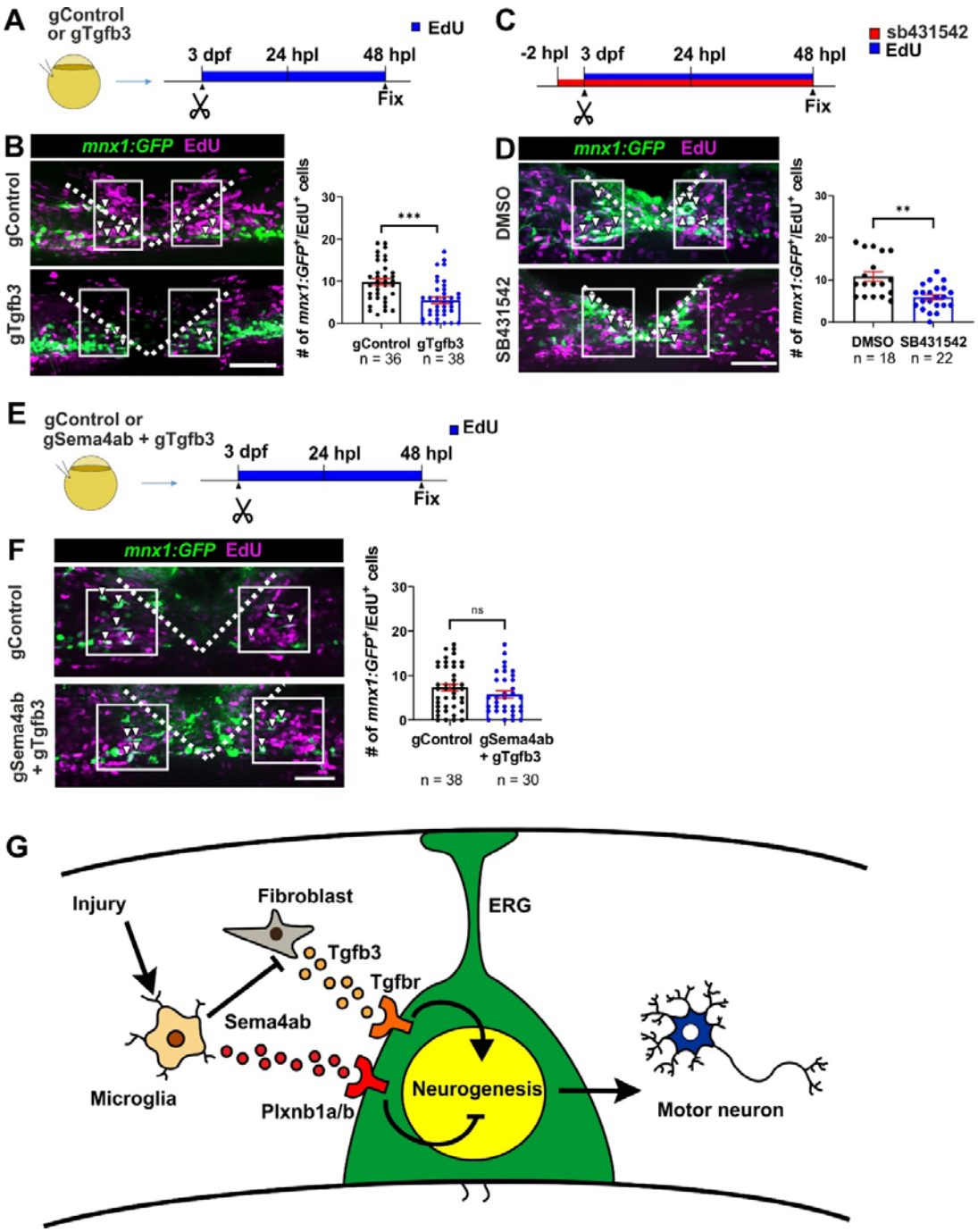

Fig. 7. Fibroblasts promote regenerative neurogenesis via *tgfb3*. (A,B) A schematic timeline of the experimental design is shown (A). Somatic mutants for

tgfb3 show a reduction in the number of newly generated motor neurons (B, gControl: 9.8 cells per larva ± 0.8; gTgfb3: 5.5 cells per larva ± 0.7; p = 0.0001). **(C,D)** A schematic of the experimental design is shown (C). Drug treatment using the small molecule inhibitor SB431542 against Tgfb-receptors mimics reduction in regenerative neurogenesis observed with *tgfb3* somatic mutants (D, DMSO: 10.8 cells per larva ± 1.15; SB431542: 5.9 cells per larva ± 0.63; p = 0.0011). **(E,F)** A schematic timeline for double gene disruption is shown (F). Double haCR injection against *sema4ab* and *tgfb3* restores control levels of regenerative neurogenesis (gControl: 8.1 cells per larva ± 0.7; gSema4ab+gTgfb3: 6.6 cells per larva ± 0.8; p = 0.1523). **(G)** A graphical summary of proposed interactions of *sema4ab* during spinal cord regeneration is shown. After spinal injury, microglia likely control neurogenesis directly by signalling through Sema4ab and Plxnb1a/b on ERGs and indirectly by controlling expression of *tgfb3*, a positive regulator of regenerative neurogenesis, in fibroblasts. Error bars show SEM. Dotted lines show the injury site. Scale bars: 50 µm.

TABLES

Top 10 downregulated genes in MM#1 (gSema4ab vs gControl)						
Gene Symbol	**p_val**	**avg_log2FC**	**pct.1**	**pct.2**	**p_val_adj**	**Fold Change**
fthl31	4.53E-10	-2.8108973	0.08	0.259	1.19E-05	-7.0172090
grn1	7.24E-18	-2.7803628	0.367	0.625	1.90E-13	-6.8702511
lyz	2.71E-09	-2.5651207	0.219	0.416	7.09E-05	-5.9180452
dyrk1aa	1.81E-08	-2.2728607	0.033	0.162	0.00047467	-4.8328048
acacb	1.75E-06	-2.1746032	0.062	0.181	0.04588534	-4.5146157
fam78ab	2.73E-06	-2.1453837	0.068	0.191	0.07138602	-4.4240991
mxf	4.21E-09	-2.1047832	0.24	0.438	0.00011024	-4.3013312
b4galt1	1.27E-06	-2.0767341	0.05	0.166	0.03338913	-4.2185117
ifitm1	2.02E-06	-2.0587836	0.13	0.266	0.05283023	-4.1663487
scp2b	1.19E-06	-2.0462101	0.092	0.225	0.03110672	-4.1301956

Table 1. Top 10 downregulated genes in MM#1 after *sema4ab* somatic mutation in scRNAseq.

SUPPLEMENTARY FIGURES

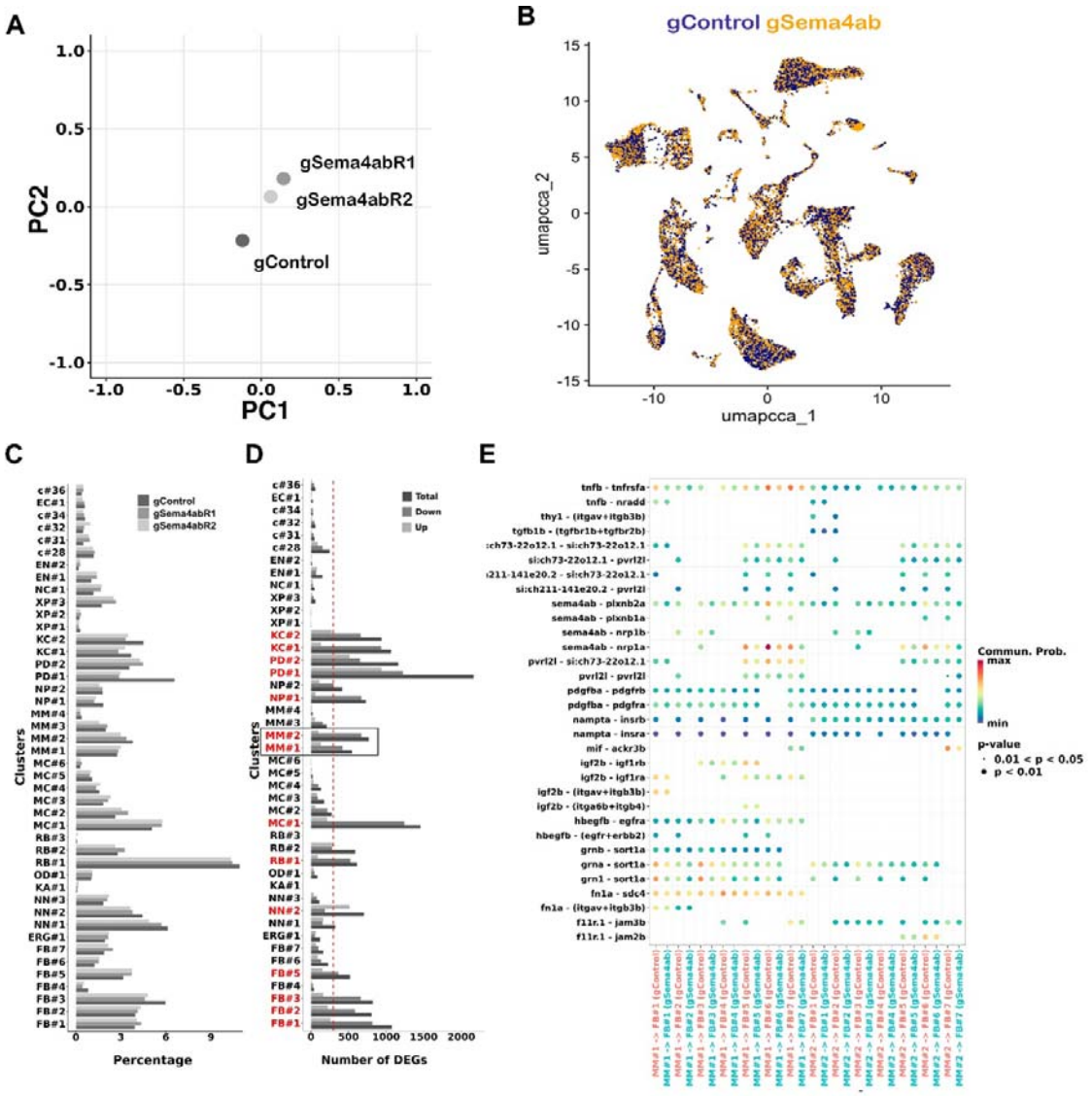

Suppl. Fig. 1 scRNAseq quality control and additional analyses. (A) Principal component analysis (PC1 and PC2) shows that gSema4ab replicates (R1 and R2) are more closely related to each other than to gControl. **(B)** A plot comparing cell numbers between samples shows no major changes in cell type representation resulting from *sema4ab* disruption (gControl in blue, gSema4ab in yellow). **(C)** A graph indicates similar percentages of cells per cluster across scRNAseq samples. **(D)** A graph indicate differential expression of genes (DEG) between samples is shown. Cell clusters with major changes (>300 DEGs) are indicated in red. Microglia clusters MM#1 and MM#2 are boxed. **(E)** A dot plot illustrates the communication probabilities of all ligand-receptor interactions identified by CellChat between microglia clusters MM#1 and MM#2 and fibroblast clusters is shown.

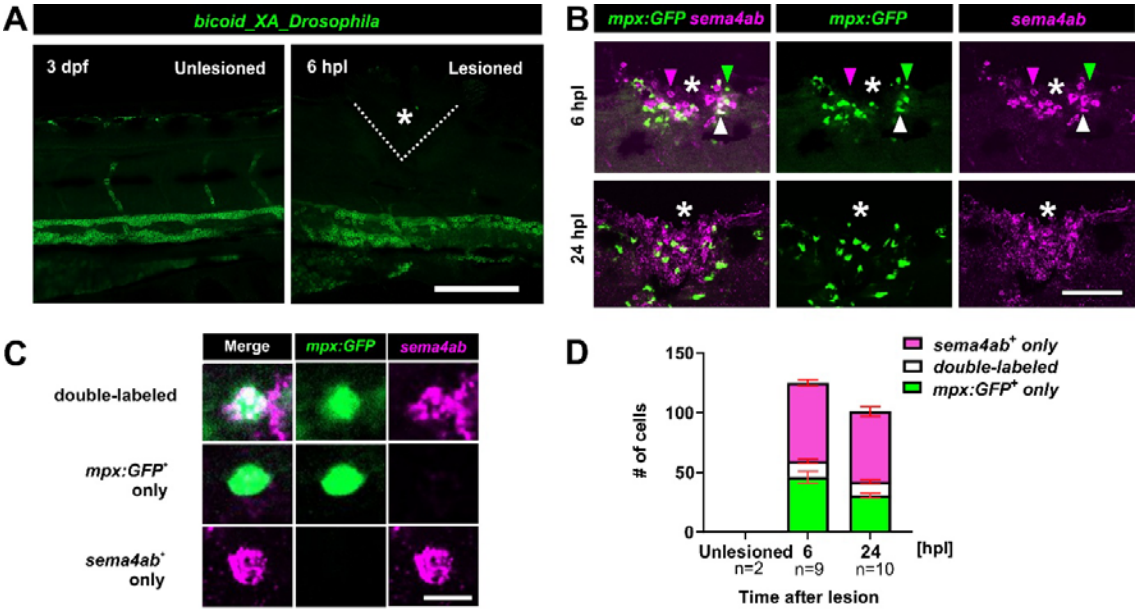

Suppl. Fig. 2 HCR-FISH method control and detection of *sema4ab* expression in neutrophils. (A) HCR-FISH for the negative control gene (*Drosophila* BicoidXA) shows non-specific labelling in some blood vessels, but not in the spinal cord in uninjured and injured larvae. **(B)** Multiplexed HCR-FISH at 6 and 24 hpl shows that a few *sema4ab*+ cells also express *mpx:GFP* (white arrows: double positive cells; green arrows: *mpx:GFP*+ only; magenta arrows: *sema4ab*+ only) **(C)** High magnifications of *mpx:GFP* and *sema4ab* double- and single-positive cells used for cell counting are shown. **(D)** A bar chart indicates numbers of *mpx:GFP* and *sema4ab* double- and single-labelled cells at different post-lesion time points. Scale bars: 100 µm (A,B), 10 µm (C).

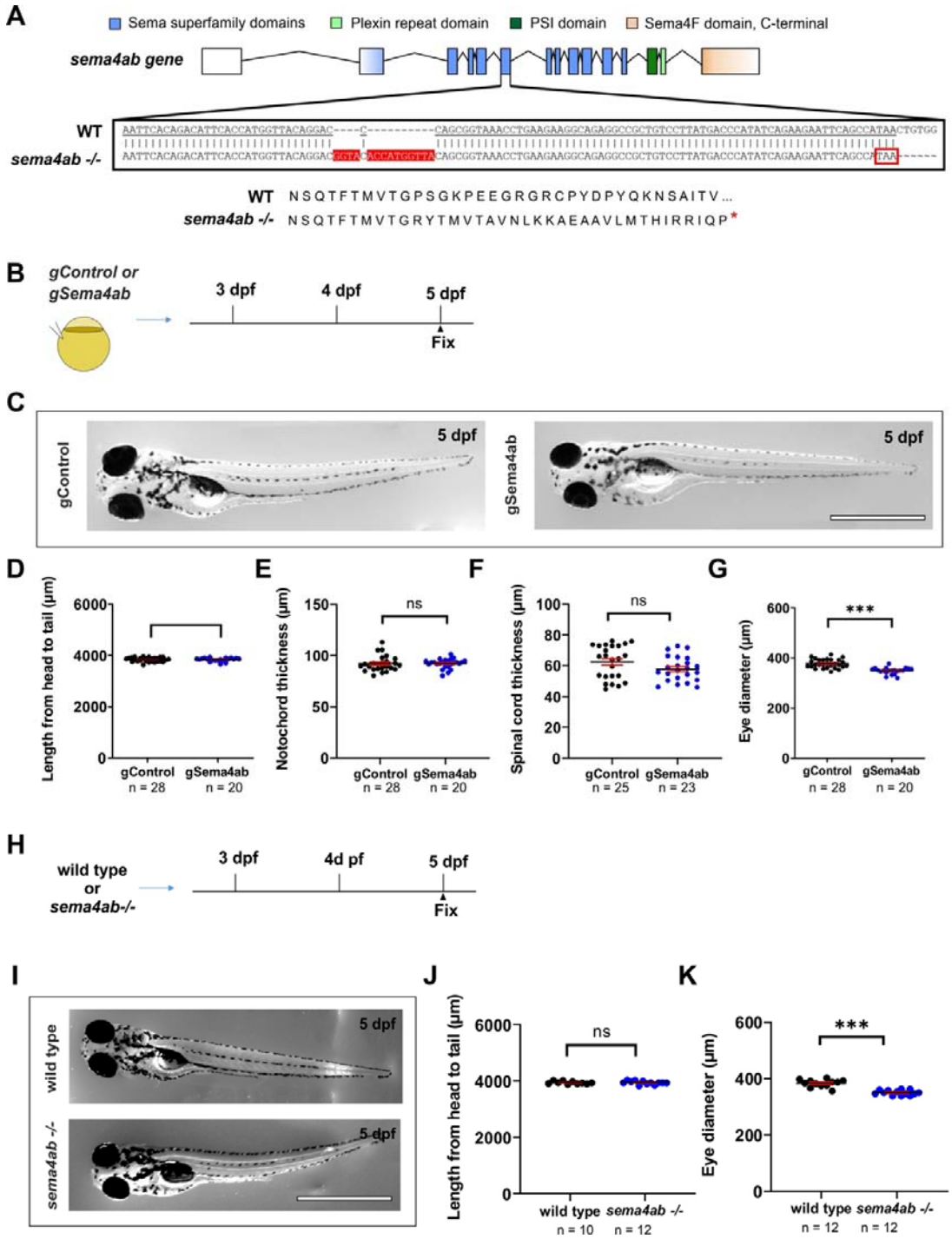
A
Sema superfamily domains
Plexin repeat domain
PSI domain
Sema4F domain, C-terminal
sema4ab gene
WT
sema4ab -/-
WT NSQTFTMVTGPSGKPEEGRGRCPYDPYQKNSAITV...
sema4ab -/- NSQTFTMVTGRYTMVTAVNLKKAEAAVLMTHIRRIQP*
B
gControl or gSema4ab
3 dpf
4 dpf
5 dpf
Fix
C
gControl
5 dpf
gSema4ab
5 dpf
D
Length from head to tail (µm)
gControl n = 28
gSema4ab n = 20
E
Notochord thickness (µm)
ns
gControl n = 28
gSema4ab n = 20
F
Spinal cord thickness (µm)
ns
gControl n = 25
gSema4ab n = 23
G
Eye diameter (µm)
***
gControl n = 28
gSema4ab n = 20
H
wild type or sema4ab-/-
3 dpf
4d pf
5 dpf
Fix
I
wild type
5 dpf
sema4ab -/-
5 dpf
J
Length from head to tail (µm)
ns
wild type n = 10
sema4ab -/- n = 12
K
Eye diameter (µm)
***
wild type n = 12
sema4ab -/- n = 12

Suppl. Fig. 3 Disruption of *sema4ab* does not lead to large changes of larval growth. (A) A schematic of the *sema4ab* gene structure and position of the mutation in the *sema4ab* germline mutant is shown. Note the insertion of 14 bp in exon 6 (sequence underlaid in red) and the frameshift that predicts a stop codon (red frame and asterisk). **(B)** A schematic indicating the experimental design for C-G is shown. **(C)** Photomicrographs of gControl and gSema4ab larvae are shown at 5 dpf. **(D-G)** Quantifications show no differences in body length (D: gControl: 3836 µm ± 15.65; gSema4ab: 3838 µm ± 15.72; t-test: $p = 0.9917$)**,** notochord thickness (E: gControl: 92.09 µm ± 1.527; gSema4ab: 92.20 µm ± 0.9314; Mann-Whitney U-test: $p = 0.3423$) or spinal cord thickness (F: gControl: 62.49 µm ± 2.215; gSema4ab: 57.83 µm ± 1.677; Mann-Whitney U-test: $p = 0.1134$) between gControl and gSema4ab larvae. Eye diameter is slightly reduced in gSema4ab larvae (G: gControl: 378.2 µm ± 3.320; gSema4ab: 349.3 µm ± 2.784; t-test: $p < 0.0001$). **(H)** A schematic indicating the experimental design for I-K is shown. **(I)** Photomicrographs show wild type and mutant larvae for *sema4ab* at 5 dpf. **(J)** No difference was observed in body length of wild type and mutant larvae (wild type: 3941 µm ± 15.95; gSema4ab: 3940 µm ± 17.50; t-test: $p = 0.6855$). **(K)** Eye diameter of mutants is slightly decreased (wild type: 383.3 µm ± 3.788; gSema4ab: 349.9 µm ± 2.56; t-test: $p < 0.0001$)**.** Error bars show SEM. Scale bars = 1 mm.

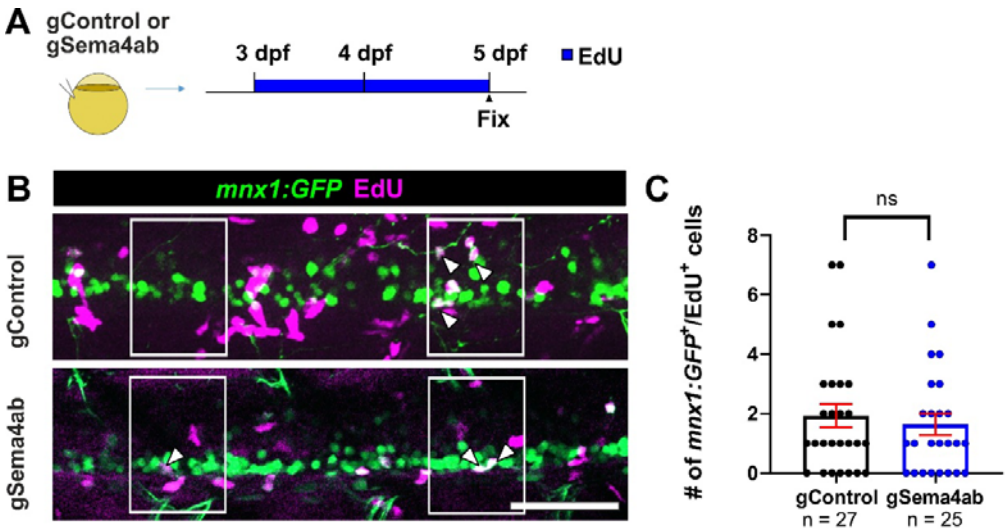

Supp. Fig. 4. *Sema4ab* loss of function does not affect ongoing developmental neurogenesis. Photomicrographs are oriented as in Fig. 1. Arrowheads indicate double-labelled cells; white boxes indicate quantification windows. **(A-C)** A schematic of the experiment is shown in (A). Ongoing developmental neurogenesis of motor neurons (double-labelled for EdU and *mnx1:GFP*) is not different between gControl and gSema4a injected unlesioned larvae (B), quantified in (C) (gControl: 1.9 cells per larvae ± 0.3920; gSema4ab: 1.7 cells per larvae ± 0.3646; Mann-Whitney U-test: p = 0.5972). Scale bar: 50 µm.

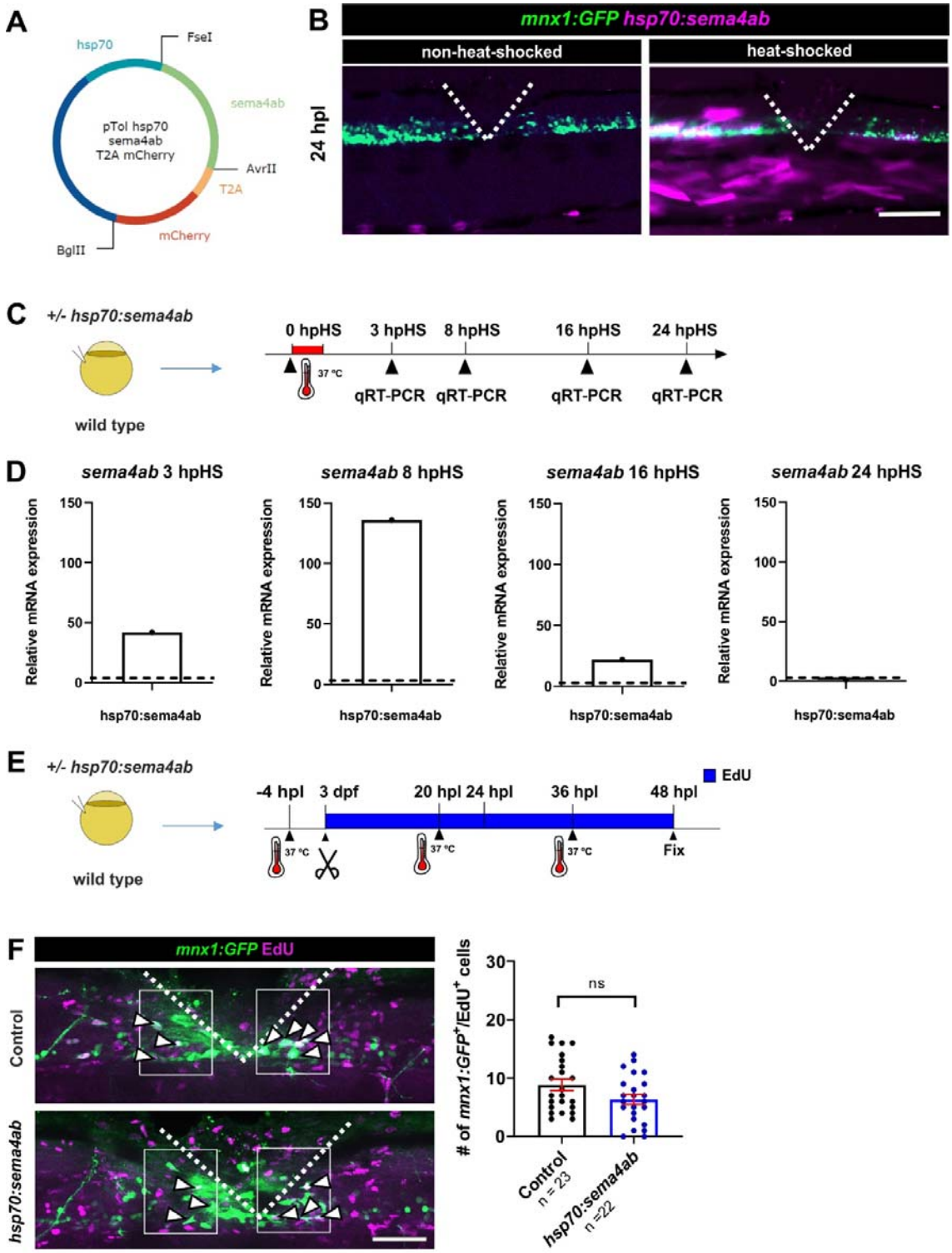
A
hsp70
FseI
sema4ab
pTol hsp70
sema4ab
T2A mCherry
AvrII
T2A
mCherry
BglII
B
mnx1:GFP hsp70:sema4ab
non-heat-shocked
heat-shocked
24 hpl
C
+/- hsp70:sema4ab
wild type
0 hpHS
3 hpHS
8 hpHS
16 hpHS
24 hpHS
37 °C
qRT-PCR
qRT-PCR
qRT-PCR
qRT-PCR
D
sema4ab 3 hpHS
sema4ab 8 hpHS
sema4ab 16 hpHS
sema4ab 24 hpHS
Relative mRNA expression
150
100
50
0
hsp70:sema4ab
E
+/- hsp70:sema4ab
wild type
EdU
-4 hpl
3 dpf
20 hpl
24 hpl
36 hpl
48 hpl
37 °C
Fix
F
mnx1:GFP EdU
Control
hsp70:sema4ab
# of mnx1:GFP+/EdU+ cells
30
20
10
0
ns
Control
n = 23
hsp70:sema4ab
n =22

Suppl. Fig. 5. Efficient heat-shock overexpression of *sema4ab* does not alter regenerative neurogenesis in lesioned wild type larvae. (A) A map of the heat-shock vector injected to over-express *sema4ab* and a reporter (*mCherry*) is shown. **(B)** Heat-shock leads to detectability of mCherry protein mainly in muscle cells surrounding the injury site (position of ventral spinal cord indicated by *mnx1:GFP* transgene) at 24 hpl. **(C,D)** Experimental timeline to assess *sema4ab* over-expression by qRT-PCR after a single heat shock is shown in (C). qRT-PCR analysis shows that a single heat-shock leads to strongly increased *sema4ab* expression for at least 16 hours after heat-shock (D). **(E,F)** A schematic of the experiment is shown in E. Over-expression of *sema4ab* does not elicit any changes in the number newly generated neurons after spinal lesion (F; gControl: 8.8 cells per larva ± 0.98; hsp70:sema4ab: 6.4 cells per larva ± 0.86; Mann-Whitney U-test: $p = 0.3850$). Error bars show SEM. Dotted lines show the injury site. Scale bars: 50 µm.

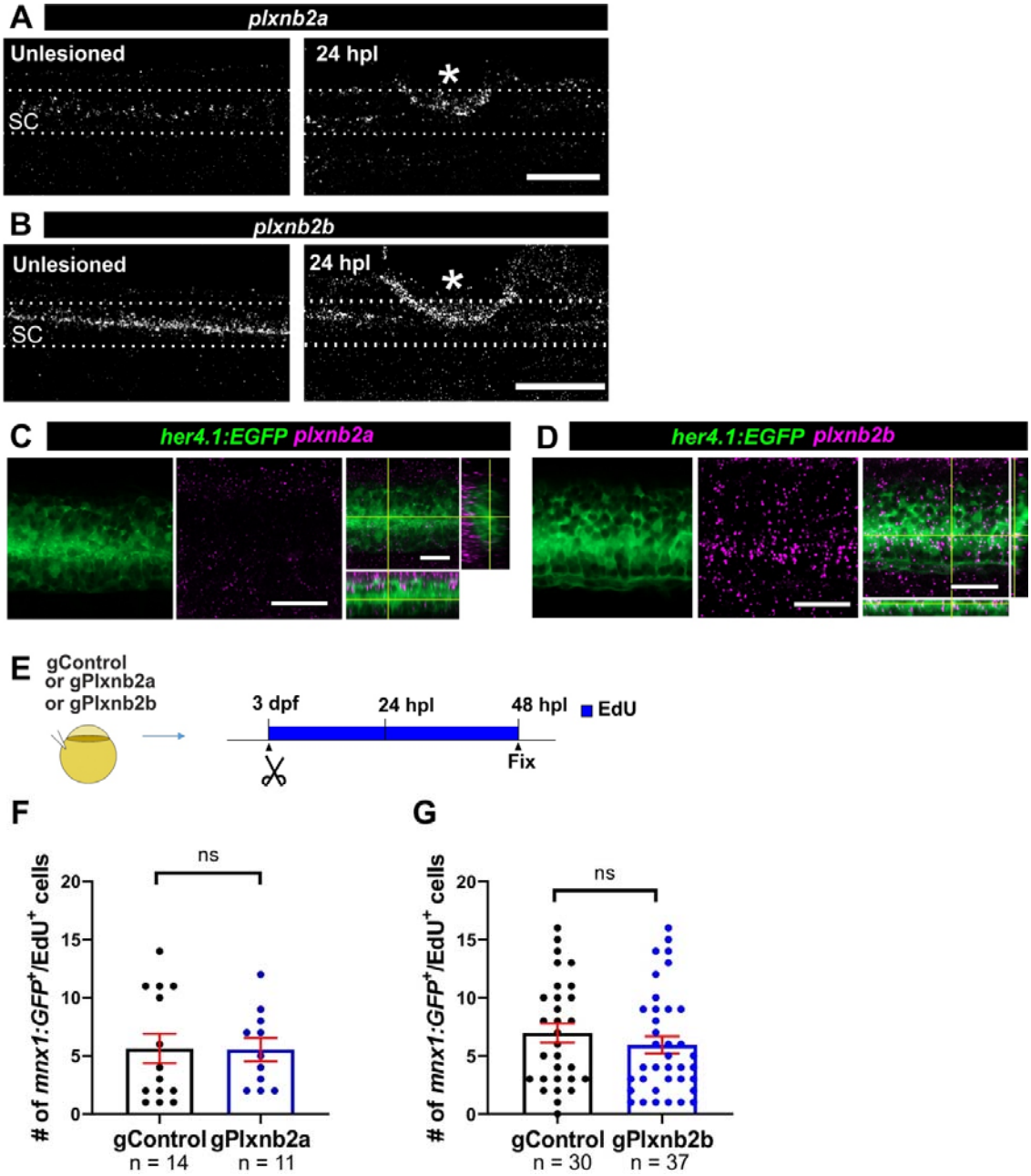
A
plxnb2a
Unlesioned
24 hpl
SC
B
plxnb2b
Unlesioned
24 hpl
SC
C
her4.1:EGFP plxnb2a
D
her4.1:EGFP plxnb2b
E
gControl
or gPlxnb2a
or gPlxnb2b
3 dpf
24 hpl
48 hpl
EdU
Fix
F
ns
# of mnx1:GFP+/EdU+ cells
gControl
gPlxnb2a
n = 14
n = 11
G
ns
# of mnx1:GFP+/EdU+ cells
gControl
gPlxnb2b
n = 30
n = 37

Suppl. Fig. 6 Somatic mutations of *plxnb2a and plxnb2b* do not affect regenerative neurogenesis. Tissue is oriented as in Fig. 1 **(A,B)** HCR-FISH shows expression of *plxnb2a* (A) and *plxnb2b* (B) in a narrow domain in the spinal cord that does not change after lesion**.** Additional signal can be observed in the injury site after lesion for both genes (asterisks). **(C,D)** High magnifications of HCR-FISH for *plxnb2a* and *plxnb2b* show no detectable expression of *plxnb2a* at the level of ERGs (C), but of *plxnb2b* in *her4.1:EGFP*+ cells (D). Note likely neuronal labelling in orthogonal views adjacent to *her4.1:GFP*+ cells in (C). **(E)** A schematic indicating the experimental design for F,G is shown. **(F,G)** haCR gene disruption of *plxnb2a* (F, gControl: 5.6 cells per larva ± 1.26 ; gPlxnb2a: 5.5 cells per larva ± 1.00; Mann-Whitney U-test: p = 0.6938) or *plxnb2b* (G, gControl: 6.9 cells per larva ± 0.83 ; gPlxnb2b: 5.9 cells per larva ± 0.73; Mann-Whitney U-test: p = 0.3336) does not lead to a change in number of newly generated motor neurons, compared to lesioned gControl injected larvae. Error bars show SEM. Dotted lines delineate the position of the spinal cord. Scale bars: 100 µm (A, B), 25 µm (C, D).

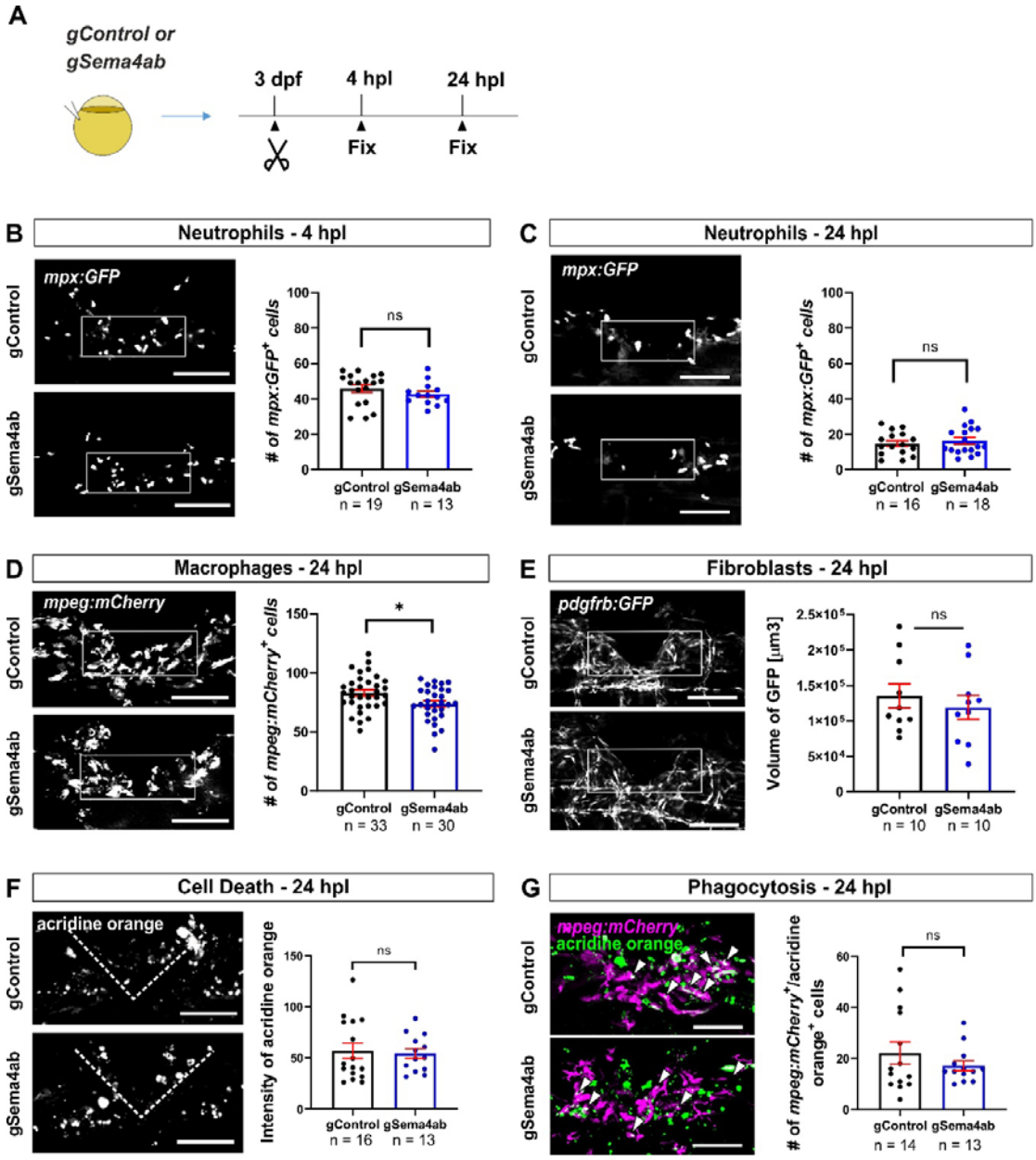
A
gControl or
gSema4ab
3 dpf
4 hpl
24 hpl
Fix
Fix
B
Neutrophils - 4 hpl
mpx:GFP
gControl
gSema4ab
# of mpx:GFP+ cells
ns
gControl
gSema4ab
n = 19
n = 13
C
Neutrophils - 24 hpl
mpx:GFP
gControl
gSema4ab
# of mpx:GFP+ cells
ns
gControl
gSema4ab
n = 16
n = 18
D
Macrophages - 24 hpl
mpeg:mCherry
gControl
gSema4ab
# of mpeg:mCherry+ cells
*
gControl
gSema4ab
n = 33
n = 30
E
Fibroblasts - 24 hpl
pdgfrb:GFP
gControl
gSema4ab
Volume of GFP [µm3]
ns
gControl
gSema4ab
n = 10
n = 10
F
Cell Death - 24 hpl
acridine orange
gControl
gSema4ab
Intensity of acridine orange
ns
gControl
gSema4ab
n = 16
n = 13
G
Phagocytosis - 24 hpl
mpeg:mCherry
acridine orange
gControl
gSema4ab
# of mpeg:mCherry+/acridine orange+ cells
ns
gControl
gSema4ab
n = 14
n = 13

Suppl. Fig. 7 Cell recruitment and phagocytosis in the injury site are hardly changed after *sema4ab* ablation. White boxes designate quantification windows. Dotted lines outline the edges of the injury site. **(A)** A schematic indicating the experimental design is shown. **(B,C)** Neutrophil numbers do not show differences at 4 hpl (A, gControl: 45.89 cells per larva ± 2.1; gSema4ab: 42.69 cells per larva ± 1.8; Mann-Whitney U-test: p = 0.1854) and 24 hpl (B, gControl: 14.63 cells per larva ± 1.7; gSema4ab: 16.33 cells per larva ± 2.5; Mann-Whitney U-test: p = 0.5005) in *sema4ab* somatic mutants compared to control gRNA-injected larvae. **(D)** There is a reduction of 12 % in the number of BDMs/microglia in gSema4ab compared to gControl larvae larvae at 24 hpl (gControl: 83.03 cells per larva ± 9.3; gSema4ab: 73.73 cells per larva ± 3.7; Mann-Whitney U-test: p= 0.0156). **(E)** The abundance of fibroblast-like cells, measured by GFP positive volume, shows no differences between controls and somatic mutants for *sema4ab* at 24 hpl (gControl: 135342 μm^3 ± 17127; gSema4ab: 118911 μm^3 ± 16774; Mann-Whitney U-test: p = 0.6842). **(F)** Cell death, measured by average labelling intensity of acridine orange in the lesion site, shows no differences between experimental groups (gControl: 56.67 ± 7.5; gSema4ab 54.27 ± 5.0; Mann-Whitney U-test: p = 0.8123). **(G)** BDMs/microglia phagocytosis, evaluated by counting *mpeg:mCherry*+ cells with engulfed acridine orange+ particles, shows no differences between groups (gControl: 22.21 cells per larva ± 4.327; gSema4ab 17.23 cells per larva ± 1.912; Mann-Whitney U-test: p = 0.9714). Error bars show SEM. Scale bars: 50 µm.

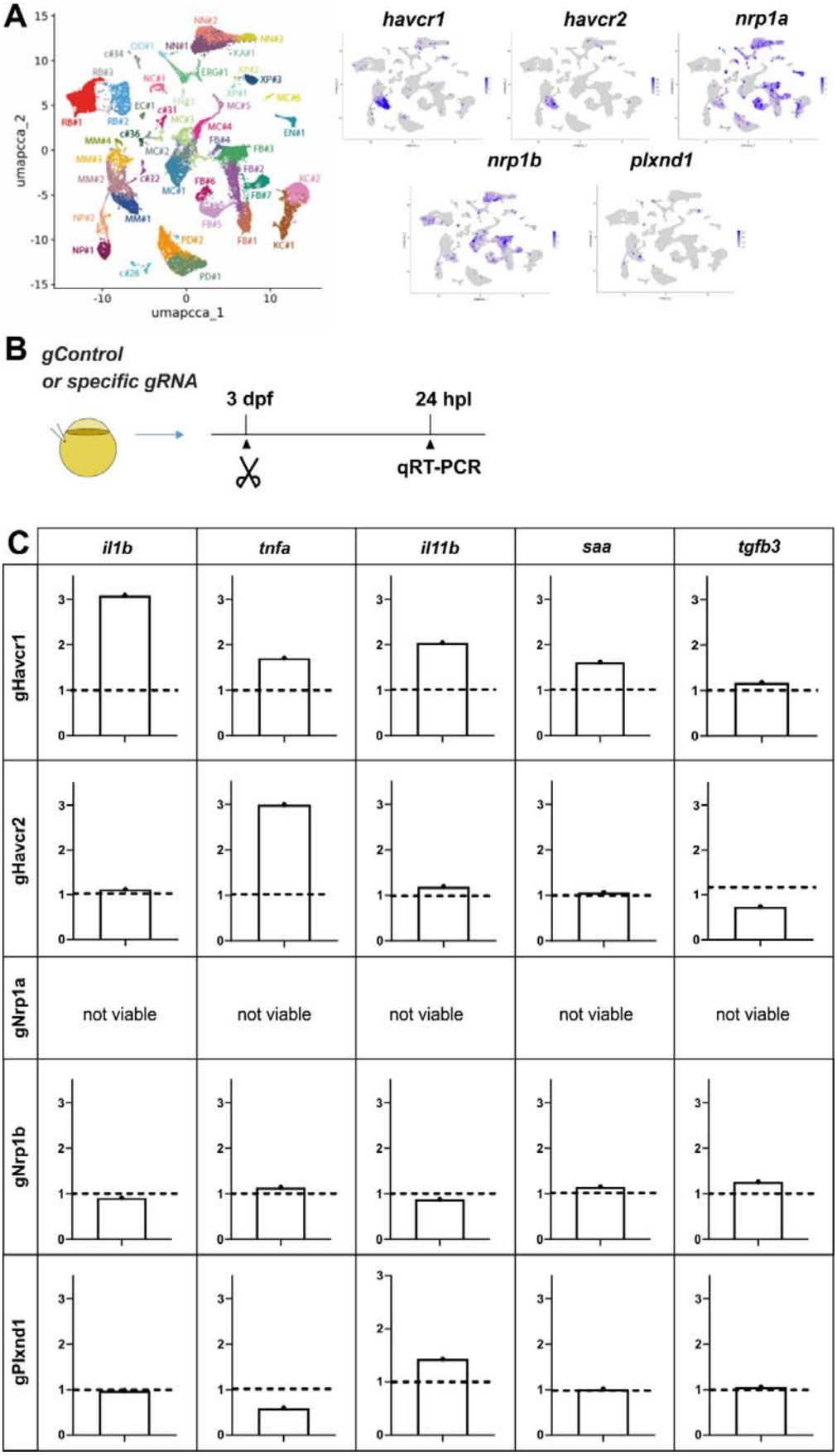
A
umapcca_2
umapcca_1
havcr1
havcr2
nrp1a
nrp1b
plxnd1
B
gControl
or specific gRNA
3 dpf
24 hpl
qRT-PCR
C
il1b
tnfa
il11b
saa
tgfb3
gHavcr1
gHavcr2
gNrp1a
gNrp1b
gPlxnd1
not viable

Suppl. Fig. 8 Disruptions of known *sema4ab* receptors do not reproduce the changes in cytokine expression observed in *sema4ab* somatic mutants. (A) Additional potential Sema4ab receptors are expressed in lesion site cells, as indicated in scRNAseq. **(B)** A schematic indicating the experimental design is shown. **(C)** Screening of somatic mutants by qRT-PCR for the indicated potential Sema4ab receptors indicates changes in the expression of some cytokines, but none of them mimics the decrease of *il1b, tnfa, il11b,* and *saa* and increase of *tgfb3* expression observed for *sema4ab* disruption (see Fig. 5). *nrp1a* haCR-injected animals were non-viable. Dotted lines indicate the expression levels of control gRNA-injected lesioned larvae set to 1, against which changes were normalised.

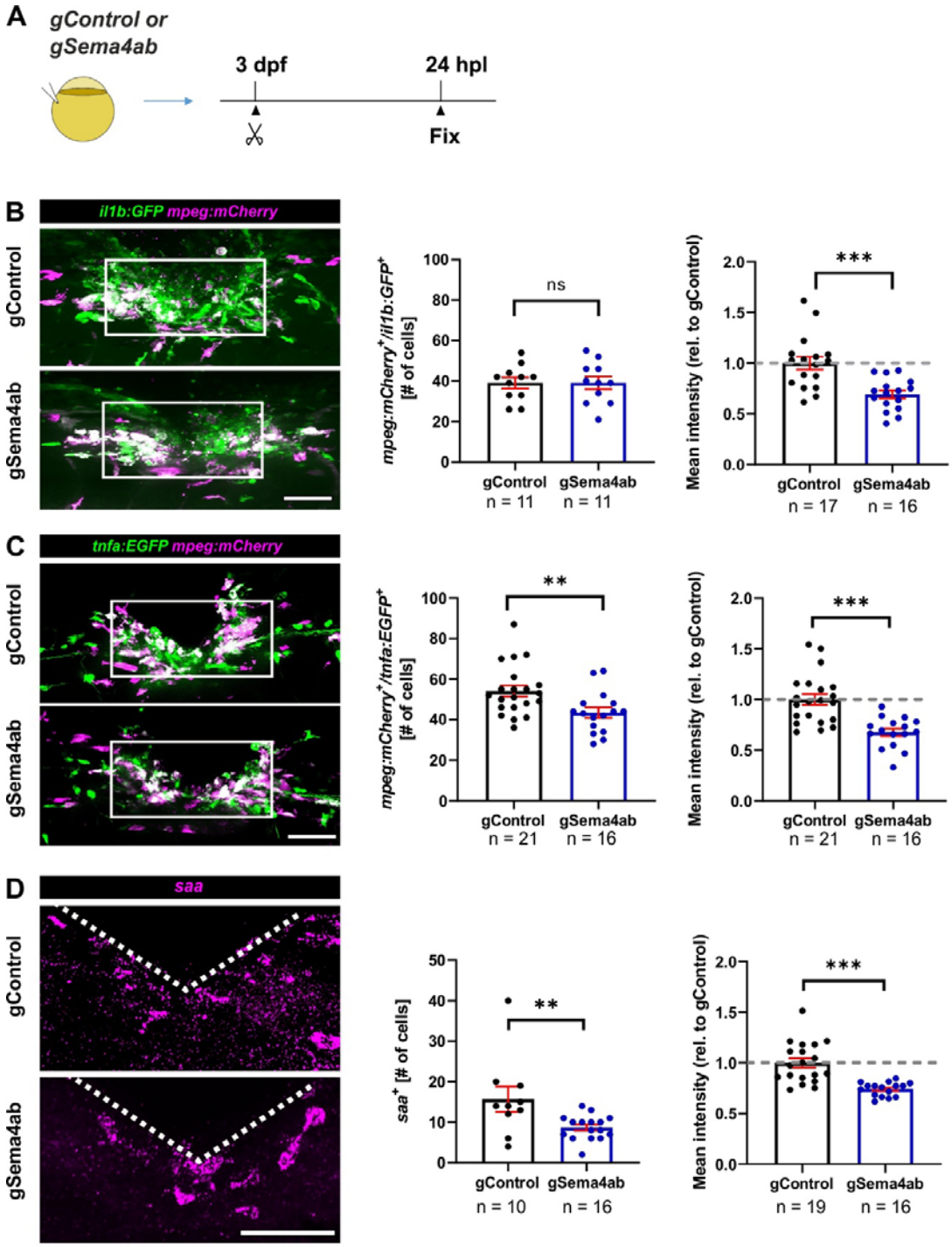
A
gControl or gSema4ab
3 dpf
24 hpl
Fix
B
il1b:GFP mpeg:mCherry
gControl
gSema4ab
mpeg:mCherry+/il1b:GFP+ [# of cells]
ns
gControl n = 11
gSema4ab n = 11
Mean intensity (rel. to gControl)
***
gControl n = 17
gSema4ab n = 16
C
tnfa:EGFP mpeg:mCherry
gControl
gSema4ab
mpeg:mCherry+/tnfa:EGFP+ [# of cells]
**
gControl n = 21
gSema4ab n = 16
Mean intensity (rel. to gControl)
***
gControl n = 21
gSema4ab n = 16
D
saa
gControl
gSema4ab
saa+ [# of cells]
**
gControl n = 10
gSema4ab n = 16
Mean intensity (rel. to gControl)
***
gControl n = 19
gSema4ab n = 16

Suppl. Fig. 9 Histological detection of changes in cytokine expression after *sema4ab* disruption. (A) A schematic indicating the experimental design for B-D is shown. **(B)** The number of *il1b:GFP* reporter gene expressing BDMs/microglia is not changed (gControl: 40.00 cells per larva ± 3.33; gSema4ab: 39.50 cells per larva ± 4.06; t-test: p = 0.9269), but *il1b:GFP* fluorescence intensity is decreased in lesioned *sema4ab* somatic mutants compared to control injected fish at 24 hpl (-1.45 fold-change; t-test: p = 0.0004). **(C)** Both the number of *mpeg:mCherry*+ cells expressing the *tnfa:EGFP* reporter gene (gControl: 54.14 cells per larva ± 2.70; gSema4ab: 43.44 cells per larva ± 2.57; t-test p = 0.0083), as well as *tnfa:EGFP* fluorescence intensity (-1.49 fold-change; t-test: p < 0.0001) are reduced in lesioned *sema4ab* somatic mutants compared to control gRNA injected lesioned larvae at 24 hpl. **(D)** *saa* expression, detected by HCR-FISH, indicates a decrease in *saa*+ cell number (gControl: 15.70 cells per larva ± 3.12; gSema4ab: 8.68 cells per larva ± 0.75; t-test p = 0.0114) and fluorescence mean intensity (-1.35 fold-change; t-test: p < 0.0001) in lesioned *sema4ab* somatic mutants compared to lesioned control gRNA-injected larvae at 24 hpl. Error bars show SEM. Dotted lines show the injury site. Squares indicate counting windows. Scale bars: 50 µm.

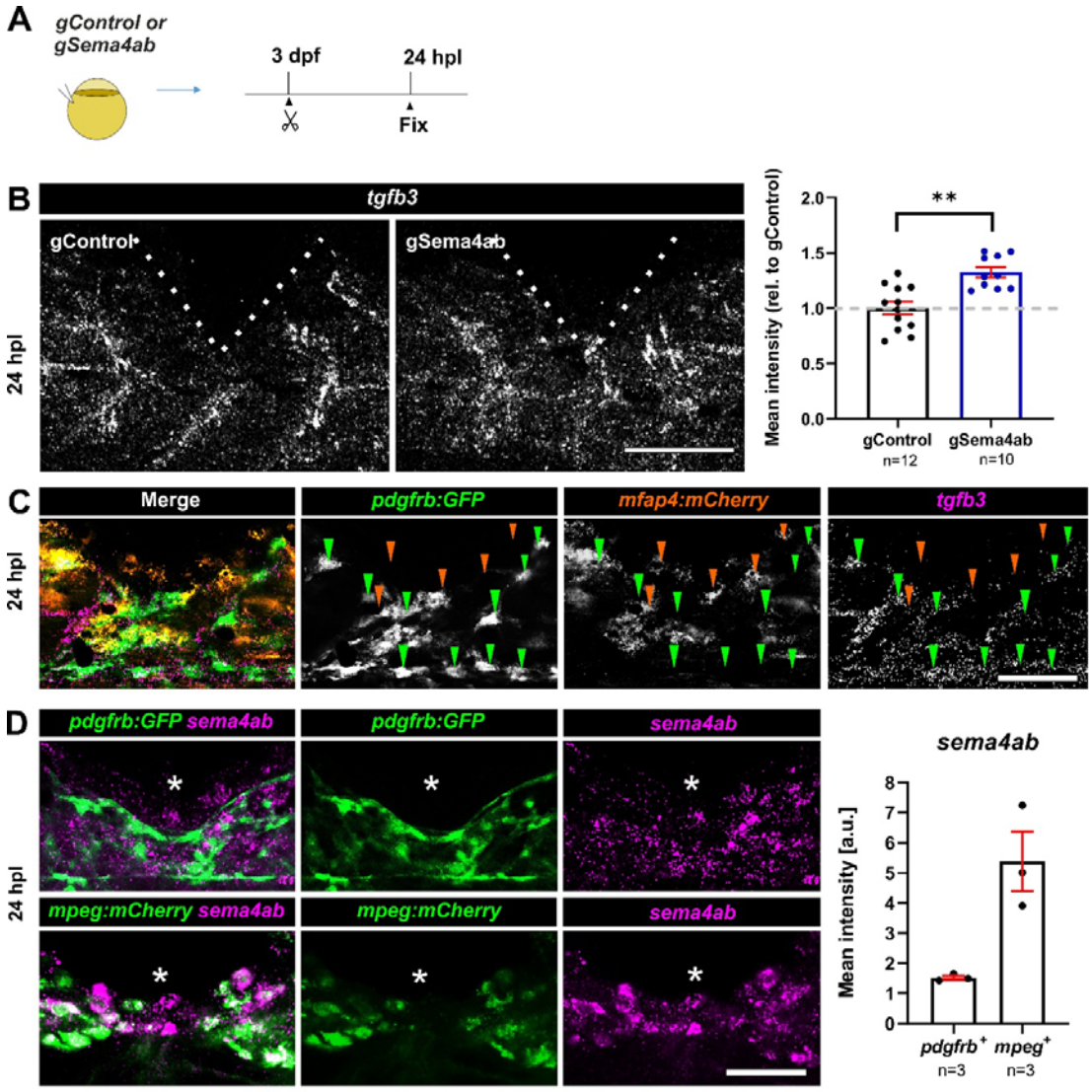
A
gControl or gSema4ab
3 dpf
24 hpl
Fix
B
tgfb3
gControl
gSema4ab
24 hpl
Mean intensity (rel. to gControl)
2.0
1.5
1.0
0.5
0.0
**
gControl
n=12
gSema4ab
n=10
C
Merge
pdgfrb:GFP
mfap4:mCherry
tgfb3
24 hpl
D
pdgfrb:GFP sema4ab
pdgfrb:GFP
sema4ab
mpeg:mCherry sema4ab
mpeg:mCherry
sema4ab
24 hpl
sema4ab
Mean intensity [a.u.]
8
7
6
5
4
3
2
1
0
pdgfrb+
n=3
mpeg+
n=3

Suppl. Fig. 10 *Tgfb3* expression is increased in lesion-site fibroblasts of *sema4ab* somatic mutants. (A) A schematic indicating the experimental design for (B-D) is shown. **(B)** HCR-FISH for *tgfb3* shows an increase in fluorescence intensity in lesioned *sema4ab* somatic mutants compared to lesioned control gRNA-injected fish at 24 hpl (gControl: 1.0 ± 0.058; gSema4ab: 1.3 ± 0.046; t-test: p = 0.0011). Dotted lines show the injury site. **(C)** HCR-FISH against *tgfb3* in the *pdgfrb:GFP* x *mfap4:mCherry* double transgenic line shows the expression of *tgfb3* only in *pdgfrb:GFP*+ cells (green arrowheads) and not in *mfap4:mCherry*+ cells (orange arrowheads). **(D)** HCR-FISH against *sema4ab* in the *pdgfrb:GFP* and *mpeg:mCherry* transgenic lines shows the expression of *sema4ab* highly enriched in *mfap4:mCherry*+ cells (overlap in white) compared to fibroblasts (*pdgfrb:GFP+)*. Asterisks indicate the position of the injury site. Error bars show SEM. Scale bars: 50 µm.

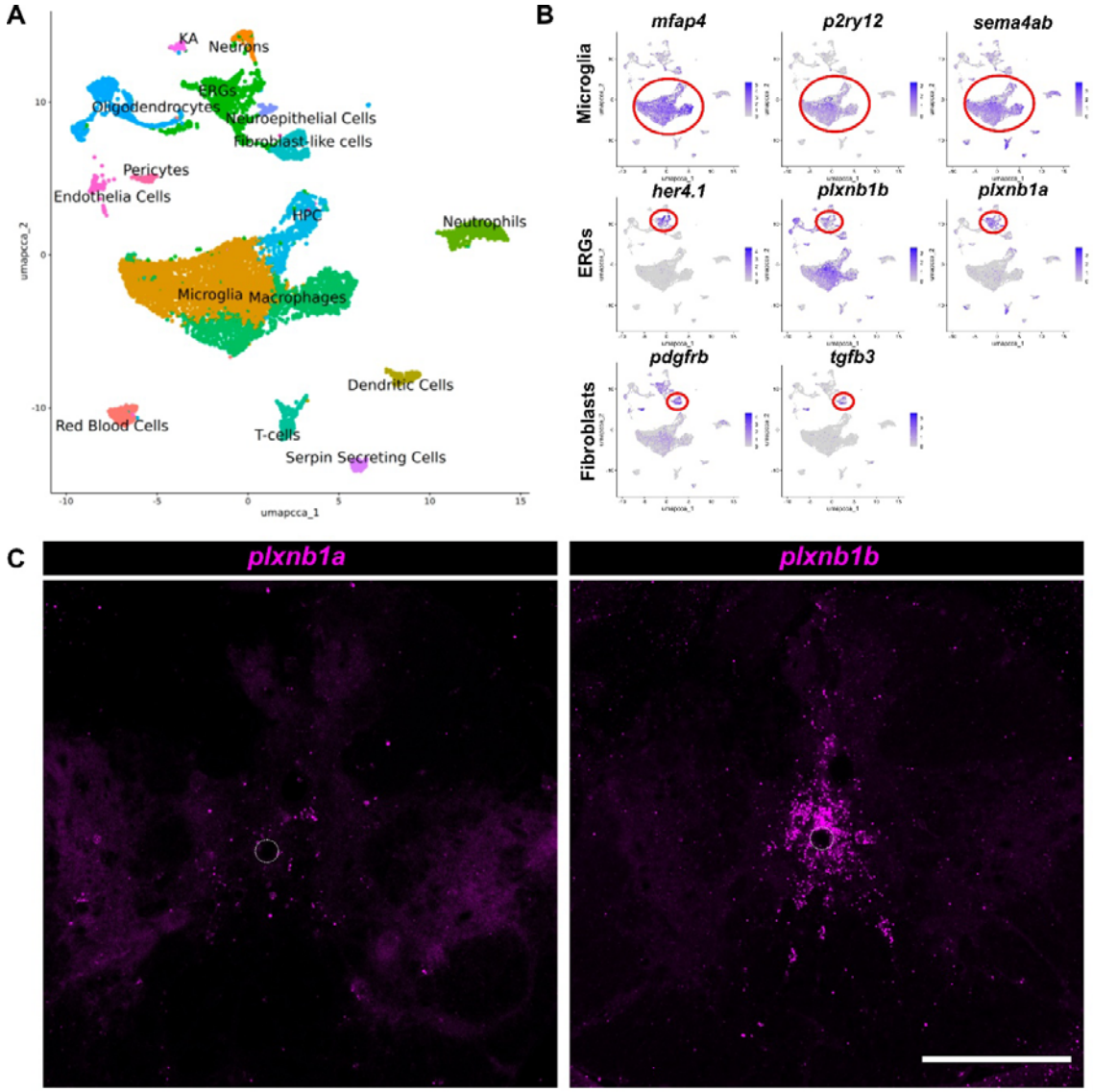
A
KA
Neurons
ERGs
Oligodendrocytes
Neuroepithelial Cells
Fibroblast-like cells
Pericytes
Endothelia Cells
HPC
Neutrophils
Microglia
Macrophages
Dendritic Cells
Red Blood Cells
T-cells
Serpin Secreting Cells
umapcca_1
umapcca_2
B
Microglia
mfap4
p2ry12
sema4ab
ERGs
her4.1
plxnb1b
plxnb1a
Fibroblasts
pdgfrb
tgfb3
C
plxnb1a
plxnb1b

Suppl. Fig. 11. scRNAseq shows that genes analysed in this study are also expressed in a spinal injury site in adult zebrafish. (A) UMAP of the main cell types from Cigliola et al. 2023 *Nat Commun* 14:4857 is shown. **(B)** Feature plots show the expression of reference genes for relevant cell types (microglia: *mfap4* and *p2ry12*; ERGs: *her4.1*; and fibroblasts-like cells: *pdgfrb*), as well as the expression of genes of interest for this study, *sema4ab, plxnb1a, plxnb1b* and *tgfb3*. Circles label expression in cell types that is conserved between larvae and adults. **(C)** HCR-FISH in cross sections of unlesioned spinal cords of 4-month-old adult zebrafish show expression of *plxnb1a and plxnb1b* in the ventricular zone. Dorsal is up and ventral is down. Dotted circle shows the central canal. Scale bar: 50 µm.

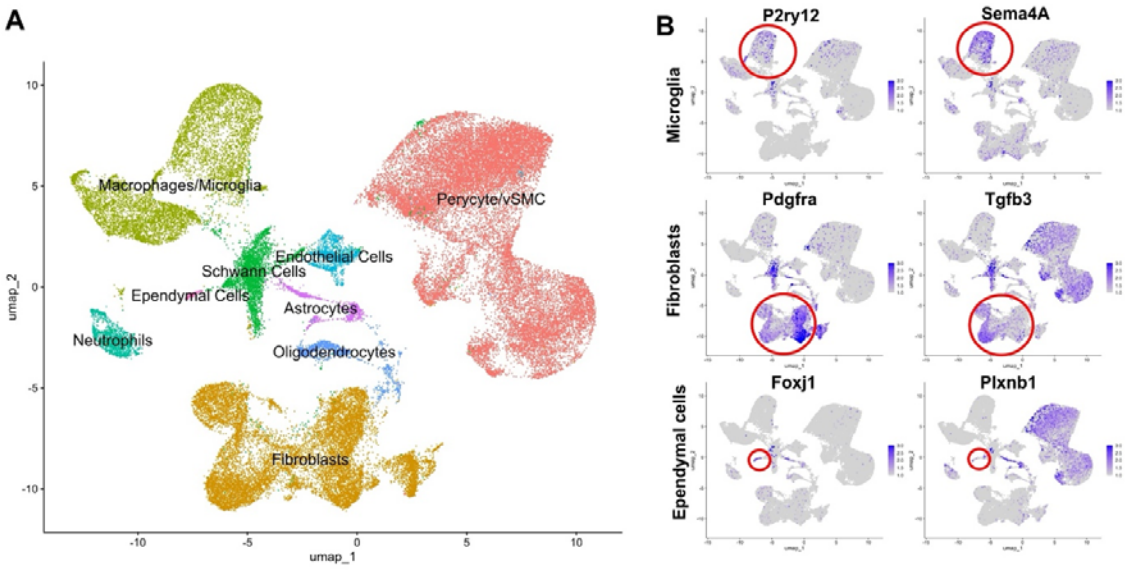

Suppl. Fig. 12 scRNAseq shows that genes analysed in this study are also expressed in a spinal injury site in adult mice. (A) A UMAP representation indicating the main cell types from Xue et al., 2024 *Nat Commun* 15:6321 is shown. **(B)** Expression pattern of mouse ortholog genes *Sema4a*, *Tgfb3* and *Plxnb1* is conserved in microglia (P2ry12), fibroblasts (Pdgfra) and ependymal cells (Foxj1), respectively. Circles label expression in cell types that is conserved between zebrafish and mouse.

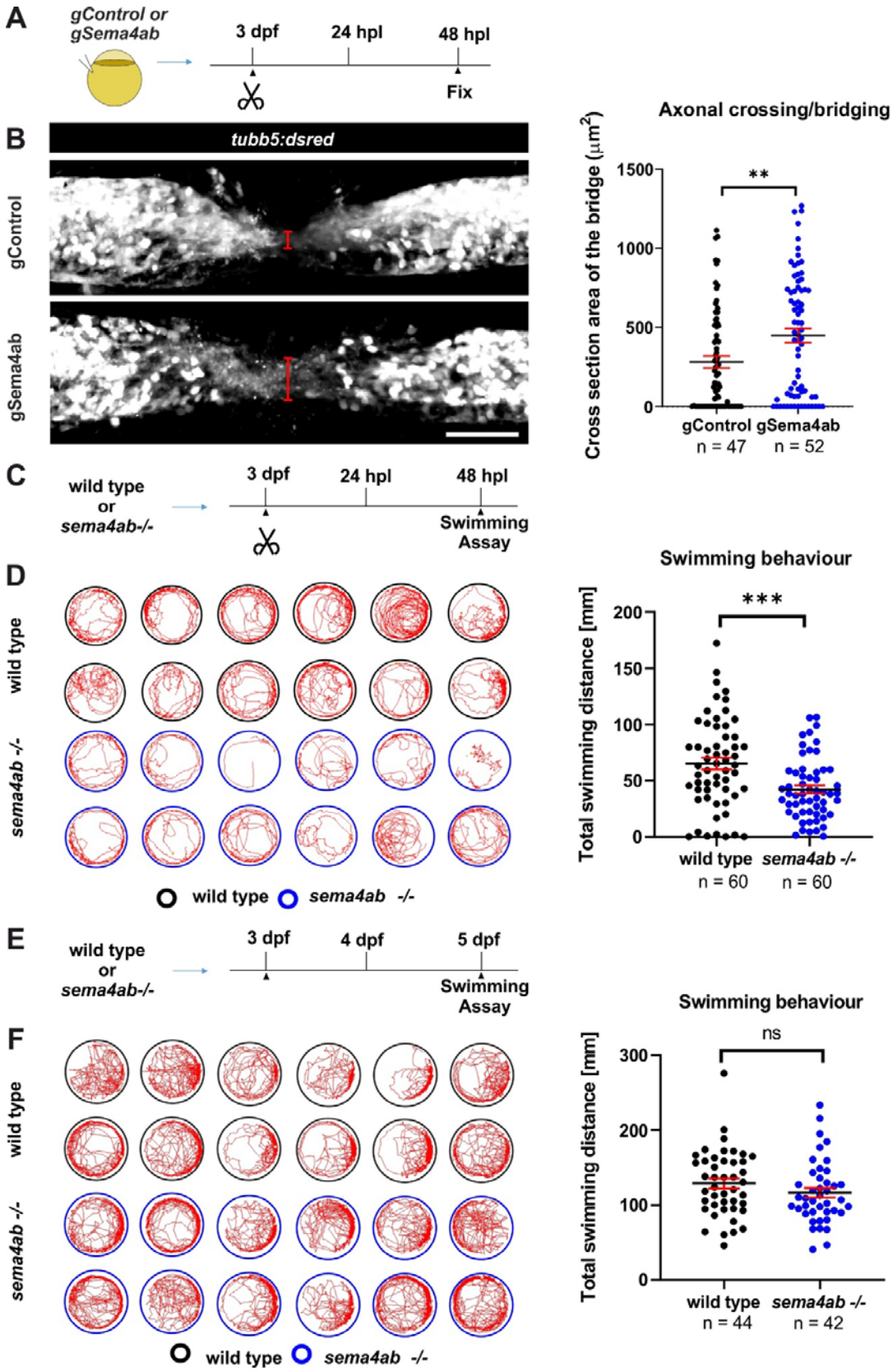
A
gControl or gSema4ab
3 dpf
24 hpl
48 hpl
Fix
B
tubb5:dsred
gControl
gSema4ab
Axonal crossing/bridging
Cross section area of the bridge (μm²)
1500
1000
500
0
**
gControl
gSema4ab
n = 47
n = 52
C
wild type or sema4ab-/-
3 dpf
24 hpl
48 hpl
Swimming Assay
D
wild type
sema4ab -/-
wild type
sema4ab -/-
Swimming behaviour
Total swimming distance [mm]
200
150
100
50
0
***
wild type
sema4ab -/-
n = 60
n = 60
E
wild type or sema4ab-/-
3 dpf
4 dpf
5 dpf
Swimming Assay
F
wild type
sema4ab -/-
wild type
sema4ab -/-
Swimming behaviour
Total swimming distance [mm]
300
200
100
0
ns
wild type
sema4ab -/-
n = 44
n = 42

Suppl. Fig. 13 Disruption of *sema4ab* enhances axonal crossing of the injury site and impairs recovery of swimming behaviour after injury. (A) A schematic indicating the experimental design to analyse axonal crossing/bridging in zebrafish larvae in B is shown. **(B)** Somatic mutation of *sema4ab* increases the thickness of the axonal fibre bundle crossing the injury site compared to controls (gControl: 281.7 μm^2 ± 36.91; gSema4ab: 448.4 μm^2 ± 44.93; Mann-Whitney U-test: p = 0.0076). **(C)** Schematic showing the experimental design to evaluate swimming behaviour in zebrafish larvae. **(D)** A test of swimming behaviour at 48 hpl shows a reduction in swimming distance in *sema4ab* germline mutants (wild type: 76.98 mm/min ± 8.846; *sema4ab* mutant: 42.15 mm/min ± 5.508; Mann-Whitney U-test: p = 0.0005). **(E)** Schematic showing the experimental design to evaluate swimming behaviour in unlesioned zebrafish larvae. **(F)** A test of swimming behaviour at 5 dpf shows no changes in swimming distance in *sema4ab* germline mutants (wild type: 128.8 mm/min ± 6.657; *sema4ab* mutant: 116.2 mm/min ± 6.504; Unpaired t-test: p = 0.1798). Error bars show SEM. Scale bars: 50 µm.

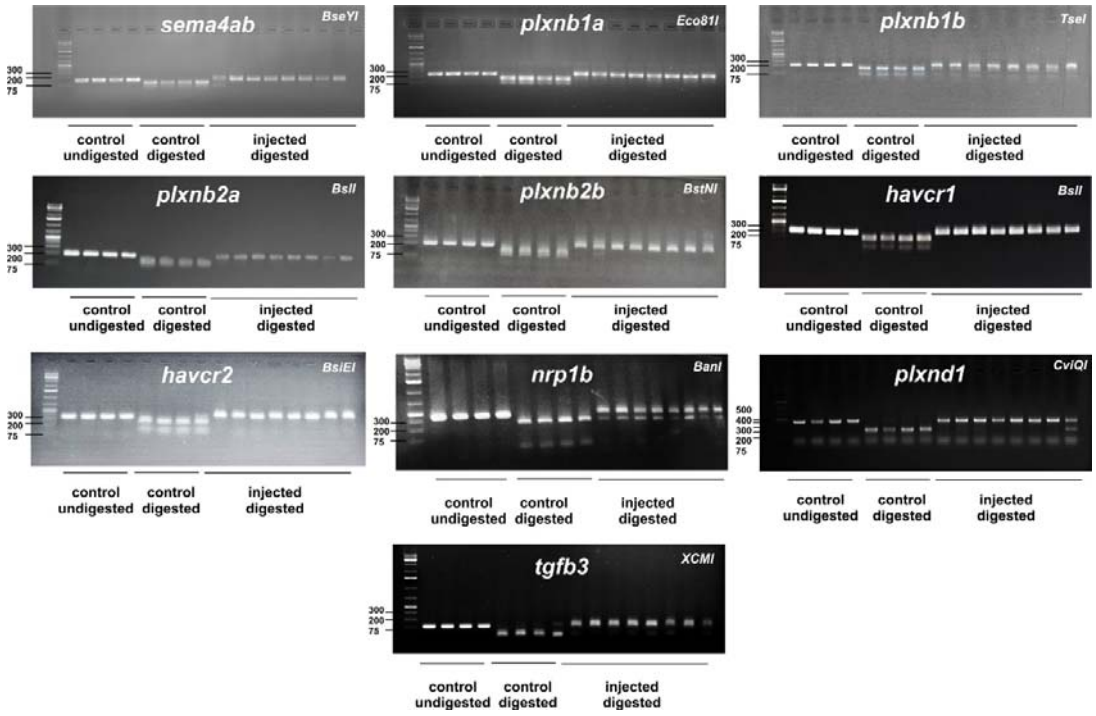

Suppl. Fig. 14. Example RFLPs of internal controls used in each somatic mutant experiment show high activity of the gRNAs. Each lane represents one larva with and without digestion with the indicated restriction enzymes and with and without targeting these sites with gRNAs as indicated. Targeting the recognition sites with haCR gRNAs leads to efficient somatic mutation, as indicated by the almost complete resistance to digestion.

SUPPLEMENTARY TABLES

	gControl	gSema4abR1	gSema4abR2
All Cells	14389	14384	14163
Cells removed	2601	2763	2833
Cells remained	11788	11621	11330
Percentage	81,92	80,79	80,00

Suppl. Table 1: Cell yields of scRNAseq experiments

	nFeature_RNA			nCount_RNA		
	mean	**median**	**total**	**mean**	**median**	**total**
gControl	2419,3	2343	28518887	9925,6	7101	117002401
gSema4abR1	2218,7	2038	25783341	9548,0	6581	110957581
gSema4abR2	2217,1	2045	25119458	9768,7	6839	110678876

Suppl. Table 2: The mean, median and total number of reads (nCount_RNA) and unique genes (nFeatures_RNA) detected per sample.

	***sema4ab* mapped total reads**	**target site total reads**	**target site intact reads**
gControl	16945	151	151
gSema4abR1	9880	4	0
gSema4abR2	10384	6	0

Suppl. Table 3: The number of reads mapped to the *sema4ab* gene and the number of reads mapped to the *sema4ab* haCR-targeted site.

scRNAseq reads of *sema4ab* gRNA target site in gSema4ab	
Reference sequence	CACAGACATTCACCATGGTTACAGGACCCAGCGGTAAACCTGAAGAAG
gSema4abR1	. .. CAGACATTCACCATGGTTACA----------
	.. . CAGACATTCACCATGGTTACAGG----------TAAACCTGAAGAAG
	. ... . . GACATTCACCATGGTTA----------
	. .. .. . GACATTCACCATGGTTACAG----------CGGTAAACCTGAAGAAG
gSema4abR2	CACAGACATTCACCATGGTTACAGG----------
	CACAGACATTCACCATGGTTACAGG----------AAACCTGAAGAAG
	CACAGACATTCACCATGGTTA----------
	. .. CAGACATTCACCATGGTTACAG----------CGGTAAACCTGAAGAAG
	. .. . . . .ACATTCACCATGGTTACAGGAACACATTCACCATGGTTACAGGA
	CACAGACATTCACCATGGTTA----------AACCTGAAGAAG
Non-targeted sequence Targeted sequence Missing/New	

Suppl. Table. 4: Examples of reads that span the haCR target site in the *sema4ab* haCR-injected samples in scRNAseq experiments

List of targeted genes using CRISPR/Cas9			
Gene	**RE**	**Sequence**	**Primer**
Sema4ab	BseYI	ACCATGGTTACAGGACCCAG	F: GCTCATGTCCACAGAATTCACA
			R: GCCACTGTTGATATACTTACCCA
Plxnb1a	Eco81I	GGCAGAACTGCCCTCAGGCT	F: GAAGTGGATGAGGAAACCGG
			R: CGTATCTACAGGCCTCTCGG
Plxnb1b	TseI	CACCATACTGTGTTGCTGCG	F: TGGGATGGTGTGTGTGACTT
			R: CGTCTCTTCCTCTGCCTCAA
Plxnb2a	BsaII	ACCTCCCGGCTTGTCCTCAAG	F: CATGGTTCCGTTTCGCCTAA
			R: CATCGACACATGAGCTGGCA
Plxnb2b	BstNI	GGACCACGCTGGCCGGCTGC	F: AAAGTGGCTCGGATGGAGAC
			R: GAGTGCAGTACCTTGACGGA
Havcr1	BslI	GAGAGGAGATATTCCCAGTA	F: GTACAGAGTTTCGAGGGTGACA
			R: ACCATCATCAACGATCAAATGGA
Havcr2	BsiEI	TTGGACAGTGGACTCGACCG	F: GCCGACACCAGTCATTGTTC
			R: GGGCCAATTGTGTTTCGGAG
Nrp1b	BanI	GCCGGACACAACGGCACCTG	F: CCCGGATAAATATCCCAACAACC
			R: CAATATGAGGACCCACTGAAAG
PlexinD1	CviQI	GTGGTTCTTGGGGAAGTACT	F: TCCGTGTACCAGGGCTTCT
			R:GTTCGCGTCGTTGTTGAAGG
Tgfb3	XCMI	GAATCCATCCAGCAGATCCC	F: GGGTCAGATCCTCAGCAAAC
			R: GAGATCCCTGGATCATGTTGA

Suppl. Table 5: Table showing the gene sequences targeted with gRNAs.

Each column represents the targeted sequence of a gene and the primers and restriction enzymes used to validate the efficiency of the mutation.

Primers use for cloning the *mfap4:mCherry-CAAX;myl7:mCerulean* vector	
Primer	**Primer sequence (5'-3')**
mfap4	**Fw:** ttt ttt gag ctc ctc gag gcg ttt ctt ggt ac
	Rev: ttt ttt ggc gcg cct gga tcc cac gat cta aag tca tga ag
mCherry-CAAX	**Fw:** aaa aaa gaa ttc gcc acc atg gtg agc aag ggc gag g
	Rev: aaa aaa tta att aat cag gag agc aca cac ttg cag ctc atg cag ccg ggg cca ctc tca tca gga ggg ttc agc tta gat ctg agt ccg gac ttg tac agc tcg tcc atg ccg aga gtg

Suppl. Table 6: Primers used for cloning the *mfap4:mCherry-CAAX;myl7:mCerulean* vector.

Primers use for cloning the *hsp70l:sema4ab-t2a-mcherry* vector	
Primer	**Primer sequence (5'-3')**
sema4ab	**Fw:** tatGGCCGGCCCAGGATGGTGATTTCGGCATCACT
	Rev: atatCCTAGGGATGGGTGTGTTGGGCAGGT
T2a-mCherry	**Fw:** atatCCTAGGGAGGGCAGAGGAAGTCTTCTAACATGCGGTGACG
	Rev: atatAGATCTCTTGTACAGCTCGTCCATGCCG

Suppl. Table 7. Primers used for cloning the *hsp70l:sema4ab-t2a-mCherry* vector.

qPCR gene primer list	
Gene name	**Primer sequence (5'-3')**
β-actin	Fw: 5'-CACTGAGGCTCCCCTGAATCCC-3 Rv: 5'-CGTACAGAGAGAGCACAGCCTGG-3
il1b	Fw: 5'-ATGGCGAACGTCATCCAAGA-3' Rv: 5'-GAGACCCGCTGATCTCCTTG-3'
tnfa	Fw: 5'-TCACGCTCCATAAGACCCAG-3 Rv: 5'-GATGTGCAAAGACACCTGGC-3'
il6	Fw: 5'-CAGCACGGAAAGATGTCTAAC-3' Rv: 5'-GTTCTTGTCAGCGCTGCCC-3'
saa	Fw: 5'-GCCGCTGGAGGTGCAAAG-3' Rv: 5'-CCTTGCAGAGCCTCCCG-3'
il11b	Fw: 5'-CAAATGAACGCaAATGAGTTGAC-3' Rv: 5'-CTGTCTGTCCGAGcTCTTG-3'
tgfb1a	Fw: 5'-GCTGTATGCGCAAGCTTTACA-3' Rv: 5'-GGACAATTGCTCCACCTTGTG-3
tgfb3	Fw: 5'-AAAACGCCAGCAACCTGTTC-3 Rv: 5'-CCTCAACGTCCATCCCTCTG-3'
neurod1	Fw: 5'-ATAACCAGCAGGCAAGTGCT-3' Rv: 5'-TCAGAGGACGGGAATTGTGC-3'

Suppl. Table 8: List of qRT-PCR primers.

Supplemental data files

Supplemental data file 1: Changes in transcript abundance for macrophage activation pathways detected by KEGG analysis. Note that most genes are down-regulated.

Supplemental movie 1: lesioned control-gRNA injected

Supplemental movie 2: lesioned *sema4ab* haCR-injected. Both movies run from 10 to 25 hpl (6 min intervals).